

This is to certify that the

dissertation entitled

Applications of Multilayer Polyelectrolyte Films in Corrosion Inhibition, Ion Separation, and Catalysis

presented by

Jinhua Dai

has been accepted towards fulfillment of the requirements for

Ph.D. degree in Chemistry

ate 11/8/02

0-12771

LIBRARY Michigan State University

PLACE IN RETURN BOX to remove this checkout from your record. TO AVOID FINES return on or before date due. MAY BE RECALLED with earlier due date if requested.

| DATE DUE | DATE DUE | DATE DUE |
|--------------|----------|----------|
| FEB 1 2 2005 | | |
| NOV 1 4 2009 | | |
| 103009 | | |
| | | |
| | | |
| | | |
| | | |
| | | |
| | | |
| | | |

6/01 c:/CIRC/DateDue.p65-p.15

APPLICATIONS OF MULTILAYER POLYELECTROLYTE FILMS IN CORROSION INHIBITION, ION SEPARATION, AND CATALYSIS

Ву

Jinhua Dai

A DISSATATION

Submitted to
Michigan State University
In partial fulfillment of the requirements
For the degree of

DOCTOR OF PHILOSOPHY

Department of Chemistry

2002

ABSTRACT

APPLICATIONS OF MULTILAYER POLYELECTROLYTE FILMS IN CORROSION INHIBITION, ION SEPARATION, AND CATALYSIS

By

Jinhua Dai

Alternating adsorption of polycations and polyanions provides a very convenient means of depositing ultrathin films with controlled thicknesses and compositions. This dissertation investigates the application of these films in areas ranging from surface protection to encapsulation of nanoparticle catalysts. In corrosion reduction, for example, deposition of multilayered poly(acrylic acid)/poly(allylamine hydrochloride) (PAA/PAH) films on Al yields ultrathin coatings that protect Al from Cl⁻-induced corrosion. Although the resistance of these films is minimal, they form a passivating layer on the surface oxide and increase oxide resistance by 2-3 orders of magnitude. Heating of PAA/PAH coatings produces cross-linked polyamides that have film resistances of about 5 M Ω cm², even when the film is only 10-nm thick. Although the resistance of these films is high, decreases in corrosion current due to cross-linked films are still result primarily from passivation of the surface oxide, as oxide resistance is larger than film resistance.

Partial Fischer esterification of PAA allows tailoring of the hydrophobicity and charge density in multilayered PAH/derivatized PAA (d-PAA) films. The hydrophobicity of these films depends on both the extent of esterification and the nature of the derivatizing alcohol. Even though PAH/d-PAA films are composed of polyelectrolytes, the presence of hydrophobic ester groups can result in advancing water contact angles as high as 101°. Cross-linking of hydrophobic PAH/d-PAA films via heat-induced amidation stabilizes

coatings over a wide pH range and allows base-promoted hydrolysis of the ester groups of PAH/d-PAA. After hydrolysis, films are extremely hydrophilic and selectively permeable to Ru(NH₃)₆³⁺ over Fe(CN)₆³⁻ due to the high density of newly formed -COO groups. To introduce fixed-charge density in PAA/PAH films, we also partially derivatized PAA using 2-nitrobenzyl bromide. Post-deposition UV irradiation of films formed using these photolabile polymers cleaves the 2-nitrobenzyl ester groups to yield fixed-charge sites. Such fixed charges can enhance Cl⁻/SO₄²⁻ selectivities up to 17-fold relative to underivatized membranes. Transport simulations suggest that both Donnan exclusion and selective diffusion contribute to selectivity.

Alternating adsorption of polyethyleneimine (PEI)-metal ion complexes and polyanions also results in the formation of multilayered polyelectrolyte films, and post-deposition reduction of the metal ions in these films yields composite coatings containing metal nanoparticles. UV/visible spectroscopy and transmission electron microscopy confirm the formation of well-dispersed nanoparticles with sizes (2-30 nm) that depend on the concentration of metal ions initially in the film. Electrodes coated with PEI-Ag (0)/PAA or PEI-Pt(0)/PAA can catalyze electrochemical reduction of methylene bromide or O₂. Interestingly, PEI-Ag(0)/PAA films are effective as antimicrobial coatings. PEI-Pd(0)/PAA-coated alumina powders catalyze the hydrogenations of structurally different unsaturated alcohols (allyl alcohol, 1-penten-3-ol, 3-methyl-1-penten-3-ol, crotyl alcohol, and 3-methyl-buten-1-ol) at very different rates. This allows selective hydrogenation of one molecule in a mixture. Additionally, the polyelectrolyte-encapsulated nanoparticles exhibit significantly lower rates of unwanted substrate isomerizations than do commercial Pd catalysts.

To my wife, Dan Xu

ACKNOWLEDGEMENTS

First, I would like to thank my advisor, Professor Merlin Bruening. I was so lucky to be accepted into your group, and have really enjoyed the four years' scientific training under your guidance. You showed me to how be insightful ('sit down and think about why is this'), to pay more attentions to details, and to be precise. You taught me how to write a paper and how to give a presentation. I owe every single piece of achievement in this dissertation to you. Thank you so very much.

Next, I want to thank my wife, Dan Xu, for your constant support in the years. You took over most of the housework, which allow me focusing on my study. I could not finish my Ph.D without you.

Professor Baker, I thank you very much for your help with my problems that I met in organic/polymeric synthesis. I was never scared of asking you questions because always greeted me with a smile.

I also would like to thank Dr. Anton Jensen for the happy cooperation in a project described in Chapter 3, and Dr. Jian Cui for his help with the anti-microbial testing.

Last, but not least, the Bruening group, past and present. Dan, a mechanist and a computer scientist in addition to a chemist, thank you so much for taking care of our computers and many set-ups in the lab. Yinda, I benefited a lot from the stimulating discussions with you. Anagi, Jeremy, Skanth, Matt, Brian, Wenxi, Kangping, Xiaoyun, Millind, Sandra, Keith, and Bo: it was so nice being with you.

This work was partially supported by the Department of Energy Office of Basic Energy Sciences, the American Chemical Society Petroleum Research Fund, and the Center for Fundamental Materials Research at Michigan State University.

v

TABLE OF CONTENTS

| List of Tables | ix |
|---|------|
| List of Figures | x |
| List of Abbreviations | xiii |
| Chapter 1: Introduction and Background | 1 |
| 1.1 Ultrathin Organic Films | 1 |
| 1.2 Layer-by-Layer Adsorption of Oppositely Charged Polyelectrolytes | 5 |
| 1.3 Fundamentals of Polyelectrolyte Films | 6 |
| 1.4 Potential Applications of Polyelectrolyte Films | 8 |
| 1.5 Motivation and Research Goals | 9 |
| 1.5.1 Polyelectrolyte Films as Protecting Coatings | 9 |
| 1.5.2 Controlling the Permeability of Layered Polyelectrolyte Films | 11 |
| 1.5.3 Controlling Ion-Transport through Layered Polyelectrolyte Membranes | 13 |
| 1.5.4 Catalytic Nanoparticle/Polyelectrolyte films | 15 |
| 1.6 References | 18 |
| Chapter 2: Ultrathin Polyelectrolyte Films as Corrosion Inhibition Coatings | 27 |
| 2.1 Introduction | 27 |
| 2.2 Experimental | 29 |
| 2.2.1 Materials | 29 |
| 2.2.2 PAA/PAH Film Synthesis | 29 |
| 2.2.3 Film Characterization | 30 |
| 2.2.4 Electrochemical Studies | 30 |
| 2.3 Results and Discussion | 31 |
| 2.3.1 Synthesis of PAA/PAH Films on Al | 31 |
| 2.3.2 Electrochemical Impedance Spectroscopy | 35 |
| 2.2.3 Protection of Al by PAA/PAH Films | 36 |
| 2.4 Conclusions | 41 |
| 2.5 References | 42 |

| through Derivatization, Cross-Linking, and Hydrolysis | 46 |
|---|--|
| 3.1 Introduction | 46 |
| 3.2 Experimental | 46 |
| 3.2.1 Materials | 46 |
| 3.2.2 Small-Scale Esterifications of PAA | 47 |
| 3.2.3 Large-Scale Ethyl-, 1-Propyl-, and 1-Butyl-PAA Syntheses | 47 |
| 3.2.4 Large-Scale Benzyl-PAA Synthesis | 48 |
| 3.2.5 Large-Scale (2-Methyl-1-butyl)-PAA Synthesis | 48 |
| 3.2.6 Film Formation | 49 |
| 3.2.7 Film Characterization | 50 |
| 3.3 Results and Discussion | 51 |
| 3.3.1 Film Formation, Cross-Linking, and Hydrolysis | 51 |
| 3.3.2 Contact Angles | 55 |
| 3.3.3 Electrochemical Studies | 57 |
| 3.3.4 Ion Detection Using Hydrolyzed Films | 61 |
| 3.4 Conclusions | 63 |
| 3.5 References | 64 |
| Chapter 4: Controlling Ion Transport through Multilayer Polyelectrolyte | |
| | |
| Membranes by Derivatization with Photolabile Functional Groups | 66 |
| 4.1 Introduction | 66 |
| • | |
| 4.1 Introduction | 66 |
| 4.1 Introduction 4.2 Experimental | 66 70 |
| 4.1 Introduction 4.2 Experimental 4.2.1 Materials | 66 70 70 |
| 4.1 Introduction 4.2 Experimental 4.2.1 Materials 4.2.2 Synthesis of 2-nitrobenzyl-derivatized PAA | 66 70 70 71 |
| 4.1 Introduction 4.2 Experimental 4.2.1 Materials 4.2.2 Synthesis of 2-nitrobenzyl-derivatized PAA 4.2.3 Synthesis of 2-nitrobenzyloxycarbonyl-derivatized PAH 4.2.4 Film Synthesis and Characterization 4.2.5 Photolysis | 66 70 70 71 71 73 74 |
| 4.1 Introduction 4.2 Experimental 4.2.1 Materials 4.2.2 Synthesis of 2-nitrobenzyl-derivatized PAA 4.2.3 Synthesis of 2-nitrobenzyloxycarbonyl-derivatized PAH 4.2.4 Film Synthesis and Characterization 4.2.5 Photolysis 4.2.6 Transport Studies | 66 70 70 71 71 73 74 74 |
| 4.1 Introduction 4.2 Experimental 4.2.1 Materials 4.2.2 Synthesis of 2-nitrobenzyl-derivatized PAA 4.2.3 Synthesis of 2-nitrobenzyloxycarbonyl-derivatized PAH 4.2.4 Film Synthesis and Characterization 4.2.5 Photolysis 4.2.6 Transport Studies 4.3 Results and Discussion | 66 70 70 71 71 73 74 74 75 |
| 4.1 Introduction 4.2 Experimental 4.2.1 Materials 4.2.2 Synthesis of 2-nitrobenzyl-derivatized PAA 4.2.3 Synthesis of 2-nitrobenzyloxycarbonyl-derivatized PAH 4.2.4 Film Synthesis and Characterization 4.2.5 Photolysis 4.2.6 Transport Studies 4.3 Results and Discussion 4.3.1 Derivatization of PAA and PAH | 66 70 70 71 71 73 74 74 75 75 |
| 4.1 Introduction 4.2 Experimental 4.2.1 Materials 4.2.2 Synthesis of 2-nitrobenzyl-derivatized PAA 4.2.3 Synthesis of 2-nitrobenzyloxycarbonyl-derivatized PAH 4.2.4 Film Synthesis and Characterization 4.2.5 Photolysis 4.2.6 Transport Studies 4.3 Results and Discussion 4.3.1 Derivatization of PAA and PAH 4.3.2 Film Formation and Photochemistry | 66 70 70 71 71 73 74 74 75 75 |
| 4.1 Introduction 4.2 Experimental 4.2.1 Materials 4.2.2 Synthesis of 2-nitrobenzyl-derivatized PAA 4.2.3 Synthesis of 2-nitrobenzyloxycarbonyl-derivatized PAH 4.2.4 Film Synthesis and Characterization 4.2.5 Photolysis 4.2.6 Transport Studies 4.3 Results and Discussion 4.3.1 Derivatization of PAA and PAH 4.3.2 Film Formation and Photochemistry 4.3.3 Ion-transport Studies | 66 70 70 71 71 73 74 74 75 75 75 |
| 4.1 Introduction 4.2 Experimental 4.2.1 Materials 4.2.2 Synthesis of 2-nitrobenzyl-derivatized PAA 4.2.3 Synthesis of 2-nitrobenzyloxycarbonyl-derivatized PAH 4.2.4 Film Synthesis and Characterization 4.2.5 Photolysis 4.2.6 Transport Studies 4.3 Results and Discussion 4.3.1 Derivatization of PAA and PAH 4.3.2 Film Formation and Photochemistry 4.3.3 Ion-transport Studies 4.3.4 Modeling of Ion Transport | 66 70 70 71 71 73 74 75 75 75 75 79 81 |
| 4.1 Introduction 4.2 Experimental 4.2.1 Materials 4.2.2 Synthesis of 2-nitrobenzyl-derivatized PAA 4.2.3 Synthesis of 2-nitrobenzyloxycarbonyl-derivatized PAH 4.2.4 Film Synthesis and Characterization 4.2.5 Photolysis 4.2.6 Transport Studies 4.3 Results and Discussion 4.3.1 Derivatization of PAA and PAH 4.3.2 Film Formation and Photochemistry 4.3.3 Ion-transport Studies 4.3.4 Modeling of Ion Transport 4.4 Conclusions | 66 70 70 71 71 73 74 75 75 75 79 81 85 |
| 4.1 Introduction 4.2 Experimental 4.2.1 Materials 4.2.2 Synthesis of 2-nitrobenzyl-derivatized PAA 4.2.3 Synthesis of 2-nitrobenzyloxycarbonyl-derivatized PAH 4.2.4 Film Synthesis and Characterization 4.2.5 Photolysis 4.2.6 Transport Studies 4.3 Results and Discussion 4.3.1 Derivatization of PAA and PAH 4.3.2 Film Formation and Photochemistry 4.3.3 Ion-transport Studies 4.3.4 Modeling of Ion Transport | 66 70 70 71 71 73 74 75 75 75 75 79 81 |

| Chapter 5: | Metal Nanoparticles/Polyelectrolyte Multilayer films: Synthesis and Catalytic Applications | 91 |
|------------|---|-----|
| 5.1 Intro | duction | 91 |
| 5.2 Expe | | 94 |
| - | ults and Discussion | 95 |
| | Synthesis of Metal Nanoparticles | 95 |
| | Electrocatalysis | 101 |
| | Inhibition of Bacteria Growth | 103 |
| 5.4 Cond | | 105 |
| | rences and Notes | 106 |
| Chapter 6: | Selective Hydrogenation Using Nanoparticle-Containing Polyelectrolyte Films | 109 |
| 6.1 Intro | duction | 109 |
| 6.2 Expe | erimental | 111 |
| • | Materials | 111 |
| 6.2.2 | Synthesis of Polyelectrolyte Films Containing Pd Nanoparticles | 113 |
| 6.2.3 | Hydrogenation | 114 |
| 6.3 Resu | alts and Discussion | 115 |
| 6.3.1 | Synthesis of Polyelectrolyte-Encapsulated Pd Nanoparticles | 115 |
| 6.3.2 | Hydrogenation | 116 |
| 6.3.3 | Competitive Hydrogenation | 120 |
| 6.3.4 | Suppression of Isomerization | 123 |
| 6.4 Cond | clusions | 124 |
| 6.5 Refe | rences | 125 |
| 6.6 App | endix | 127 |
| Chapter 7: | Conclusions and Future Work | 130 |

LIST OF TABLES

| Table 2.1 | Film thicknesses and equivalent circuit parameters for Al electrodes coated with cross-linked 9-bilayer PAA/PAH films. | 39 |
|-----------|---|-----|
| Table 2.2 | Equivalent circuit parameters for Al electrodes coated with unheated PAA monolayers and 9-bilayer PAA/PAH films that were deposited at pH 3.5 and pH 4.5. | 39 |
| Table 3.1 | Thicknesses and advancing water contact angles for 6-bilayer PAH/d-PAA films. | 56 |
| Table 4.1 | Fluxes and selectivities through membranes prepared from PAA, PAH, NBPAA, and NBPAH deposited on porous alumina. | 80 |
| Table 4.2 | Estimated charge densities, diffusion coefficients, Donnan selectivities, and diffusional selectivities for derivatized PAA/PAH membranes. | 83 |
| Table 6.1 | Rates of hydrogenation for structurally related unsaturated alcohols using commercial 5%-Pd-on-alumina or PEI-Pd(0)/PAA-on-alumina as catalysts. | 118 |

LIST OF FIGURES

| Figure 1.1 | (A) A Langmuir-Blodgett trough for deposition of monolayers on solid substrates; (B) Transfer of a LB film from the water-air | |
|------------|--|----|
| | interface to a solid, hydrophilic substrate. | 3 |
| Figure 1.2 | A schematic diagram of the formation of a self-assembled monolayer. | 4 |
| Figure 1.3 | Formation of an ultrathin film by alternating polyelectrolyte adsorption. | 5 |
| Figure 1.4 | Schematic diagram of heat-induced cross-linking of PAA/PAH films. Cross-linking converts polyelectrolyte films into passivating coatings. | 10 |
| Figure 1.5 | A composite separation membrane with a selective skin layer and a porous support. | 13 |
| Figure 1.6 | Schematic drawing of the introduction of net, fixed charges into a polyelectrolyte membrane via photolysis | 15 |
| Figure 1.7 | Reduction of metal ions in a polyelectrolyte film to form a uniform dispersion of metal nanoparticles. | 17 |
| Figure 2.1 | Synthesis and cross-linking of layered PAA/PAH films. | 28 |
| Figure 2.2 | External reflection FTIR spectra of 1, 3, 5, 7, and 9-bilayer PAA/PAH on aluminum. | 33 |
| Figure 2.3 | External reflection FTIR spectra of 9-bilayer PAA/PAH films before and after heating at 215 °C for 2h under N ₂ protection. | 34 |
| Figure 2.4 | Equivalent circuits used to simulate impedance data. | 36 |
| Figure 2.5 | Impedance plots for 'bare' Al, and Al coated with 9 bilayers of PAA/PAH, 9 bilayers of cross-linked PAA/PAH, or a monolayer of unheated PAA. | 37 |
| Figure 2.6 | Tafel plots of 'bare' Al and Al coated with 9 bilayers of cross-linked PAA/PAH (deposited at pH 4.5). | 40 |
| Figure 3.1 | Synthesis, cross-linking, and hydrolysis of PAH/d-PAA films. | 45 |
| Figure 3.2 | External reflection FTIR spectra of a PAH/PAA film and several different PAH/d-PAA films on Au. | |

| Figure | 3.3 External reflection FTIR spectra of unheated, heated, and hydrolyzed PAH/Pr-PAA films (six bilayers) on Au. | 54 |
|--------|---|----|
| Figure | in 0.5 M Na ₂ SO ₄ at Au electrodes coated with different PAH/d-PAA films. | 58 |
| Figure | at Au electrodes coated with cross-linked, hydrolyzed PAH/d-PAA films. | 60 |
| Figure | 23.6 Cyclic voltammograms of Ru(NH ₃) ₆ Cl ₃ in 0.1M NaCl containing different concentration of Ca ²⁺ at Au electrodes coated with 6 bilayers of cross-linked, hydrolyzed PAH/Pr-PAA films. | 62 |
| Figure | 4.1 Schematic drawing of the formation of multilayer polyelectrolyte membrane and subsequent introduction of net, fixed charges via photolysis. | 69 |
| Figure | 4.2 ¹ H NMR spectra of PAA and PAH that were 50% derivatized with 2-nitrobenzyl and 2-nitrobenzyloxycarbonyl groups, respectively | 72 |
| Figure | 4.3 Reflection FTIR spectra of a 10.5-bilayer 50%NBPAA/PAH film on an Al-coated wafer before (a) and after (b) UV irradiation. Spectrum (c) is that of the irradiated film after a 30 min immersion in pH 9.2 buffer solution and rinsing with ethanol. | 77 |
| Figure | 4.4 Reflection FTIR spectra of a 10.5-bilayer PAA/50%NBPAH film on an Al-coated wafer before (a) and after (b) UV irradiation. | 78 |
| Figure | 4.5 Schematic diagram of a model for ion transport through a multilayer polyelectrolyte membrane. | 82 |
| Figure | 25.1 UV-visible spectra (A) and TEMs (B,C) of PEI-protected silver colloids reduced with NaBH ₄ . The absorbance decreased 50% in the first 10 hours, and average particle size increased from 8 nm at 1h (B) to 21 nm at 10 h (C). | 96 |
| Figure | 25.2 UV-visible spectra of NaBH ₄ -reduced PEI-Ag(0)/PAA films and TEM image of a NaBH ₄ -reduced PEI-Ag(0)/PAA film.). Silver particle size is 4.0 ± 0.6 nm, | 98 |
| Figure | 5.3 TEM image of a 5.5-bilayer PEI-Pt(0)/PAA (NaBH ₄ reduced) film. | 99 |

| Figure 5.4 | TEM images of thermally reduced (heating for 2 h at 150 °C under N ₂) 5.5-bilayer PEI-Ag(0)/PAA films prepared using different concentrations of Ag ⁺ during PEI adsorption. | 100 |
|------------|---|-----|
| Figure 5.5 | Reflection FTIR spectra of a 5.5-bilayer PEI-Ag ⁺ /PAA film on Al before and after heating at 150 °C for 2h under N ₂ . | 100 |
| Figure 5.6 | (A) Cyclic voltammograms of CH ₂ Br ₂ (25 mM) at bare, PEI/PAA-coated, and PEI-Ag(0)/PAA-coated Au electrodes, and at a bulk Ag electrode. (B) Cyclic voltammograms at bare, PEI/PAA-coated, and PEI-Pt(0)/PAA-coated Au electrodes in O ₂ -saturated 1.0 M H ₂ SO ₄ . | 102 |
| Figure 5.7 | (left) E. Coli. solutions photographed after 12 h of growth at 37 °C in LB broth. The test tubes were coated with different films as noted on the picture. (right) Visible spectra of the solutions in the four test tubes. | 104 |
| Figure 6.1 | TEM image of 5 bilayers of PEI-Pd(0)/PAA on a carbon-coated copper grid. | 106 |
| Figure 6.2 | Percent of substrates hydrogenated vs reaction time for allyl alcohol, 1-penten-3-ol, and 3-methyl-1-penten-3-ol on a commercial 5%-Pd-on alumina catalyst and on a 7-bilayer PEI-Pd(0)/PAA-coated alumina catalyst. | 119 |
| Figure 6.3 | Gas chromatograms of reaction mixtures from competitive hydrogenations of allyl alcohol and 1-penten-1-ol (left), and allyl alcohol and 3-methyl-1-penten-3-ol (right). | 121 |
| Figure 6.4 | Gas chromatograms from competitive hydrogenations of allyl alcohol, crotyl alcohol, and 3-methyl-1-buten-1-ol on 5%-Pd-on-alumina and on 7-bilayer PEI-Pd(0)/PAA-on-alumina. | 122 |
| Figure 6.5 | Gas chromatograms of the reaction mixture from hydrogenation of 1-penten-3-ol on 5%-Pd-on-alumina and on 7-bilayer PEI-Pd(0)/PAA-on-alumina catalysts. Substrate isomerization was greatly suppressed by the polyelectrolye films. | 123 |

LIST OF ABBREVIATIONS

 α ion transport selectivity

Ben benzyl

 C_f capacitance of film C_{ox} capacitance of oxide

CV cyclic voltammograms (or voltammetry)
DBU 1,8-diazabicyclo[5.4.0]undec-7-ene

DMSO dimethyl sulfoxide d-PAA derivatized PAA

Et ethyl

FTIR Fourier-transform infrared

 i_{cor} corrosion current

J flux

LB Langmuir-Blodgett mBu 2-methyl-1-butyl

MPA 3-mercaptopropionic acid MPF multilayer polyelectrolyte films MSA monolayer self-assembly

NB 2-nitrobenzyl

NBOC 2-nitrobenzyloxycarbonyl NEt₄Cl tetraethylammonium chloride

PAA poly(acrylic acid)

PAH poly(allylamine hydrochloride)

PEI polyethyleneimine

PEPdN polyelectrolyte-encapsulated Pd nanoparticles

PF polyelectrolyte film

Pr 1-propyl

PSS poly(sodium 4-styrenesulfonate)

 $\begin{array}{ll} \text{PVP} & \text{poly(4-vinylpyridine)} \\ R_f & \text{resistance of film} \\ R_{ox} & \text{resistance of oxide} \end{array}$

TEM transmission electron microscopy
TGA thermogravimetric analysis

TOF turnover frequency

Chapter 1

Introduction and Background

1.1 Ultrathin Organic Films

Thin (µm) to ultrathin (nm) films are important for applications ranging from corrosion prevention to drug delivery. For example, protective layers in microelectronic devices must be very thin due to space limitations, and anti-corrosion coatings on heat-exchangers should be thin enough that they do not greatly diminish heat transfer. In membrane separations, for a given material with a specific selectivity, the separation layer should be as thin as possible in order to achieve high fluxes. Additionally, pharmaceutical tablets often contain very thin coatings that protect drugs from oxygen, moisture, and light (the three key causes of drug degradation), and simultaneously allow rapid release of drug compounds to the body.

Polymers are probably the most ubiquitous coating materials because they are relatively robust and inexpensive. The wide variety of available polymers also affords a range of material properties, and methods for deposition of these macromolecules allow coating of substrates ranging from automobiles to pharmaceuticals. Films are often prepared by dissolving the appropriate polymer in organic solvent(s), applying a coating of the material, and allowing the solvent(s) to evaporate. The biggest drawback to this strategy is the unavoidable release of volatile organic solvents. Furthermore, commonly used methods for film formation such as brushing, rolling, spraying, dip coating, and curtain coating are not suitable for forming ultrathin films with controlled thicknesses.

In ideal cases, spin coating may yield ultrathin films on smooth, flat surfaces, but this technique does not allow for preparation of films on a large scale.

The Langmuir-Blodgett (LB) technique is a powerful method for forming ultrathin organic films of amphiphilic molecules with control over film thickness on the nm scale. Langmuir carried out the first systematic study of monolayers of amphiphilic molecules at the water-air interface as early as in 1917, and Blodgett developed a method to transfer the Langmuir films onto solid substrates.⁸ In a typical experiment, a drop of a dilute solution (~1%) of an amphiphilic molecule in a volatile solvent (e.g., CHCl₃) is spread on the water-air interface of a trough (Fig. 1.1A). The amphiphiles orient themselves so that their hydrophilic head groups are dispersed at the water surface while their hydrophobic tails protrude to the air. Moving a barrier in the trough changes surface area and controls the film density. Films are transferred onto a surface by withdrawal of a substrate from the water (for hydrophilic surfaces) or insertion of the substrate into the water (for hydrophobic surfaces) (Fig. 1.1B). Multilayers can be obtained through retraction and immersion cycles. The LB method provides chemists with the capability of constructing ordered, ultrathin molecular assemblies, but the technique demands an experienced operator and careful control of experimental environment and purity of chemicals. For example, some groups recommend that the LB trough be installed on a shock absorber in a laminar-flow hood to minimize vibration and to ensure a dust-free atmosphere. The system has little tolerance to organic contamination, and thus necessitates meticulous cleaning procedures and high purity reagents. Additionally, the need for amphiphilic constituents limits film composition, while the weak van der Waals

forces holding films together result in a fragile system. ¹⁰ Thus in spite of its appeal, the LB technique is not likely to yield practical coatings.

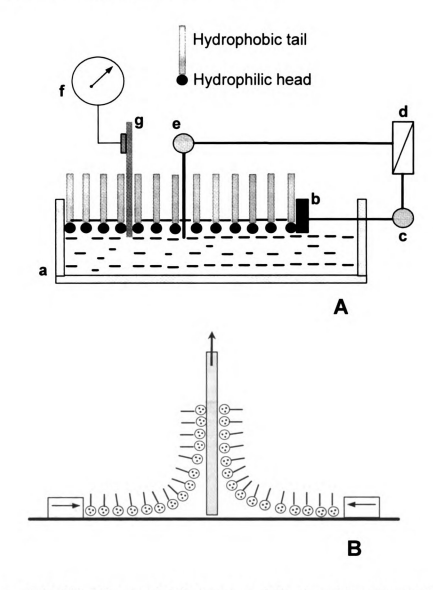


Figure 1.1: (A) A Langmuir-Blodgett trough for deposition of monolayers on solid substrates. a, bath; b, a moving barrier that allows control of the pressure applied to the monolayer; e, a motor that moves the barrier; d, a processor for controlling pressure; e, a balance that measures the surface pressure; f, a motor with a gearbox that lowers and raises the substrate; g, a solid substrate. (B) Transfer of a LB film from the water-air interface to a solid, hydrophilic substrate. Figures are adapted from reference 8.

Monolayer self-assembly (MSA) provides another method to form ultrathin films. ^{9,11-13} This technique is more convenient than the LB procedure and also produces more robust films. Amphiphilic molecules with thiol, carboxylate, or silane groups spontaneously form assemblies that are covalently or ionically connected to substrates such as Au, Al₂O₃/Al, and SiO₂/Si (Fig. 1.2). Although the procedure for film formation is convenient, simply involving immersion of a substrate in a dilute solution of the amphiphile, the film is usually limited to one layer. Substrate requirements also restrict the applications of these films.

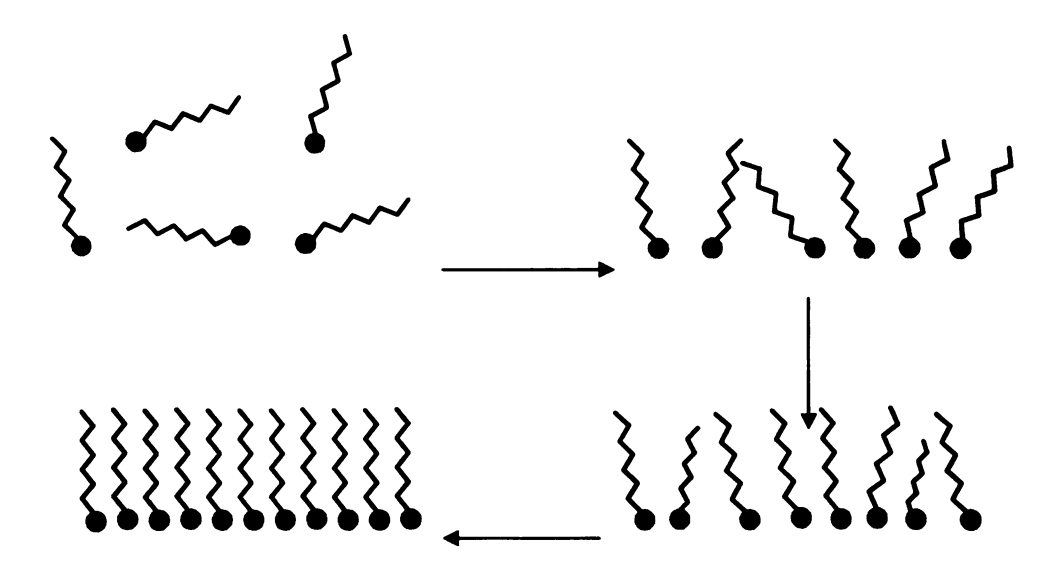


Figure 1.2: A schematic diagram of the formation of a self-assembled monolayer.

1.2 Layer-by-Layer Adsorption of Oppositely Charged Polyelectrolytes

Formation of ultrathin films by alternating adsorption of polycations and polyanions overcomes many of the limitations imposed by the LB and MSA methods. Figure 1.3 schematically portrays the principle of this technique. 14 A charged (negatively charged in

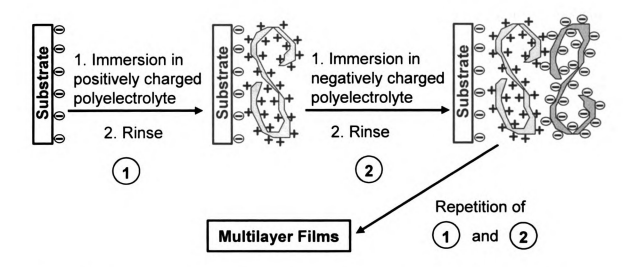


Figure 1.3: Formation of an ultrathin film by alternating polyelectrolyte adsorption.

the figure) substrate is first immersed into a solution containing an oppositely charged polyelectrolyte for a few minutes. The polymer adsorbs onto the substrate due to electrostatic interactions, and the sign of the surface charge reverses. After rinsing with water to remove any physisorbed polymer, the substrate is then immersed into a second solution of polyelectrolyte to produce another layer of polymer. This procedure may be repeated as many times as desired to produce multilayer films.

Film formation by alternating polyelectrolyte deposition has the following assets. 1.

Film formation is extremely easy and convenient, involving only a simple "dip and rinse" procedure. 2. Film thicknesses are tunable on the nanometer scale simply by controlling

the number of layers^{14, 15} or deposition conditions such as the pH or ionic strength of the deposition solutions.¹⁵⁻¹⁸ 3. Any multiply charged species (polymeric, inorganic, or biological) can be selected to construct films (vide infra). This asset contributes largely to the versatility of the method. 4. Films can form on a wide variety of surfaces, as the only required characteristic of the substrate is that it must be charged. This requirement is easily met because many solid substrates are naturally charged. Importantly, films can be deposited on irregular substrates such as small particles¹⁹ or test tubes.²⁰ 5. Film synthesis is environmentally friendly because in most cases the only solvent used is water.

1.3 Fundamentals of Polyelectrolyte Films

Sequential adsorption of oppositely charged colloids was first reported in a seminal paper by Iler.²¹ Decher and coworkers "rediscovered" this concept of layer-by-layer growth of films and extended it to preparation of mutilayers of polymeric polyelectrolytes.^{14, 22, 23} Although film formation is based on electrostatic attractions between positively and negatively charged species, the true driving force is presumably due to an entropy increase rather than an enthalpy change.²⁴ Due to the requirement of electrical neutrality, the number of ionic bonds in the system is the same before and after adsorption, and thus adsorption results in a negligible enthalpy change. Nevertheless, complexation of polyions to a charged surface releases many monovalent and divalent counterions that were previously associated with the polyelectrolytes and the surface, thus increasing the entropy of the system.

Although multilayer polyelectrolyte films are formed by sequential adsorption of polycations and polyanions, they generally do not have a highly stratified structure.

Neighboring layers are highly intertwined in most of cases because of loops and tails in the polyions. ^{14, 25, 26} These tails and loops may be in part responsible for the charge overcompensation at the film surface, ²⁷ and the entanglement of adjacent layers also facilitates complete charge compensation within multilayer films. Several studies detected no counterions in the bulk of polyelectrolyte films, suggesting that polycations are completely charge-compensated by the neighboring polyanions, and vice versa. ^{24,27}

The thicknesses of multilayer polyelectrolyte films are highly dependent on adsorption conditions. For a given substrate and polyelectrolyte system, variables that affect film thickness include the pH and ionic strength of deposition solutions, deposition time, rinsing and drying methods, and solvent composition.²⁸ The effects of pH and ionic strength are more pronounced than other factors. For polycarboxylates and polyamines, pH affects film thickness because it controls the charge density in the polyelectrolytes by altering the degree of protonation/deprotonation.¹⁶ In most cases, a high charge density results in relatively thin films because chains are in an extended configuration parallel to the substrate surface. Moreover, with high charge densities, charge compensation of the surface can be accomplished with less polymers. Addition of supporting electrolyte to the deposition solution also allows adjustment of film thickness over a wide range.

Though there are exceptions, high concentrations of salt generally increases thickness and density.^{15, 25, 29-32} The salt screens neighboring charges on the polyelectrolytes and allows formation of loops and tails.

1.4 Potential Applications of Polyelectrolyte Films

Since the early studies of alternating polyelectrolyte adsorption by Decher and coworkers, ^{14, 22, 23} the simplicity and versatility of this method have stimulated investigations of possible applications of multilayer polyelectrolyte films. As previously mentioned, virtually any multiply charged species may be used to construct films with this technique, and even when considering only functional polymers, the scope of films that can be formed is vast. Conducting, ^{33, 34} light-emitting, ^{35, 36} redox-active, ^{25, 31, 37, 40} and reactive polymers ^{41, 43} have been used for film formation. Specifically modified polyelectrolytes including polymeric metal-ion complexes, ^{36, 40, 44} polymers bearing dyes for non-linear optics, ^{41, 45, 48} and labeled polymers (e.g., biotin-, ^{49, 50} dye-, ⁵¹⁻⁵⁴ or fluorescent marker-labeled ⁵⁵⁻⁵⁸ systems) were also prepared for possible applications as conducting films, optical devices, modified electrodes, and bio/chemical sensors.

In addition to synthetic polymers, natural polyelectrolytes have been used for layer-by-layer electrostatic adsorption. Biomacromolecules employed include nucleic acids, ^{59,60} proteins, ^{49,61-64} and polysaccharides, ⁶⁵ as well as certain charged supramolecular biological assemblies like viruses ⁶⁶ and membrane fragments. ⁶⁷⁻⁶⁹ These investigations were primarily motivated by a desire to achieve biological properties such as enzymatic activity and biocompatibility in a controlled synthetic system.

The inclusion of charged nanoparticles (predominantly inorganic) in polyelectrolyte films further expands the spectrum of useful materials that can be prepared by layer-by-layer electrostatic adsorption. These charged nanoparticles (or platelets) can be considered to be rigid polyelectrolytes, and most of the particles used thus far were deposited as negatively charged colloids. Stable colloidal dispersions of silica, 70-73 metal

oxides, ^{1, 21, 74-78} polyoxometalates, ^{76, 79-82} semiconductor nanoparticles, ⁸³⁻⁸⁷ fullerenes, ⁵⁵ metal colloids, ⁸⁸⁻⁹⁵ metallo-supramolecular complexes, ⁹⁷⁻¹⁰⁰ charged latex spheres, ^{19, 21, 96, 97} or microcrystallites ⁹⁸ have been successfully employed to prepare coatings. The resulting films are nanoparticle-polymer hybrids, which sometimes combine the unique properties (e.g., electrical, optical, magnetic, catalytic) of nanoparticles with the mechanical properties of polymers (e.g., flexibility, strength). These studies have laid the foundation for possible preparation of miniaturized photoelectronic or magnetic recording devices and efficient catalysts using alternating polyelectrolyte deposition.

1.5 Motivation and Research Goals

1.5.1 Polyelectrolyte Films as Protecting Coatings

For applications of thin films as protective coatings, membranes, and controlledrelease coatings, film permeability is among the first factors that must be considered. In
the case of anti-corrosion coatings, films should be highly impermeable so that the
corrosive species cannot access the substrate. As mentioned earlier, in some cases
protective coatings should also be as thin as possible so as not to mask substrate
properties. Although alternating polyelectrolyte deposition allows formation of ultrathin
films, these coatings are usually rather permeable due to their hydrophilic nature and the
fact that they swell in aqueous solution.¹⁷ Harris and coworkers reported a technique for
cross-linking of polyelectrolyte films to reduce their permeability.⁹⁹ In this procedure,
heating of poly(acrylic acid) (PAA)/poly(allylamine hydrochloride) (PAH) films on gold
allows formation of amide bonds from the -COO groups of PAA and the -NH₄⁺ groups

of PAH (Fig. 1.4). These cross-linked, ultrathin films have a resistance of $\sim 10^5 \, \Omega \cdot \text{cm}^2$. Chapter 2 of this thesis describes deposition of such films on aluminum and examination of their ability to inhibit corrosion. Electrochemical impedance studies and polarization curves show that cross-linked PAA/PAH films with thicknesses of only 10 nm decrease the rate of Al corrosion by 2-3 orders of magnitude. In note that after the publication of this work, Farhat and Schlenoff reported that an ultrathin polyelectrolyte multilayer film can suppress the corrosion of stainless steel under anodic conditions in salt solutions.

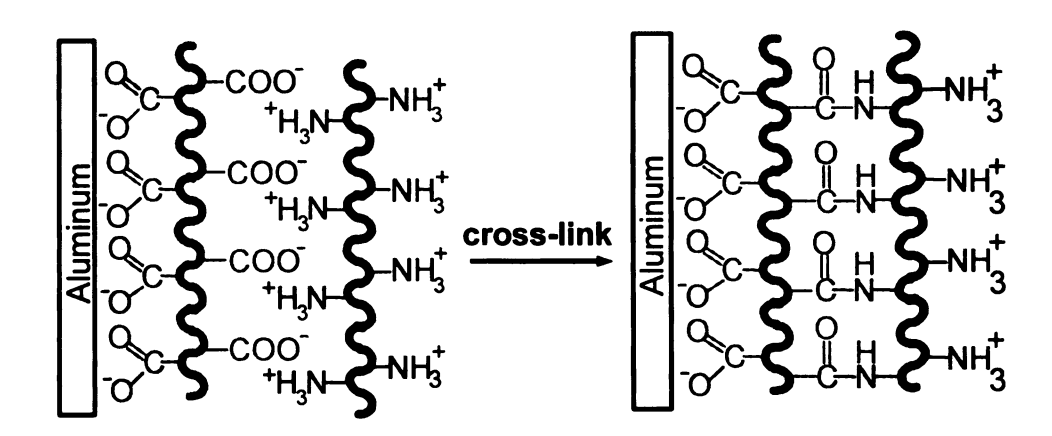


Figure 1.4: Schematic diagram of heat-induced cross-linking of PAA/PAH films. Cross-linking converts polyelectrolyte films into passivating coatings.

1.5.2 Controlling the Permeability of Layered Polyelectrolyte Films

The minimal thickness of polyelectrolyte films could also be exploited to prepare high-flux membranes, but this will require formation of films that are selectively permeable. This thesis is particularly concerned with ion-transport through polyelectrolyte films. A few groups performed fundamental studies in this area. Using voltammetry at rotating disk electrodes coated with poly(sodium 4-styrenesulfonate) (PSS)/poly(diallylmethylammonium chloride) films, Schlenoff and coworkers¹⁰² investigated the transport of electroactive ions through polyelectrolyte multilayers. They found that limiting currents are strongly attenuated by films with thicknesses on the order of a few hundred A, and that the rate of diffusion of ions through these films decreases with increasing ion charge. Ion transport also depends on the sign of the charge at the film surface, presumably because of Donnan exclusion. Möhwald and von Klitzing examined the transport of neutral quenchers in polyelectrolyte films using timedependent fluorescence.^{58, 103} They observed that the quenchers diffuse more slowly in the bulk of the film than in the outer layers, indicating that the outer part of the film is more loosely packed, probably due to less entanglement. They also found that preparation of films without added salt gives a dramatic increase in permeability. Electrochemical and in situ ellipsometric investigations of layered polyelectrolyte films by our group showed that the permeability of PSS/PAH and PAA/PAH films to Fe(CN)₆³⁻ and Ru(NH₃)₆³⁺ depends on the solution pH, the number of bilayers in the film, the concentration of salt, and the nature of constituent polymers.¹⁷ More recently. Sukhorukov¹⁰⁴ and Donath¹⁰⁵ investigated the release of fluorescein and ibufrofen from layer-by-layer polyelectrolyte mutilayer capsules, and revealed that the diffusion of the

core molecules is dependent on several parameters such as the crystal size, the polyelectrolyte capsule thickness, and the solubility of the core material in the bulk solutions. Among the results of the above studies, two are particularly important to this thesis. The first is that ion transport varies with the composition of polyelectrolyte films. The second is that Donnan inclusion/exclusion plays an important role in ion transport.

In this work, we further probed the effects of film constituents and charge density on ion transport through polyelectrolyte films. Specifically, we partially derivatized PAA with different alkyl groups through Fischer esterification reactions (Scheme 1.1). These partially derivatized PAAs (d-PAAs) still contain –COO groups that are essential for formation of PAH/d-PAA films. In contrast to underivatized PAA/PAH, the d-PAA/PAH films are highly impermeable to Fe(CN)₆³⁻ and Ru(NH₃)₆³⁺ due to the hydrophobicity of substituent alkyl groups. Interestingly, after cross-linking followed by base-catalyzed hydrolysis of ester groups, Ru(NH₃)₆³⁺ flux through the films is 10-fold higher than that of Fe(CN)₆³⁻. This occurs due to the removal of hydrophobic alkyl groups and the introduction of negative –COO groups during hydrolysis. Chapter 3 of this thesis presents electrochemical studies that demonstrate control of the permeability of multilayered polyelectrolyte films through derivatization, cross-linking, and hydrolysis.

PAA
$$\begin{array}{c}
 + R - OH \xrightarrow{H_2SO_4} \\
 \hline
COOH \\
 \hline
R
\\
NaOH
\\
Scheme 1.1$$

$$\begin{array}{c}
 + R - OH \xrightarrow{H_2SO_4} \\
 \hline
COO \\
 COO \\
 \hline
COO \\
 C$$

1.5.3 Controlling Ion-Transport through Layered Polyelectrolyte Membranes

Building on the work described in Chapter 3, Chapter 4 of this thesis reports studies on controlling ion transport through multilayer polyelectrolyte *membranes* by derivatization with photolabile functional groups. Membrane separations are attractive because of their operational simplicity and low energy cost, and polymer membranes are used extensively due to their low cost and relatively easy manufacture. Simultaneously achieving high flux and selectivity, however, is an ongoing challenging in most membrane applications.¹⁰⁷ This problem stems from the fact that selectivity is generally inversely proportional to permeability over a wide range of membrane materials.^{107, 108} Synthesis of ever-thinner membranes provides a means of increasing flux without decreasing selectivity, but deposition of membranes with a selective, defect-free layer that is less than 50 nm thick is very difficult. Adsorption of ultrathin polyelectrolyte films on porous supports may provide a way to overcome this challenge (Fig. 1.5). The porous support supplies mechanical strength, while the ultrathin polyelectrolyte 'skin', which is responsible for selectivity, should allow high flux.

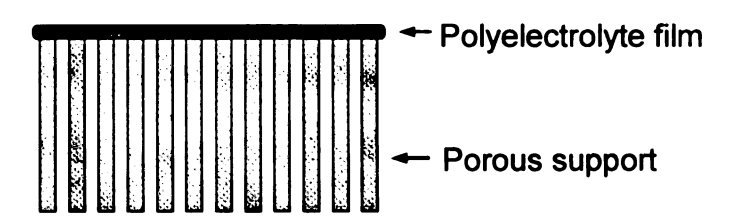


Figure 1.5: A composite separation membrane with a selective skin layer and a porous support.

Previous studies indicate, however, that simple polyelectrolyte films do not show particularly high ion-transport selectivity. Harris, ¹⁰⁹ Stair ¹¹⁰ and coworkers compared transport of Cl⁻, SO₄²⁻, and Fe(CN)₆³⁻ through PSS/PAH and PAA/PAH films coated on porous alumina supports. They obtained a selectivity of 4-9 for Cl⁻/SO₄²⁻ and a selectivity of 310-1500 for Cl⁻/Fe(CN)₆³⁻ using 5-bilayer films. Once complete pore coverage occurs, the presence of additional polyelectrolyte bilayers decreases anion flux, but has little impact on selectivity. Krasemann and Tieke did similar research and observed a selectivity of 45 for Cl⁻/SO₄²⁻ and 113 for Na⁺/Mg²⁺. ³² The differences in Cl⁻/SO₄²⁻ selectivity between the two studies are likely due to different supports and deposition conditions. Krasemann and Tieke used 60 bilayers of PSS/PAH coated on a porous polymer support. Both studies suggest that selectivity likely results from Donnan exclusion of multiply charged ions.

Assuming that Donan exclusion does play an important role in ion transport through polyelectrolyte films, the introduction of net charges into polyelectrolyte films should greatly enhance ion-transport selectivity. Although polyelectrolyte films contain a high concentration of charges, polycations and polyanions electrically compensate each other and there is little net charge in these films.^{25,31} To introduce net charge, we partially derivatized PAA with photolabile functional groups, and then formed derivatized PAA/PAH films on porous alumina supports. Photolysis of specific functional nitrobenzyl ester groups liberates –COO groups in the film that must be charge-compensated by ions in solution (Fig. 1.6).¹¹¹ Photolysis is preferable to base-catalyzed hydrolysis because it is mild and does not corrode the alumina support. Transport studies show that the introduction of net charges into polyelectrolyte films increase Cl'/SO₄²⁻

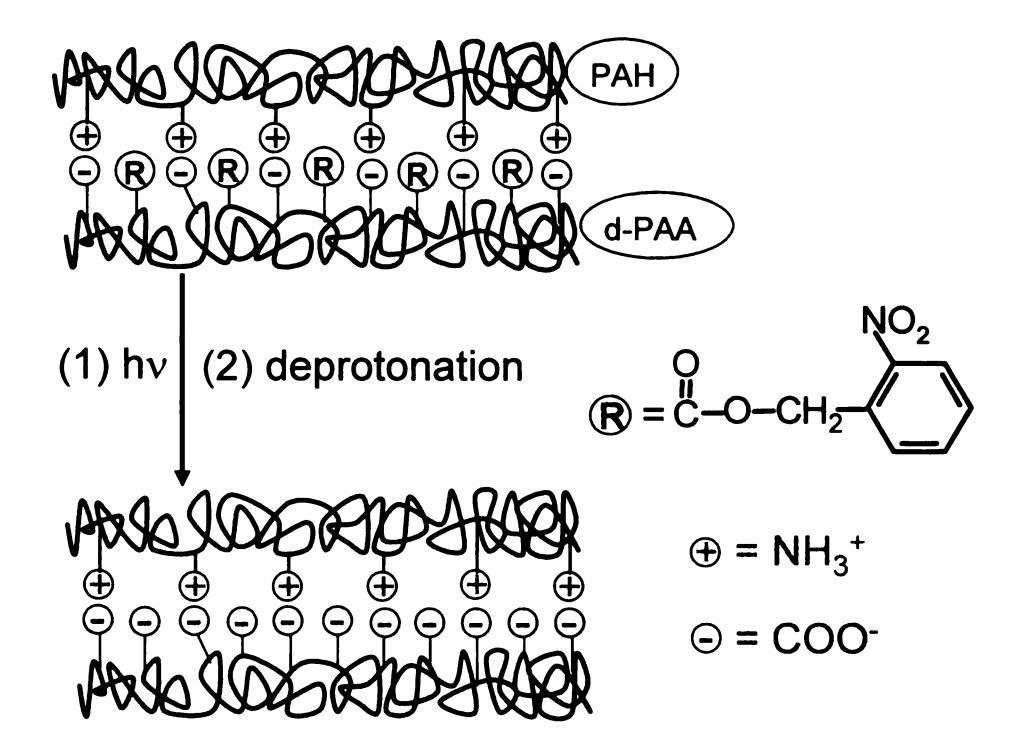


Figure 1.6: Schematic drawing of the introduction of net, fixed charge into a polyelectrolyte membrane via photolysis.

selectivity by as much as 17-fold, and the selectivity is tunable by controlling the degree of derivatization. We also simulated ion transport through this system using a simple model. The simulations indicate that Donnan exclusion is not entirely responsible for ion-transport selectivity. Diffusivity differences between various ions are also important, and in some cases dominant, in determining selectivity.

1.5.4 Catalytic Nanoparticle/Polyelectrolyte films

Chapter 5 of this thesis focuses on developing new methods for preparing polyelectrolyte films containing catalytic nanoparticles. This study expands the applications of polyelectrolyte films to include preparation of catalysts for electrodes, membranes, and synthesis of fine chemicals. Interestingly, although a number of

studies described development of nanoparticle/polyelectrolyte films, we are unaware of studies of catalysis with these systems.

Nanoparticles are attractive catalysts because of their high surface area and unique size-dependent properties.^{1,114} However, practical application of these materials will require their immobilization on supports so that the catalysts can be recovered and recycled. Because of their easy manipulation and relatively cheap price, polymeric catalyst supports have been explored recently by several groups.¹¹⁸⁻¹²³ Examples include immobilization of Pd nanoparticles on poly(vinylpyridine) nanospheres,¹¹⁵ in the interior of a block copolymer shell,^{116,117} or in the inside of dendrimers.¹¹⁸⁻¹²⁰ The polymers stabilize nanoparticles, regulate the access of reactant to the particles, and expedite catalyst recovery.^{119,121,122,124} In applications, the polymer-capped nanoparticles are generally dispersed in solutions in a batch reactor. In spite of the improvements in encapsulation, the complete recovery of catalysts is still challenging. Uniformly dispersed catalytic nanoparticle/polymer composite membranes should have advantages in this area,¹²¹ but as discussed earlier, making ultrathin polymer films is challenging.

In Chapter 5, I present a new method of forming ultrathin films that contain catalytic metal nanoparticles (Fig. 1.7).²⁰ This method circumvents the cumbersome procedures for preparation of colloids that are commonly adapted in constructing inorganic nanoparticle/polyelectrolyte composites.^{88, 89, 93, 95, 122-125} I also demonstrate that metal nanoparticle-containing polyelectrolyte films are active as electrocatalysts and antimicrobial films.

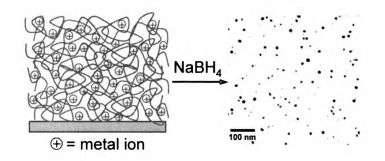


Figure 1.7: Reduction of metal ions in a polyelectrolyte film to form a uniform dispersion of metal nanoparticles

The final work in this thesis aims at utilizing catalytic nanoparticle/polyelectrolyte films to afford selective hydrogenations. Such selective catalysis may allow the performance of organic reactions such that purification is not needed after each step.

This work, described in Chapter 6, represents the culmination of this thesis as it combines selective transport through polyelectrolyte films with nanoparticle catalysis.

1.6 References

- Fendler, J. H. Nanoparticles and Nanostructured Films: Preparation, Characterization and Applications; Wiley-VCH: Weinhein, 1998.
- Bellucci, F.; Nicodemo, L.; Monetta, T.; Kloppers, M. J.; Latanision, R. M. Corrosion Sci. 1992, 33, 1203-1226.
- 3 Negi, Y. S.; Goyal, R. K. Mol. Crys. Liq. Crys. Sci. Tech., C: Mol. Mater. 2001, 14, 103-120.
- 4 Melo, L. F.; Bott, T. R. Exp. Therm. Fluid Sci. 1997, 14, 375-391.
- Johnson, J. L. In *Coatings Technology Handbook*; Satas, D., Tracton, A. A., Eds.; Marcel Dekker: New York, **2001**, pp 863-866.
- Wicks, Z. W.; Jones, F. N.; Pappas, S. P. Organic Coatings: Science and Technology, 2nd ed.; John Wiley & Sons: New Yorker, **1999**.
- 7 Langmuir, I. J. Am. Chem. Soc. 1917, 39, 1848-1852.
- 8 Blodgett, K. B. J. Am. Chem. Soc. 1935, 57, 1007-1010.
- 9 Ulman, A. An Introduction to Ultrathin Organic Films: from Langmuir-Blodgett to Self-Assembly; Academic Press: San Diego, 1991.
- Embs, F.; Funhoff, D.; Laschewsky, A.; Licht, U.; Ohst, H.; Prass, W.; Ringsdorf, H.; Wegner, G.; Wehrmann, R. Adv. Mater. 1991, 3, 25-30.
- 11 Allara, D. L.; Nuzzo, R. G. *Langmuir* **1985**, *1*, 45-52.
- 12 Nuzzo, R. G.; Fusco, F. A.; Allara, D. L. J. Am. Chem. Soc. 1987, 109, 2358-2368.
- 13 Nuzzo, R. G.; Dubois, L. H. Chem. Rev. 1996, 96, 1533-1554.
- 14 Decher, G. Science 1997, 277, 1232-1237.

- 15 Dubas, S. T.; Schlenoff, J. B. *Macromolecules* **1999**, *32*, 8153-8160.
- 16 Yoo, D.; Shiratori, S. S.; Rubner, M. F. *Macromolecules* **1998**, *31*, 4309-4318.
- 17 Harris, J. J.; Bruening, M. L. *Langmuir* **2000**, *16*, 2006-2013.
- 18 Caruso, F.; Niikura, K.; Furlong, D. N.; Okahata, Y. *Langmuir* **1997**, *13*, 3422-3426.
- 19 Caruso, F. Adv. Mater. 2001, 13, 11-22.
- 20 Dai, J.; Bruening, M. L. Nano Letters 2002, 2, 497-501.
- 21 Iler, R. K. J. Coll. Int. Sci 1966, 21, 569-594.
- 22 Decher, G.; Hong, J. D. Macromol. Chem., Macromol. Symp. 1991, 46, 321-327.
- 23 Decher, G.; Hong, J. D. Ber. Bunsenges. Phys. Chem. 1991, 95, 1430-1434.
- Arys, X.; Jonas, A. M.; Laschewsky, A.; Legras, R. In *Supramolecular Polymers*; Ciferri, A., Ed.; Marcel Dekker: New York, **2000**, pp 505-564.
- 25 Schlenoff, J. B.; Ly, H.; Li, M. J. Am. Chem. Soc. 1998, 120, 7626-7634.
- 26 Joly, S.; Kane, R.; Radzilowski, L.; Wang, T.; Wu, A.; Cohen, R. E.; Thomas, E. L.; Rubner, M. F. Langmuir 2000, 16, 1354-1359.
- 27 Lowack, K.; Helm, C. A. *Macromolecules* **1998**, *31*, 823-833.
- Bertrand, P.; Jonas, A.; Laschewsky, A.; Legras, R. *Macromol. Rapid Commun.* **2000**, *21*, 319-348.
- 29 Lvov, Y.; Decher, G.; Möhwald, H. Langmuir 1993, 9, 481-486.

- 30 Clark, S. L. M., Martha F.; Hammond, Paula T. *Macromolecules* **1997**, *30*, 7237-7244.
- 31 Laurent, D.; Schlenoff, J. B. Langmuir 1997, 13, 1552-1557.
- 32 Krasemann, L.: Tieke, B. *Langmuir* **2000**, *16*, 287-290.
- Lukkari, J.; Salomaeki, M.; Viinikanoja, A.; Aeaeritalo, T.; Paukkunen, J.; Kocharova, N.; Kankare, J. J. Am. Chem. Soc. 2001, 123, 6083-6091.
- 34 Fou, A. C.; Rubner, M. F. *Macromolecules* **1995**, *28*, 7115-7120.
- 35 Liu, Y. O.; Ma, H.; Jen, A. K. Y. Chem. Commun. 1998, 2747-2748.
- 36 Wu, A.; Yoo, D.; Lee, J.-K.; Rubner, M. F. J. Am. Chem. Soc. 1999, 121, 4883-4891.
- 37 Hodak, J.; Etchenique, R.; Calvo, E. J. *Langmuir* **1997**, *13*, 2708-2716.
- 38 Kaschak, D. M.; Lean, J. T.; Waraksa, C. C.; Saupe, G. B.; Usami, H.; Mallouk, T. E. J. Am. Chem. Soc. 1999, 121, 3435-3445.
- 39 Meier, L. P.; Heule, M.; Caseri, W. R.; Shelden, R. A.; Suter, U. W. *Macromolecules* **1996**, *29*, 718-723.
- 40 Keller, S. W.; Johnson, S. A.; Brigham, E. S.; Yonemoto, E. H.; Mallouk, T. E. J. Am. Chem. Soc. 1995, 117, 12879-12880.
- Koetse, M.; Laschewsky, A.; Mayer, B.; Rolland, O.; Wischerhoff, E. *Macromolecules* **1998**, *31*, 9316-9327.
- Laschewsky, A.; Mayer, B.; Wischerhoff, E.; Arys, X.; Jonas, A.; Kauranen, M.; Persoons, A. Angew. Chem. Int. Ed. Engl. 1997, 36, 2788-2791.
- 43 Sun, J.; Wu, T.; Sun, Y.; Wang, Z.; Zhang, X.; Shen, J.; Cao, W. *Chem. Commun.* **1998**, 1853-1854.

- 44 Lee, J.-K.; Yoo, D.; Rubner, M. F. Chem. Mater. 1997, 9, 1710-1712.
- Lindsay, G. A.; Roberts, M. J.; Chafin, A. P.; Hollins, R. A.; Merwin, L. H.; Stenger-Smith, J. D.; Yee, R. Y.; Zarras, P.; Wynne, K. J. *Chem. Mater.* **1999**, *11*, 924-929.
- 46 Roberts, M. J.; Lindsay, G. A.; Herman, W. N.; Wynne, K. J. J. Am. Chem. Soc. 1998, 120, 11202-11203.
- Laschewsky, A.; Wischerhoff, E. *Macromolecules* **1997**, *30*, 8304-8309.
- 48 Balasubramanian, S.; Wang, X.; Wang, H. C.; Ke Yang; Kumar, J.; Tripathy, S. K. *Chem. Mater.* **1998**, *10*, 1554-1560.
- 49 Hong, J. D.; Lowack, K.; Schmitt, J.; Decher, G. *Prog. Colloid Polym. Sci.* **1993**, 93, 98-102.
- 50 Cassier, T.; Lowack, K.; Decher, G. Supramol. Sci. 1998, 5, 309-315.
- 51 Fischer, P.; Laschewsky, A. *Macromolecules* **2000**, *33*, 1100-1102.
- 52 Ferreira, M.; Rubner, M. F. *Macromolecules* **1995**, *28*, 7107-7114.
- Delcorte, A.; Bertrand, P.; Wischeroff, E.; Laschewsky, A. *Langmuir* 1997, 13, 5125-5136.
- 54 Dante, S.; Advincula, R.; Frank, C. W.; Stroeve, P. Langmuir 1999, 15, 193-201.
- 55 Liu, Y.; Wang, Y.; Lu, H.; Claus, R. O. J. Phys. Chem. B 1999, 103, 2035-2036.
- Kerimo, J.; Adams, D. M.; Barbara, P. F.; Kaschak, D. M.; Mallouk, T. E. J. Phys. Chem. B 1998, 102, 9451-9460.
- 57 Kaschak, D. M.; Mallouk, T. E. J. Am. Chem. Soc. 1996, 118, 4222-4223.
- 58 Klitzing, R. v.; Möhwald, H. *Macromolecules* **1996**, *29*, 6901-6906.

- 59 Sukhorukov, G. B.; Möhwald, H.; Decher, G.; Lvov, Y. M. Thin Solid Films 1996, 220-223.
- Montrel, M. M.; Sukhorukov, G. B.; Shabarchina, L. I.; Apolonnik, N. V.; Sukhorukov, B. I. *Mater. Sci. Eng. C* **1998**, *C5*, 275-279.
- 61 Ladam, G.; Schaaf, P.; Cuisinier, F. J. G.; Decher, G.; Voegel, J.-C. *Langmuir* **2001**, 17, 878-882.
- 62 Caruso, F.; Möhwald, H. J. Am. Chem. Soc. 1999, 121, 6039-6046.
- 63 Caruso, F.; Niikura, K.; Furlong, D. N.; Okahata, Y. *Langmuir* **1997**, *13*, 3427-3433.
- 64 Eremenko, A.; Kurochkin, I.; Chernov, S.; Barmin, A.; Yaroslavov, A.; Moskvitina, T. *Thin Solid Films* 1995, 260, 212-216.
- 65 Lvov, Y.; Onda, M.; Ariga, K.; Kunitake, T. J. of Biomater. Sci., Polym. Ed. 1998, 9, 345-355.
- 66 Lvov, Y.; Haas, H.; Decher, G.; Möhwald, H. Langmuir 1994, 10, 4232-4236.
- 67 He, J.-A.; Samuelson, L.; Li, L.; Kumar, J.; Tripathy, S. K. Adv. Mater. 1999, 11, 435-446.
- 68 He, J.-A.; Samuelson, L.; Li, L.; Kumar, J.; Tripathy, S. K. J. Phys. Chem. B 1998, 102, 7067-7072.
- 69 He, J.-A.; Samuelson, L.; Li, L.; Kumar, J.; Tripathy, S. K. *Langmuir* **1998**, *14*, 1674-1679.
- 70 Caruso, F.; Caruso, R. A.; Möhwald, H. Science 1998, 282, 1111-1114.
- 71 Caruso, F.; Lichtenfeld, H.; Giersig, M.; Möhwald, H. J. Am. Chem. Soc. 1998, 120, 8523-8524.
- 72 Caruso, F.; Möhwald, H. *Langmuir* **1999**, *15*, 8276-8281.

- 73 Lvov, Y.; Ariga, K.; Onda, M.; Ichinose, I.; Kunitake, T. *Langmuir* **1997**, *13*, 6195-6203.
- 74 Cassagneau, T.; Fendler, J. H.; Mallouk, T. E. Langmuir 2000, 16, 241-246.
- Aliev, F. G.; Correa-Duarte, M. A.; Mamedov, A.; Ostrander, J. W.; Giersig, M.; Liz-Marzan, L. M.; Kotov, N. A. Adv. Mater. 1999, 11, 1006-1010.
- 76 Keller, S. W.; Kim, H.-N.; Mallouk, T. E. J. Am. Chem. Soc. 1994, 116, 8817-8818.
- 77 Rosidian, A.; Liu, Y.; Claus, R. O. Adv. Mater. 1998, 10, 1087-1091.
- 78 Chen, Z.-h.; Yang, Y.-a.; Qiu, J.-b.; Yao, J.-n. *Langmuir* **2000**, *16*, 722-725.
- 79 Caruso, F.; Kurth, D. G.; Volkmer, D.; Koop, M. J.; Müller, A. *Langmuir* **1998**, *14*, 3462-3465.
- 80 Ichinose, I.; Tagawa, H.; Mizuki, S.; Yuri Lvov, a.; Kunitake, T. *Langmuir* **1998**, *14*, 187-192.
- 81 Moriguchi, I.; Fendler, J. H. *Langmuir* **1998**, *10*, 2205-2211.
- 82 Cheng, L.; Niu, L.; Gong, J.; Dong, S. Chem. Mater. 1999, 11, 1465-1475.
- 83 Cassagneau, T.; Mallouk, T. E.; Fendler, J. H. J. Am. Chem. Soc. 1998, 120, 7848-7859.
- 84 Kotov, N. A.; Dékány, I.; Fendler, J. H. J. Phys. Chem. 1995, 99, 13065-13069.
- 85 Sun, Y.; Hao, E.; Zhang, X.; Yang, B.; Shen, J.; Chi, L.; Fuchs, H. *Langmuir* 1997, 13, 5168-5174.
- 86 Gao, M.; Richter, B.; Kirstein, S.; Möhwald, H. J. Phys. Chem. B 1998, 102, 4096-4103.
- 87 Zhang, X.; Shen, J. Adv. Mater. 1999, 11, 1139-1143.

- 88 Feldheim, D. L.; Grabar, K. C.; Natan, M. J.; Mallouk, T. E. J. Am. Chem. Soc. 1996, 118, 7640-7641.
- 89 Schrof, W.; Rozouvan, S.; Van Keuren, E.; Horn, D.; Schmitt, J.; Decher, G. Adv. Mater. 1998, 10, 338-341.
- 90 Cassagneau, T.; Fendler, J. H. J. Phys. Chem. B 1999, 103, 1789-1793.
- 91 Schmitt, J.; Decher, G.; Dressick, W. J.; Brandow, S. L.; Geer, R. E.; Shashidhar, R.; Calvert, J. M. Adv. Mater. 1997, 9, 61-65.
- 92 Liu, Y.; Claus, R. O. J. Appl. Phys. **1999**, 85, 419-424.
- 93 Liu, Y.; Wang, Y.; Claus, R. O. *Chem. Phys. Lett.* **1998**, 298, 315-319.
- 94 Yonezawa, T.; Onoue, S.-y.; Kunitake, T. Adv. Mater. 1998, 10, 414-416.
- 95 He, J.-A.; Valluzzi, R.; Yang, K.; Dolukhanyan, T.; Sung, C.; Kumar, J.; Tripathy, S. K. Chem. Mater. 1999, 11, 3268-3274.
- 96 Caruso, F.; Susha, A. S.; Giersig, M.; Möhwald, H. Adv. Mater. 1999, 11, 950-953.
- 97 Serizawa, T.; Takeshita, H.; Akashi, M. Langmuir 1998, 14, 4088-4094.
- 98 He, J.-A.; Yang, K.; Kumar, J.; Tripathy, S. K. J. Phys. Chem. B 1999, 103, 11050-11056.
- 99 Harris, J. J.; DeRose, P. M.; Bruening, M. L. J. Am. Chem. Soc. 1999, 121, 1978-1979.
- 100 Dai, J.; Sullivan, D. M.; Bruening, M. L. Ind. Eng. Chem. Res. 2000, 39, 3528-3535.
- 101 Farhat, T. R.; Schlenoff, J. B. Electrochem. Solid-State Lett. 2002, 5, B13-B15.
- 102 Farhat, T. R.; Schlenoff, J. B. *Langmuir* **2001**, *17*, 1184-1192.

- 103 Klitzing, R. v.; Möhwald, H. Thin Solid Films 1996, 352-356.
- 104 Antipov, A. A.; Sukhorukov, G. B.; Donath, E.; Möhwald, H. J. Phys. Chem. B **2001**, 105, 2281-2284.
- 105 Qiu, X.; Leporatti, S.; Donath, E.; Möhwald, H. Langmuir 2001, 17, 5375-5380.
- 106 Dai, J.; Jensen, A. W.; Mohanty, D. K.; Erndt, J.; Bruening, M. L. Langmuir 2001, 17, 931-937.
- 107 Liu, C.; Martin, C. R. Nature (London) 1991, 352, 50-52.
- 108 Liu, C.; Espenscheid, M. W.; Chen, W.-J.; Martin, C. R. J. Am. Chem. Soc. 1990, 112, 2458-2459.
- 109 Harris, J. J.; Stair, J. L.; Bruening, M. L. Chem. Mater. 2000, 12, 1941-1946.
- 110 Stair, J. L.; Harris, J. J.; Bruening, M. L. Chem. Mater. 2001, 13, 2641-2648.
- 111 Dai, J.; Balachandra, A. M.; Lee, J. I.; Bruening, M. L. *Macromolecules* **2002**, *35*, 3164-3170.
- 112 Bengtson, G.; Scheel, H.; Theis, J.; Fritsch, D. Chem. Eng. J. 2002, 85, 303-311.
- 113 Vankelecom, I. F. J.; Jacobs, P. A. Catalysis Today 2000, 56, 147-157.
- 114 Rao, C. N. R.; Kulkarni, G. U.; Thomas, P. J.; Edwards, P. P. Chem. Eur. J. 2002, 8, 28-35.
- 115 Pathak, S.; Greci, M. T.; Kwong, R. C.; Mercado, K.; Surya Prakash, G. K.; Olah, G. A.; Thompson, M. E. *Chem. Mater.* **2000**, *12*, 1985-1989.
- 116 Bronstein, L. M.; Chernyshov, D. M.; Volkov, I. O.; Ezernitskaya, M. G.; Valetsky, P. M.; Matveeva, V. G.; Sulman, E. M. J. Catalysis 2000, 196, 302-314.
- 117 Underhill, R. S.; Liu, G. Chem. Mater. 2000, 12, 3633-3641.

- 118 Rahim, E. H.; Kamounah, F. S.; Frederiksen, J.; Christensen, J. B. *Nano Lett.* **2001**, *1*, 499-501.
- 119 Yeung, L. K.; Crooks, R. M. Nano Lett. 2001, 1, 14-17.
- 120 Niu, Y.; Yeung, L. K.; Crooks, R. M. J. Am. Chem. Soc. 2001, 123, 6840-6846.
- 121 Liu, C.; Xu, Y.; Liao, S.; Yu, D. Appl. Catal., A 1998, 172, 23-29.
- 122 Lvov, Y.; Munge, B.; Giraldo, O.; Ichinose, I.; Suib, S. L.; Rusling, J. F. *Langmuir* **2000**, *16*, 8850-8857.
- 123 Mamedov, A. A.; Belov, A.; Giersig, M.; Mamedova, N. N.; Kotov, N. A. J. Am. Chem. Soc. 2001, 123, 7738-7739, and references therein.
- 124 Ostrander, J. W.; Mamedov, A. A.; Kotov, N. A. J. Am. Chem. Soc. 2001, 123, 1101-1110.
- 125 Liu, Y.; Wang, A.; Claus, R. O. Appl. Phys. Lett. 1997, 71, 2265-2267.

Chapter 2

Ultrathin Polyelectrolyte Films as Corrosion Inhibition Coatings

2.1 Introduction

In spite of the fact that surface passivation generally increases with coating thickness, there are applications where ultrathin coatings would be advantageous. In heat-exchangers, for example, coatings should be thin enough that they do not drastically reduce heat-transfer coefficients.¹ Thin coatings are also important for protecting electronic materials²⁻⁴ and microelectrode arrays.⁵

To provide satisfactory protection, a film must exhibit high chemical resistance in a corrosive environment and good adhesion to the underlying structure. Langmuir-Blodgett films are not attractive in either aspect and thus are rarely used as anti-corrosion coatings. Self-assembled monolayers are chemically adsorbed onto substrates, and full coverage on very uniform structures may occur. Although they can supply good short-term protection in some cases, they frequently have defects, and lack thermal and mechanical stability. Self-assembled monolayers

The strong electrostatic attachment of polyelectrolytes to surfaces provides good adhesion to the substrate, and layered polyelectrolyte films have many advantages as described in the introduction of this thesis (section 1.2). Unfortunately, layered polyelectrolyte films are relatively permeable because their ionic composition allows them to absorb water. Because of this, we investigated conversion of poly(acrylic acid)/(poly(allylamine hydrochloride) (PAA/PAH) films into cross-linked polyamides

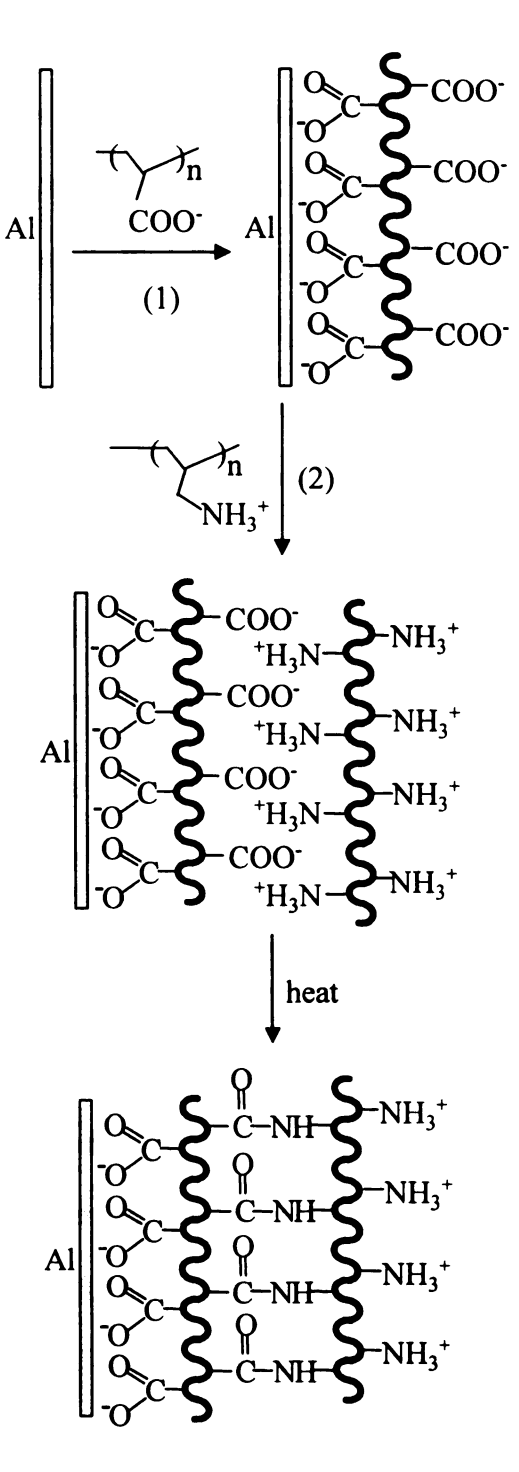


Figure 2.1: Synthesis and cross-linking of layered PAA/PAH films. Repetition of steps 1 and 2 produces multilayers.

through heating (Fig. 2.1). These cross-linked, nylon-like films are highly passivating. ¹⁴ Here we report on the possibility of using these films to protect Al from corrosion. Electrochemical studies show that such films protect the native oxide layer of Al, and even a 10 nm-thick, nylon-like film reduces corrosion currents by 2-3 orders of magnitude. For comparison, we also investigated corrosion inhibition by non-cross-linked PAA/PAH films and PAA monolayers. The ultrathin cross-linked films discussed here should have a stability advantage over non-cross-linked and monolayer films, but they do have the disadvantage of needing a heat-treatment. The heat treatment (215 °C), however, is compatible with most metals, and such treatments are common in the deposition of practical expoxy coatings. ¹⁵

2.2 Experimental

- 2.2.1 Materials. Poly(acrylic acid) ($M_w\sim90,000,25$ wt % solution in water) and poly(allylamine hydrochloride) ($M_w\sim70,000$) were obtained from Aldrich. Solutions of 0.01 M PAA, 0.01 M PAH and 0.5 M NaCl were prepared in 18.2 M Ω cm Millipore water, and pH values were adjusted with 0.1 M NaOH or HCl. (For polymers, concentration is given with respect to the repeating unit). Al substrates were made by sputtering 200 nm of Al on Si(100) wafers. This substrate has a native oxide layer with an ellipsometric thickness of about 40 Å after 15 minutes of cleaning in a UV/ozone cleaner. In this chapter, when we refer to Al or "bare" Al, we mean Al with its native oxide.
- 2.2.2 PAA/PAH film synthesis. Al substrates were cleaned for 15 minutes in a UV/ozone cleaner (Boekel Industries, model 135500) and subsequently immersed in a

- 0.01 M PAA solution for 5 minutes to form the first PAA layer on Al. The wafers were then rinsed with H₂O for 1 minute, immersed in a 0.01 M PAH solution for 5 min, and rinsed with water for 1 min. This cycle was repeated until the desired number of bilayers was deposited, and the films were then blown dry with N₂. Cross-linking was performed by heating at 215 °C under N₂ flow for 2 hours. The temperature was measured with a mercury thermometer that touched the bottom of the round-bottom flask next to the substrate. Heating at lower temperatures results in less cross-linking and higher permeability.¹⁴
- 2.2.3 Film Characterization. External reflection FTIR spectra of films were obtained with a Nicolet Magna-IR 560 spectrometer using a Pike grazing angle (80°) attachment. The whole instrument was enclosed in a glove box that was purged with the N₂ from the sample compartment. This decreases unwanted peaks due to water vapor. Film thicknesses were measured with a M-44TM rotating analyzer spectroscopic ellipsometer (J. A. Woollam), and the films were assumed to have a reflective index of 1.5. For thickness calculations, the Al/Al₂O₃ system was assumed to be one homogeneous substrate, and values of refractive index, n, and absorption coefficient, k, for this system were determined on each substrate prior to film deposition. Modeling Al/Al₂O₃ with two layers while assuming literature values for n and k of Al and Al₂O₃ allowed determination of the oxide thickness. This two-layer substrate model gives the same thicknesses for adsorbed polyelectrolyte films (within experimental error) as the assumption of a homogeneous substrate.
- **2.2.4 Electrochemical studies.** Impedance data and polarization curves were obtained with a CH Instruments electrochemical analyzer (Model 604). Measurements were made

using a Ag/AgCl (3M KCl) reference electrode and a platinum wire counter electrode. The working electrode was "bare" or coated Al contained within an O-ring holder that exposed 2.2 cm² of the sample. We intentionally used a rather corrosive electrolyte solution (0.5 M NaCl, adjusted to pH 3.0 with HCl) for electrochmical measurements to differentiate between the impedances of "bare" and film-coated Al. At neutral pH, the impedance of "bare" Al is as high as $10^7 \Omega$ -cm² after a 4 h immersion in 0.5 M NaCl due to its native oxide. Impedance data acquisition started after four hours of immersion in NaCl solutions to achieve stable values. For "bare" Al, the impedance data were acquired at the open circuit potential (ca. -1.20 V vs Ag/AgCl) using a sinusoidal voltage of 5 mV. Other impedance measurements were made at a DC potential of -0.75 V vs. Ag/AgCl, because coated Al has a much more positive open circuit potential (-0.48 to -0.75 V) than does "bare" Al. Applying potentials higher than -0.7 V (pitting potential of Al⁴) causes rapid corrosion in some cases. The frequency range for impedance measurements was 10⁵ Hz to 10 mHz, and fitting of impedance data to equivalent circuits was performed using LEVM 7.0 software written by J. Ross MacDonald (available from Solatron). Polarization curves (scan rate of 1 mV/sec) were acquired 10 minutes after finishing impedance measurements (after a total of 5 hours of immersion). All electrochemical experiments were performed on at least three different electrodes.

2.3 Results and Discussion

2.3.1 Synthesis of PAA/PAH Films on Al. Synthesis of PAA/PAH films on Al occurs in a controlled layer-by-layer fashion (Fig. 2.1). We begin the synthesis by immersing an Al-coated wafer into a solution of PAA to form carboxylate linkages to the oxidized

surface.^{14,15} Subsequent alternating immersions in PAH and PAA solutions produce a multilayer film. External reflection FTIR spectra (Figure 2.2) demonstrate the layer-by-layer growth of these coatings as absorbances increase regularly with the number of deposited bilayers. The dominant peaks in these spectra are due to the -COO⁻ asymmetric (1575 cm⁻¹) and symmetric (1400 cm⁻¹) stretches, and the -COOH carbonyl stretch (1710 cm⁻¹).

By varying the pH of deposition solutions, one can vary the thickness and composition of PAA/PAH films.¹⁶ The FTIR spectra in Figure 2.3 show that the ratio of -COOH to -COO groups increases with a decrease in deposition pH. When depositing at pH 5.5, the ratio of the absorbances (peak heights) due to the acid carbonyl and the -COO asymmetric stretch is 0.1 (Fig. 2.3a). At pH 3.5 this ratio increases to 0.5 (Fig. 2.3b). This change is explained by the variation of protonation/deprotonation of PAA with pH. Rubner and coworkers noted that bilayer thicknesses in PAA/PAH films vary dramatically with the pH at which films are deposited.¹⁶ This is certainly true in the present case as 9-bilayer films deposited at pH 5.5 are 30% as thick as 9-bilayer films deposited at pH 4.5 (See Table 2.1 on page 39).

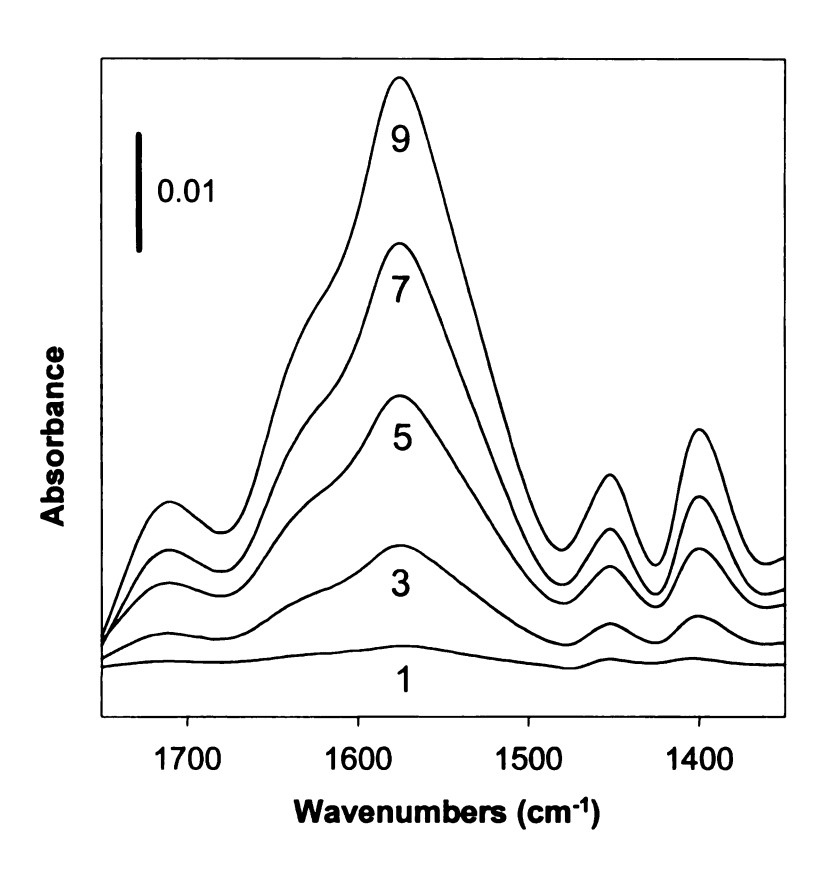


Figure 2.2: External reflection FTIR spectra of 1, 3, 5, 7, and 9 bilayers of PAA/PAH on aluminum. Films were synthesized at pH 5.5.

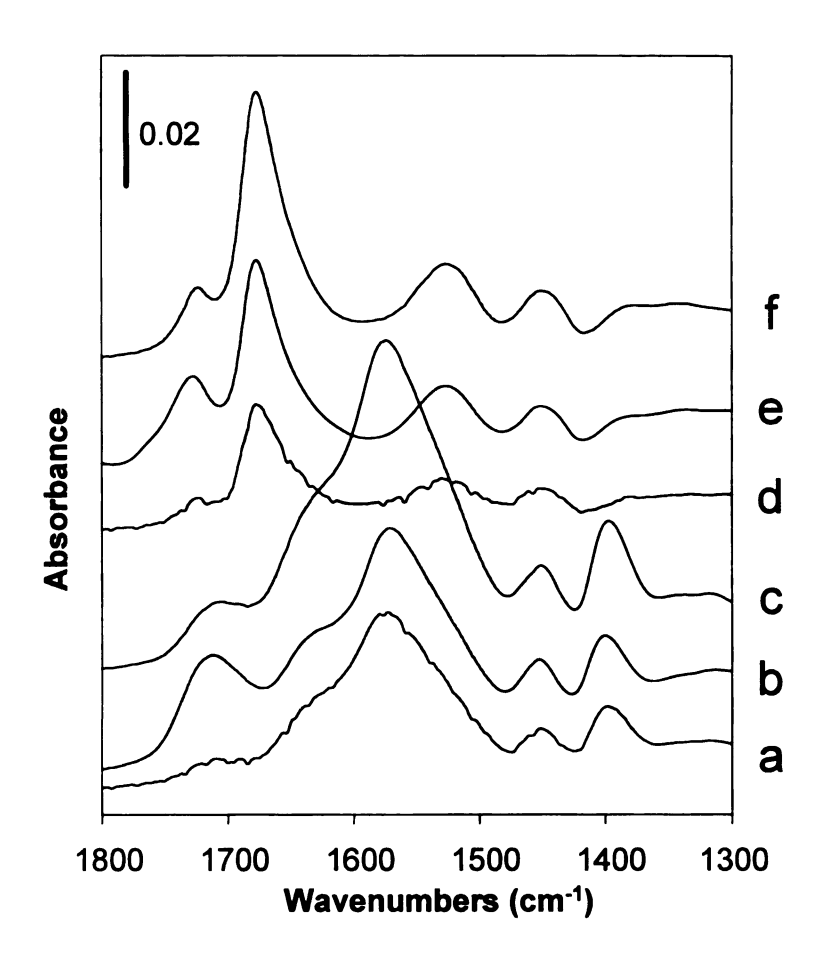


Figure 2.3: External reflection FTIR spectra of 9-bilayer PAA/PAH films before (a, b, c) and after d, e, f) heating at 215 °C for 2h under N₂ protection. Deposition pH values were as follows: pH 5.5, a and d; pH 3.5, b and e; pH 4.5, c and f. The spectra of films deposited at pH 5.5 (a and d) were multiplied by 2 for figure clarity.

In a procedure similar to a method for forming nylon, heating PAA/PAH films at 215 °C under N₂ efficiently converts carboxylate/ammonium salts into amide groups.¹⁷ Upon heating, absorbance peaks due to amide groups (1675 and 1530cm⁻¹) appear in external reflection FTIR spectra, and peaks due to -COO groups vanish (Fig. 2.3). The spectra suggest nearly complete conversion of carboxylates to amides. Amide formation occurs for films deposited at all of the pH values, but the number of remaining -COOH groups does vary with deposition pH. As expected, deposition at lower pH results in more residual -COOH groups (Fig. 2.3).

2.3.2 Electrochemical Impedance Spectroscopy. Electrochemical impedance spectroscopy is one of the most powerful methods for studying corrosion because it often provides mechanistic information about corrosion processes. ¹⁷⁻²⁶ In this technique, one determines the impedance of an electrochemical cell over a wide range of frequencies and then uses an equivalent circuit to describe impedance as a function of frequency. Various equivalent circuit models were proposed to simulate the impedance behavior of coated aluminum, ^{19,23-25,27-29} and most of these are similar to the circuits shown in Figure 2.4. For "bare" Al, the insulating oxide film forms a leaky capacitor resulting in circuit A. The presence of an organic coating that is highly blocking complicates the circuit by the addition of another leaky capacitor as shown in circuit B. As a parallel RC element results in a semicircle in a plot of real versus imaginary components of impedance, the introduction of an organic coating often results in a plot with two partial semicircles. ^{17,18,23} Note that the magnitude of the diameter of each semicircle is proportional to the resistance in the parallel RC circuit. ³⁰ Thus, larger semicircles in

impedance plots represent better corrosion protection. Scully and Hensley suggest that coating resistances need to be at least $10^7 \,\Omega\text{-cm}^2$ to provide effective protection of Al.³¹

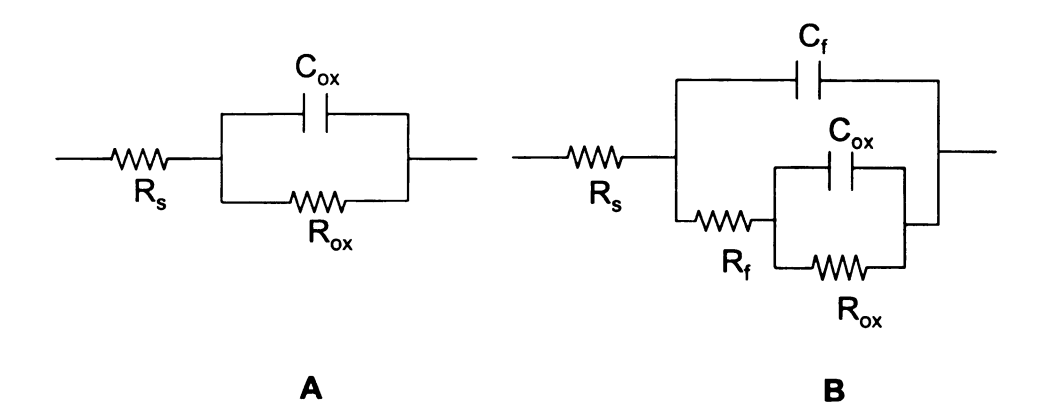


Figure 2.4: Equivalent circuits used to simulate impedance data. Circuit A was used to fit "bare" Al and Al coated with non-cross-linked PAA/PAH films. Circuit B was used to fit Al coated with cross-linked PAA/PAH films. The physical meaning of the different symbols is R_s , solution resistance, R_{ox} , oxide resistance, R_f , film resistance, R_f , film capacitance, and R_f , oxide capacitance.

2.3.3 Protection of Al by PAA/PAH Films. Impedance data show that PAA/PAH films protect the underlying aluminum oxide layer. Figure 2.5 shows impedance plots for "bare" Al (inset) and Al coated with 9-bilayers of cross-linked (triangles) and unheated (squares) PAA/PAH films. Figure 2.5 also shows the impedance plot for Al coated with a monolayer of PAA (diamonds). All of the coated Al electrodes have values of R_{ox} that are 2-3 orders of magnitude higher than for "bare" Al (Tables 2.1 and Table 2.2).

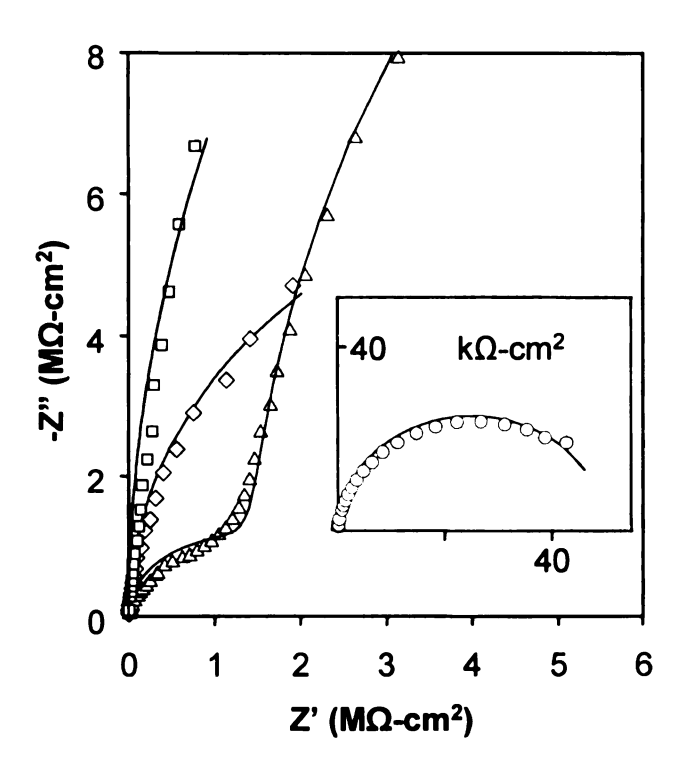


Figure 2.5: Impedance plots for 'bare' Al (circles, inset) and Al coated with 9-bilayer PAA/PAH (squares), 9-bilayer cross-linked PAA/PAH (triangles), or a monolayer of unheated PAA (diamonds). Films were deposited at pH 4.5. Lines represent fits to the data using the equivalent circuits in figure 2.4. All impedance data were measured in 0.5 M NaCl at pH 3.0 after a 4-h immersion time.

Tafel plots in Figure 2.6 also confirm the protective value of PAA/PAH coatings. The corrosion currents for "bare" Al are 2-3 orders of magnitude higher than those for Al coated with cross-linked PAA/PAH films. This is in excellent agreement with the 2-3 order of magnitude increase in oxide resistance determined by impedance. For unheated PAA/PAH films and PAA monolayers, it is difficult to obtain complete Tafel plots like those in Figure 2.6 due to their very positive open circuit potential (ca. –0.48 V). A couple of plots that we did obtain show corrosion currents within the same order of magnitude as those for Al coated with cross-linked films.

The impedance data explain why ultrathin films reduce the corrosion current for Al. Binding of a monolayer of PAA to the surface passivates the oxide layer and, in turn, protects Al (Table 2.2). The film resistance of a single PAA layer or unheated PAA/PAH films should be small, but the film apparently inhibits dissolution of the oxide. We surmise that a protective layer of Al carboxylates is forming on the surface similar to protective layers formed by corrosion inhibitors and self-assembled monolayers. All the layer inhibits Cl adsorption, thus protecting the oxide. This layer will not be as ordered as protective films of self-assembled monolayers, but it does passivate the oxide film. Multilayer PAA/PAH films likely provide more complete coverage than do PAA monolayers, resulting in higher Rox values (Table 2.2).

Although passivation of the surface oxide likely dominates corrosion currents, impedance plots show definite differences between cross-linked and unheated PAA/PAH films. As seen in Figure 2.5, the impedance plot for Al coated with cross-linked films

Table 2.1: Film thicknesses and equivalent circuit parameters^a for Al electrodes coated with cross-linked 9-bilayer PAA/PAH films.

| | | Coated at | Coated at | Coated at | |
|---|-----------------|-----------------|-----------------|---------------------|--|
| | Bare Al | pH 3.5 | pH 4.5 | pH 5.5 ^c | |
| Thickness before heating (Å) ^b | _ | 330 ± 20 | 410 ± 30 | 130 ± 15 | |
| Thickness after heating (Å) ^b | - | 260 ± 20 | 320 ± 20 | 100 ± 10 | |
| $R_f (M\Omega - cm^2)$ | - | 4 ± 0.8 | 3 ± 0.6 | 7 ± 1 | |
| $R_{ox} (M\Omega - cm^2)$ | 0.07 ± 0.02 | 80 ± 60 | 60 ± 44 | 70 ±50 | |
| $C_f (\mu F/cm^2)$ | - | 0.55 ± 0.05 | 0.75 ± 0.10 | 2.4 ± 0.6 | |
| $C_{ox} (\mu F/cm^2)$ | 7.5 ± 1.0 | 2.5 ±0.1 | 2.6 ± 0.2 | 0.8 ± 0.4 | |
| icor (nA/cm²) | 800 ± 150 | 3.5 ± 1 | 3.5 ± 1 | 3.5 ± 1 | |

^a Equivalent circuit elements are defined in Figure 2.4 and were determined from impedance spectroscopy.

Table 2.2: Equivalent circuit parameters for Al electrodes coated with unheated PAA monolayers and 9-bilayer PAA/PAH films that were deposited at pH 3.5 and pH 4.5.

| | Monolayer | | 9 bilayer PAA/PAH | | |
|---------------------------|---------------|---------------|-------------------|---------------|--|
| | pH 3.5 | pH 4.5 | pH 3.5 | pH 4.5 | |
| $R_{ox} (M\Omega - cm^2)$ | 11 ± 2 | 10 ± 2 | 40 ± 10 | 30 ± 10 | |
| $C_{ox} (\mu F/cm^2)$ | 4.2 ± 0.1 | 4.3 ± 0.1 | 4.4 ± 0.3 | 4.5 ± 0.3 | |

^b Thicknesses were determined using ellipsometry.

^c Impedance plots for films deposited at pH 5.5 do not show two apparent semicircles as do plots for films deposited at pH 3.5 and 4.5. However, phase angle-frequency plots suggest two time constants in all cases, so data were fit with circuit B in figure 2.4.

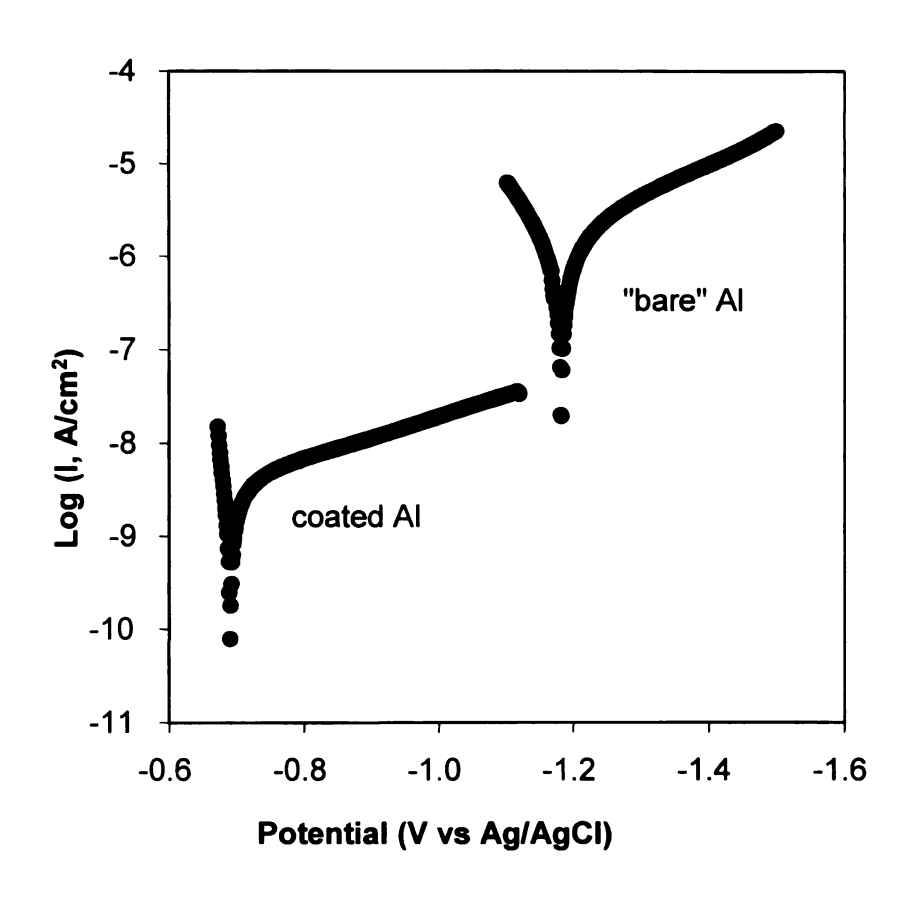


Figure 2.6: Tafel plots of bare Al and Al coated with 9-bilayer of cross-linked PAA/PAH (deposited at pH 4.5). The data were taken after a 5-h immersion time in 0.5 M NaCl adjusted to a pH of 3.0.

contains two semicircles, while that for unheated films contains only one. Plots of phase-angle versus frequency also show that there is an additional time constant for cross-linked films. The film resistance, R_f , for unheated films is negligible, ¹⁴ while values of R_f for cross-linked films are around 5 M Ω -cm² (Table 2.1). Even though this value is substantial, film resistance will not significantly decrease corrosion currents because R_{ox} is the dominant resistance in these systems. As mentioned earlier, R_f is generally > 10^7 Ω -cm² in films used for practical corrosion protection. One has to consider, however, that the R_f values in this study result from films as thin as 100 Å.

Both R_f and R_{ox} show little variation with deposition pH (Table 2.1). As gauged by the value of R_f per unit thickness, cross-linked films deposited at pH 5.5 are superior to films deposited at pH 3.5 and 4.5, but the differences in R_f /thickness are less than an order of magnitude. Thus the presence of excess -COOH groups does not appreciably increase the permeability of cross-linked films in acidic conditions.

2.4 Conclusions

PAA/PAH films can be synthesized on Al by simple "dip and rinse" layer-by-layer methods, and heating of these films results in amidation of PAA/PAH. Cross-linking by amidation yields films with resistances of 5 $M\Omega$ -cm², whereas film resistance before cross-linking is negligible. Interestingly, even unheated PAA monolayers provide substantial short-term protection for Al by passivating the surface oxide. Although the resistance of cross-linked PAA/PAH films is probably not sufficient for practical corrosion protection, considering the thickness of these films, 5 $M\Omega$ -cm² is encouraging.

2.5 References

- 1 Melo, L. F.; Bott, T. R. Exp. Therm. Fluid Sci. 1997, 14, 375-391.
- 2 Kirchner, C.; George, M.; Stein, B.; Parak, W. J.; Gaub, H. E.; Seitz, M. Adv. Funct. Mater. 2002, 12, 266-276.
- Negi, Y. S.; Goyal, R. K. Mol. Crys. Liq. Crys. Sci. Tech., C: Mol. Mater. 2001, 14, 103-120.
- Bellucci, F.; Nicodemo, L.; Monetta, T.; Kloppers, M. J.; Latanision, R. M. Corrosion Sci. 1992, 33, 1203-1226.
- 5 Schmitt, G.; Faßbender, F.; Lüth, H.; Schöning, M. J.; Schultze, J.-W.; Buß, G. *Mater. Corr.* **2000**, *51*, 20-25.
- 6 Jaiswal, A.; Singh, R. A.; Dubey, R. S. Corrosion 2001, 57, 307-312.
- 7 Ulman, A. An Introduction to Ultrathin Organic Films: from Langmuir-Blodgett to Self-Assembly; Academic Press: San Diego, 1991.
- 8 Tsuji, N.; Nozawa, K.; Armaki, K. Corros. Sci. 2000, 42, 1523-1538.
- 9 Zamborini, F. P.; Crooks, R. M. *Langmuir* **1998**, *14*, 3279-3286.
- 10 French, M.; Creager, S. E. Langmuir 1998, 14, 2129-2133.
- Harris, J. J.; Bruening, M. L. *Langmuir* **2000**, *16*, 2006-2013.
- 12 Lösche, M.; Schmitt, J.; Decher, G.; Bouwman, W. G.; Kjaer, K. *Macromolecules* 1998, 31, 8893-8906.
- 13 Schlenoff, J. B.; Ly, H.; Li, M. J. Am. Chem. Soc. 1998, 120, 7626-7634.
- 14 Harris, J. J.; DeRose, P. M.; Bruening, M. L. J. Am. Chem. Soc. 1999, 121, 1978-1979.
- 15 Grandle, J. A.; Taylor, S. R. Corrosion 1994, 50, 792-803.
- 16 Macdonald, J. R. Solid State Ionics 1992, 58, 97-107.
- Deflorian, F.; Fedrizzi, L.; Bonora, P. L. *Progress in Organic Coatings* **1993**, 23, 73-88.

- Deflorian, F.; Miskovic-Stankovic, V. B.; Bonora, P. L.; Fedrizzi, L. *Corrosion* **1994**, *50*, 438-446.
- 19 Kendig, M.; Scully, J. Corrosion 1990, 46, 22-29.
- 20 Mansfeld, F.; Chen, C.; Lee, C. C.; Xiao, H. Corros. Sci. 1996, 38, 497-513.
- 21 Bonora, P. L.; Deflorian, F.; Fedrizzi, L. *Electrochim. Acta* 1996, 41, 1073-1082.
- 22 Griffin, A. J. J.; Brotzen, F. R. J. Electrochem. Soc. 1994, 141, 3473-3479.
- 23 Su, P.-C.; Devereux, O. F. Corrosion 1998, 54, 419-427.
- 24 Mertens, S. F.; Xhoffer, C.; De Cooman, B. C.; Temmerman, E. *Corrosion* **1997**, 53, 381-388.
- 25 Scholl, H.; Jimenez, M. M. D. Corros. Sci. 1992, 33, 1967-1978.
- 26 Lin, S.; Shih, H.; Mansfeld, F. Corrosion Science 1992, 33, 1331-1349.
- 27 Bessone, J.; Mayer, C.; Jüttner, K.; Lorentz, W. J. *Electrochim. Acta.* **1983**, *28*, 171-175.
- 28 Bellucci, F.; Kloppers, M.; Latanision, R. M. J. Electrochem Soc. 1991, 138, 40-48.
- 29 Mansfeld, F.; Kendig, M. W.; Tsai, S. Corrosion 1982, 38, 478-485.
- Bard, A. J.; Faulkner, L. R. *Electrochemical Methods: Fundamentals and Applications*; 2nd ed.; John Wiley & Sons: New York, **2001**.
- 31 Scully, J. R.; Hensley, S. T. *Corrosion* **1994**, *50*, 705-716.
- 32 Heeg, B.; Klenerman, D. Langmuir **2000**, 16, 1783-1792.
- 33 Brusic, V.; Frisch, M. A.; Eldridge, B. N.; Novak, F. P.; Kaufman, F. B.; Rush, B. M.; Frankel, G. S. *J. Electrochem. Soc.* **1991**, *138*, 2253-2259.
- 34 Ogawa, H.; Chihera, T.; Taya, K. J. Am. Chem. Soc. 1985, 107, 1365-1369.
- 35 EI-Awady, A. A.; Abd-EI-Nabey, B. A.; Aziz, S. G. J. Chem. Soc. Faraday Trans. 1993, 89, 795-802.

Chapter 3

Controlling the Permeability of Multilayered Polyelectrolyte Films through Derivatization, Cross-Linking, and Hydrolysis

3.1 Introduction

The convenience and versatility of layer-by-layer polyelectrolyte deposition make polyelectrolyte films (PFs) attractive for possible applications in sensors, ¹⁻³ separation membranes, ⁴⁻¹¹ capillary electrophoresis, ¹² light-emitting diodes, ^{13,14} and corrosion protection. ¹⁵ Several of these applications require control over film permeability. Development of corrosion-resistant coatings, for example, requires PFs that are impermeable to ions, while separation membranes composed of PFs should be selectively permeable. Synthesis of impermeable PFs will likely require development of hydrophobic ¹⁶ or highly cross-linked films. ^{17,18} In contrast, PFs are attractive for ion-separation membranes in part because their high charge density may result in Donnan exclusion of multiply charged ions. ^{4,5}

This chapter describes the preparation (see Fig. 3.1) and use of partially esterified poly(acrylic acid) (d-PAA) to control both hydrophobicity and charge density in poly(allylamine hydrochloride) (PAH)/d-PAA films. The hydrophobicity of PAH/d-PAA films results in coatings that passivate surfaces. In contrast, ester hydrolysis affords highly charged films that are selectively permeable to ions. We employ only partial esterification of PAA because unreacted -COO groups are necessary for formation of PFs. Esterification of 50-70% of the -COOH groups of PAA still results in very hydrophobic PAH/d-PAA films (advancing water contact angles of up to 101°) that greatly restrict access to an underlying electrode.

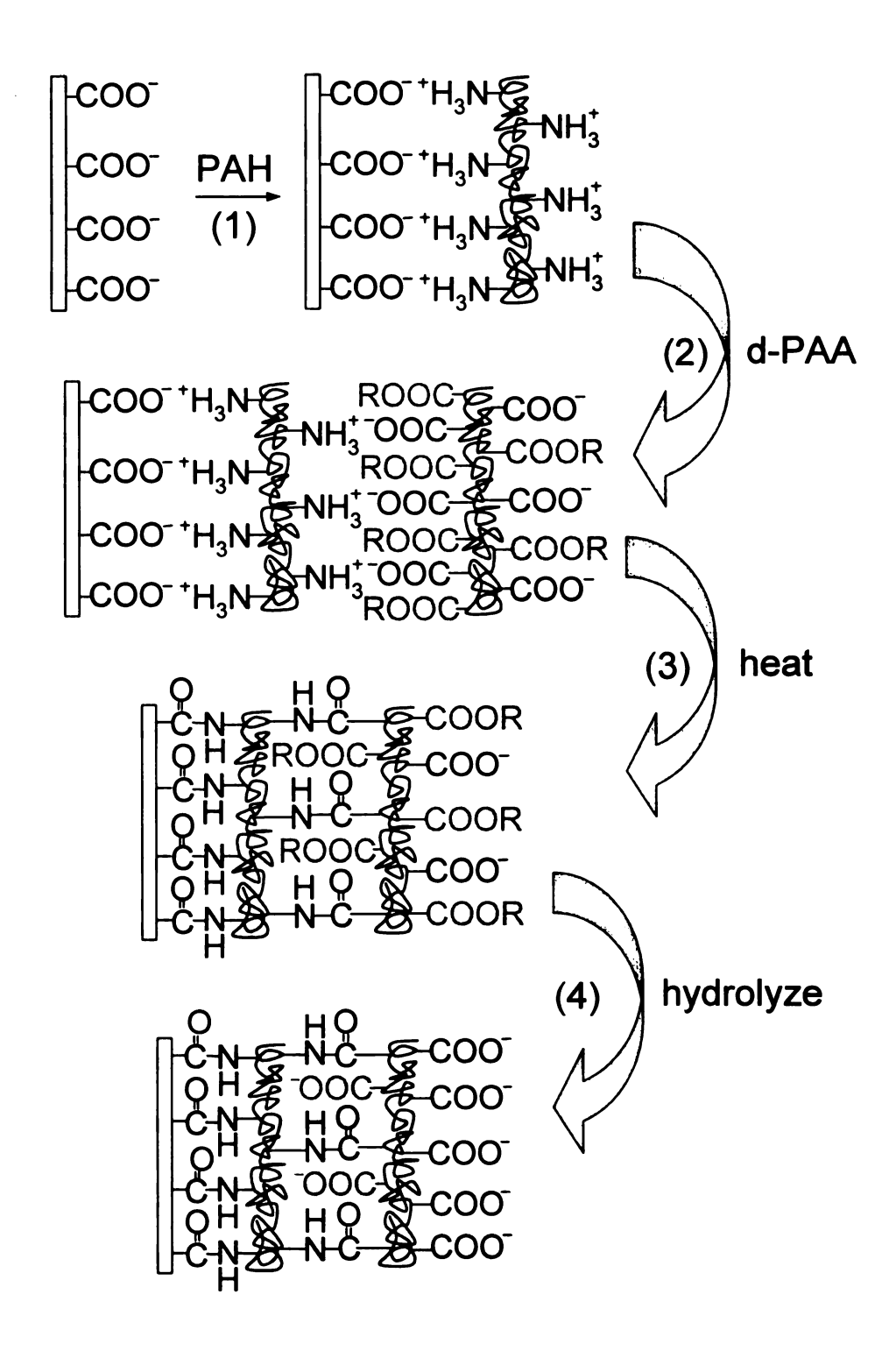


Figure 3.1: Synthesis, cross-linking (heating), and hydrolysis of PAH/d-PAA films. Repetition of steps 1 and 2 produces multilayer films.

To increase charge density in a PAH/d-PAA coating, we first heat the film to form amide cross-links from carboxylate-ammonium ion pairs. Subsequently, basic hydrolysis of ester groups results in a high density of -COO groups in the film. Unlike the -COO groups present during deposition of PAH/d-PAA, carboxylates formed by hydrolysis are not charge-compensated by a neighboring ammonium group in PAH. Several previous studies show that charge compensation in many PFs is almost completely intrinsic (polycations are compensated by polyanions, and vice versa). 19-21 The charges on carboxylate groups formed by hydrolysis, however, must be charge-compensated by cations from the solution (extrinsic compensation). Binding of divalent cations to extrinsically compensated -COO sites in hydrolyzed PAH/d-PAA films dramatically alters film permeability and provides a possible means of sensing low concentrations of ions such as Ca²⁺, even in a 5 order of magnitude excess of Na⁺.

3.2 Experimental Section

3.2.1 Materials. PAA (Aldrich, $M_w = 750\,000$), PAH (Aldrich, $M_w = 70\,000$), 3-mercaptopropionic acid (MPA) (Aldrich), K₃Fe(CN)₆ (Mallinckrodt), Ru(NH₃)₆Cl₃ (Alfa Aesar), AlCl₃·6H₂O (Spectrum), CaCl₂·2H₂O (Baker), NaCl (Baker), Na₂SO₄ (Baker), ethanol (Pharmco, 200 proof), 1-butanol (Fisher, Certified ACS), 2-methyl-1-butanol (Fisher, Certified ACS), pentane (Aldrich, HPLC grade), diethyl ether (Fisher, anhydrous), and sulfuric acid (Fisher, Certified ACS) were used as received. Propanol and benzyl alcohol were distilled over magnesium and iodine. All aqueous solutions were prepared with 18 M Ω cm Milli-O water

3.2.2 Small-Scale Esterifications of PAA. Fischer esterification reactions were performed and described by Dr. Anton Jensen and his associates at Central Michigan University. Small-scale reactions were initially run to test the reactivity of the alcohols. This involved adding 0.5-1.0 g of PAA, 10-20 mL of alcohol, and 3 drops of concentrated sulfuric acid to a round-bottom flask fitted with a condenser. The mixtures were then heated with stirring to reflux (ethanol, 1-propanol, and 1-butanol) or about 100 °C (benzyl alcohol). IR spectra were taken at regular intervals by placing a drop from the solution onto a salt plate and drying. At these same intervals, 2 mL aliquots were removed from the reaction for ¹H NMR analysis. These aliquots were added to distilled water, pentane, or diethyl ether to precipitate the polymer, which was then dried in a vacuum oven for about an hour. About 50 mg of dried precipitate was then dissolved in d₆-DMSO for analysis. The extent of derivatization was calculated from the ¹H NMR spectra. Once small-scale reactions were analyzed by IR and ¹H NMR, a correlation could be made between relative intensities of ester and acid carbonyl peaks in the IR spectra and extent of derivatization. Thermogravimetric analysis (TGA) of the polymers was conducted at a heating rate of 10 °C/min under nitrogen using a DuPont 2900 TGA. These data were collected by Dr. Dilip Mohanty of Central Michigan University. 3.2.3 Large-Scale Ethyl., 1-Propyl., and 1-Butyl-PAA Synthesis. For the ethyl, 1propyl, and 1-butyl ester derivatives, large-scale reactions were run by adding 10 g of PAA, about 130 mL of alcohol, and 10 drops of sulfuric acid to a round-bottom flask fitted with a reflux condenser. The solution was then heated with stirring to reflux. The reactions were followed via IR by comparing the relative intensities of ester and sour carbonyl stretches with the small-scale-reaction IR spectra. Thus, reactions were allowed to proceed until the desired percent derivatization, as estimated by IR, was reached. The products were then precipitated and analyzed by ¹H NMR as with the small scale reactions. For the ethyl derivative, after 3 h of reflux PAA was 67% ethyl esterified (82% yield). For the 1-propyl derivative, after 1 h and 50 min of reflux PAA was 61% 1-propyl esterified (66% yield). For the 1-butyl derivative, after 40 min of reflux PAA was 69% 1-butyl esterified (71% yield). The 19% ethyl ester polymer that was used in the film studies was the first aliquot removed from a small-scale reaction after 30 min of heating.

- 3.2.4 Large-Scale Benzyl-PAA Synthesis. For the benzyl ester derivative, a large scale reaction was run by adding 3.0 g of PAA, about 30 mL of alcohol, and 3-4 drops of sulfuric acid to a round-bottom flask fitted with a reflux condenser. The clear, gelatinous slurry was then heated to 100 °C. The product was precipitated as a white solid, soxhlet extracted with diethyl ether, and dried under high vacuum with minimal heating before analysis by ¹H NMR. After 2 h and 10 min of reflux, PAA was 52% benzyl esterified (quantitative yield).
- 3.2.5 Large-Scale (2-Methyl-1-butyl)-PAA Synthesis. Only a large-scale reaction was run for the 2-methyl-1-butyl ester derivative. This was done by adding 10 g of PAA, 220 mL of 2-methyl-1-butanol, and 6 drops of sulfuric acid into a round-bottom flask fitted with a reflux condenser and a mechanical stirrer. The solution was heated to 105 °C. The mixture was heated initially for 3 h, stopped for 11 h, and recommenced for an additional 4.5 h, all with continuous stirring. At the end of the heating, the polymer was precipitated in pentane, dried under vacuum for 20 h at 62 °C, and analyzed by ¹H NMR. The product was found to be 30% derivatized (93% yield).

3.2.6 Film Formation. To synthesize PAH/d-PAA films, we first cleaned a gold-coated Si slide $(2.4 \times 1.2 \text{ cm piece of a Si}(100))$ wafer that was sputter-coated with 20 nm of Cr followed by 200 nm of Au) for 15 min in a Boekel UV/ozone cleaner. Next, we formed a monolayer of MPA on the gold by immersing the slide in 2 mM MPA in ethanol for 45 min, rinsing with ethanol, and drying with N₂. (MPA was used because it can be crosslinked to PAH in a later step. Otherwise, 3-mercapto-1-propanesulfonic acid might be a better choice because it is not pH-sensitive.²²) Deposition of a layer of PAH occurred by immersion (5 min) of the MPA-coated slide into an aqueous 0.02 M PAH, 0.2 M NaCl solution that was adjusted to pH 5.5 with NaOH. (Salt was added to increase the thickness of PAH layers. 19, 20, 23, 24 The molarity of the polymer is given with respect to the repeating unit.) The slide was then removed from solution, rinsed with water for 1 min, dried with N₂, and immersed in a solution containing PAA or d-PAA for 5 min. Rinsing again with water and drying with N₂ completed the synthesis of the first bilaver of PAH/PAA. Subsequent bilayers were prepared with the same PAH/PAA deposition steps.

Derivatized PAA molecules were not soluble in water, so deposition solutions for these polymers were prepared in mixtures of water and methanol or water and THF.^{19, 25} Solutions containing PAA derivatized with ethyl, 1-propyl, or 2-methyl-1-butyl alcohol (Et-, Pr-, and mBu-PAA) were prepared by dissolving 200 mg of polymer in 90 mL of methanol, adding 10 mL of water, and adjusting the apparent pH (measured with a pH meter) to 7.0 with a few drops of 0.1 M NaOH. To prepare solutions for deposition of PAA derivatized with butyl alcohol (Bu-PAA), 200 mg of polymer was dissolved (with sonication) in 90 mL of methanol, and then 60 μL of *N*-methylmorpholine (added to

deprotonate the -COOH groups of Bu-PAA) and 10 mL of water were added to this solution. (Bu-PAA precipitates in solutions of methanol and water in the absence of *N*-methylmorpholine.) Solutions for deposition of PAA derivatized with benzyl alcohol (Ben-PAA) were prepared by dissolving 200 mg of Ben-PAA in 90 mL of THF and adding 60 μL of *N*-methylmorpholine and 10 mL of water. (Ben-PAA does not dissolve in methanol). For deposition of underivatized PAA, we used 0.01 M aqueous solutions of PAA that were adjusted to pH 5.0 with NaOH.

Cross-linking of films was performed by heating at 180 °C under N₂ for 2 h. Heating at higher temperatures causes more loss of ester groups, while lower temperatures result in less cross-linking.¹⁸ Hydrolysis of cross-linked films was effected by immersion of the sample in a solution of 2.0 M NaOH in 90%methanol+10%water for 4 h at 60 °C followed by rinsing with 1 mM NaOH and drying with N₂. We rinsed with 1 mM NaOH rather than pure water to avoid protonation of -COO groups.

3.2.7 Film Characterization. External reflection FTIR spectra were obtained with a Nicolet Magna-560 FTIR spectrometer using a Pike grazing angle attachment (80° angle of incidence). The spectrometer employs a MCT detector. Film thickness was measured with a rotating analyzer ellipsometer (J. A. Woollam model M-44), assuming a film refractive index of 1.5. Contact-angle measurements were performed with a FTÅ200 (First Ten Angstroms) contact angle analyzer. We used the following procedure in measuring the advancing contact angle of water. A 2 μ L drop of water was formed on the tip of a stainless steel syringe needle and placed on a film by raising the substrate until contact was made between the drop and sample. Subsequently water was added to the drop at a rate of 0.2 μ L/s for about 7 s to produce the advancing contact angle. Then

an image of the drop was taken and the left and the right contact angles were determined and averaged. The needle was in the drop when the contact angle was measured. All samples were dried in a flask under flowing N₂ for 2 h before contact angle measurement.

Cyclic voltammograms were obtained with a CH Instruments electrochemical analyzer (model 604). Measurements were made using a Ag/AgCl (3 M KCl) reference electrode and a platinum wire counter electrode. The working electrode was one of the Au-coated Si slides contained within a plastic/O-ring holder that exposed 0.1 cm² of the sample.

3.3 Results and Discussion

3.3.1 Film Formation, Cross-Linking, and Hydrolysis. Formation of PAH/d-PAA films occurs by alternating immersion of MPA-coated Au slides in solutions containing PAH or d-PAA as shown schematically in Figure 3.1. External reflectance FTIR spectra (Fig. 3.2) confirm the formation of PAH/d-PAA films and show significant differences among the different PAH/d-PAA coatings. Peaks due to the -COO asymmetric (1575 cm⁻¹) and symmetric (1400 cm⁻¹) stretches and the ester C=O (1735 cm⁻¹) and C-O (1170 and 1265 cm⁻¹) stretches appear in the spectra of all PAH/d-PAA films. (The ester carbonyl peaks probably also contain a small contribution from the carbonyl stretch of underivatized, un-ionized -COOH groups.) The ratio of absorbances of the ester carbonyl peaks to those of -COO peaks is not the same in each of the spectra, and this ratio is affected both by the extent of derivatization and by the nature of derivatized groups. Higher percentages of derivatization lead to higher ratios of ester carbonyl peak heights

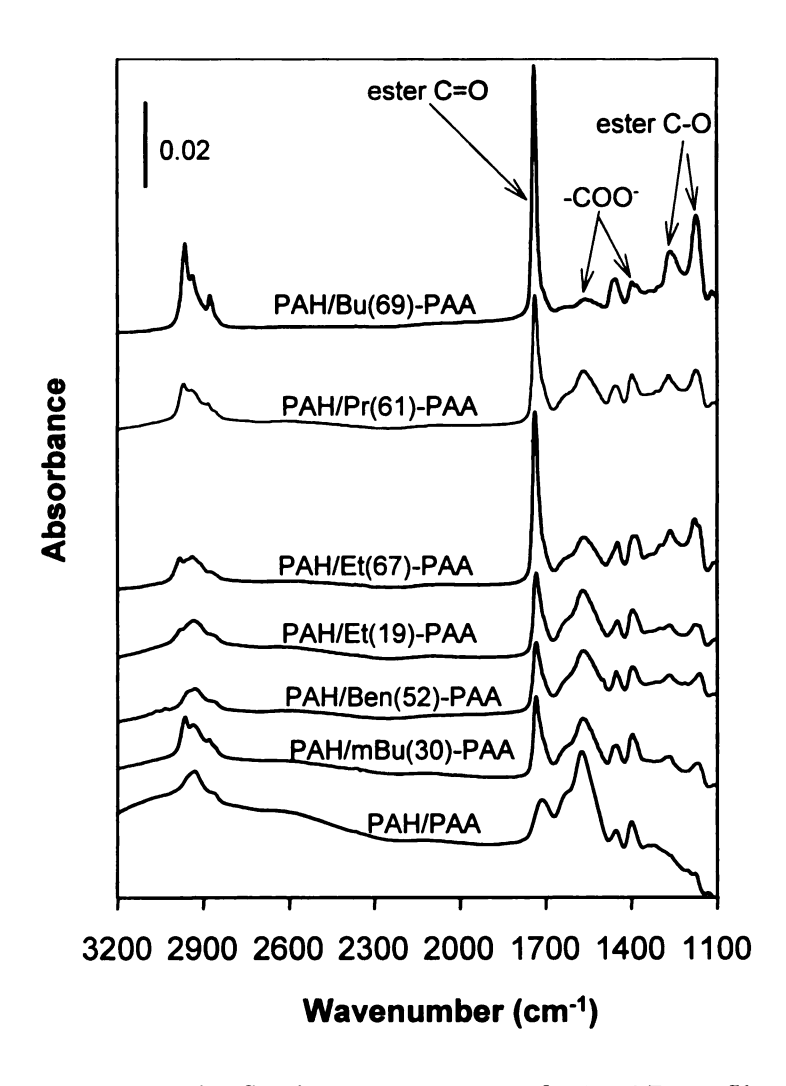


Figure 3.2: External reflection FTIR spectra of a PAH/PAA film and several different PAH/d-PAA films on Au. The fraction of -COOH groups in d-PAA that were esterified is given in parentheses. The films contained six bilayers.

to -COO peak heights as shown by the spectra of PAH/Et(67)-PAA and PAH/Et(19)-PAA in Figure 3.2. PAH/Bu-PAA films have unusually small -COO peaks. The high hydrophobicity of these films may result in higher pK_a values for -COOH groups and hence smaller -COO peaks. An additional reason for the low -COO peaks in spectra of PAH/Bu-PAA films may be the fact that due to the low solubility of Bu-PAA, PAH/Bu-PAA films were prepared under different conditions than most other films (see Experimental Section). However, preparation of PAH/Pr-PAA films under the conditions used for PAH/Bu-PAA films did not alter the IR spectrum of PAH/Pr-PAA.

Heating PAH/d-PAA films at 180 °C under N₂ cross-links coatings by converting carboxylate-ammonium salts into amides (Fig. 3.1, step 3). The reflectance FTIR spectra in Figure 3.3 give evidence for this transformation. Upon heating, peaks due to amide groups appear (1675 and 1530 cm⁻¹), and peaks due to -COO groups vanish. The spectra suggest nearly complete conversion of carboxylates to amides. After heating, the height of the peak due to the ester carbonyl stretch drops 15-25% for all PAH/d-PAA films except PAH/Bu-PAA, which shows no significant change. We speculate that drops in carbonyl absorbance result from partial conversion of ester groups to amides. The lack of conversion of esters to amides in PAH/Bu-PAA films may be due to higher thermal stability of the butyl ester (TGAs for Et-, Pr-, and Ben-PAA show a ~10% weight loss at 150-180 °C. Weight loss for Bu-PAA occurs at higher temperatures.).

Reflectance FTIR spectra also demonstrate the success of base-promoted hydrolysis of esters in cross-linked PAH/d-PAA films (Fig. 3.3). After exposure of films to 2 M NaOH in 90% MeOH for 4 h (60 °C),²⁶ ester carbonyl peaks decrease by at least 65%, and -

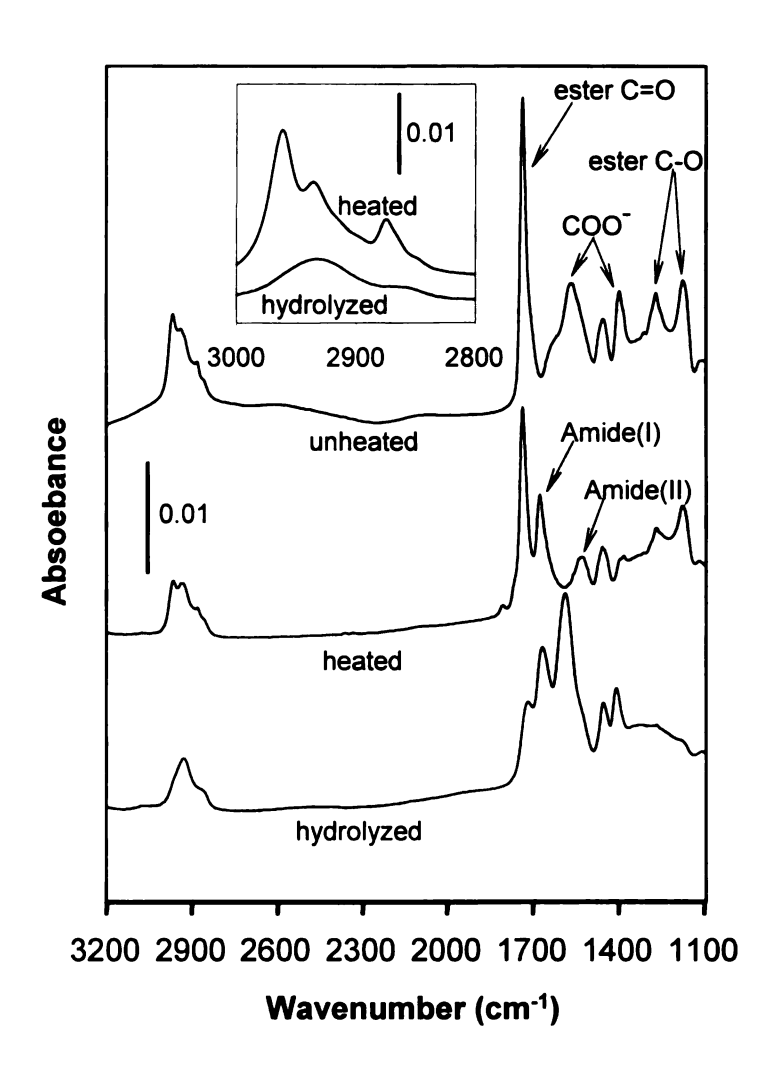


Figure 3.3: External reflection FTIR spectra of unheated, heated, and hydrolyzed PAH/Pr-PAA films (six bilayers) on Au. The inset shows the IR spectra (2800 cm⁻¹ to 3000 cm⁻¹) of heated and hydrolyzed PAH/Bu-PAA films.

ester groups that were hydrolyzed using the carbonyl region of the spectrum, because the ester-carbonyl peak and the acid-carbonyl peak overlap. However, the nearly complete disappearance of methyl (2965 and 2880 cm⁻¹) and C-O stretches (1170 and 1265 cm⁻¹) of ester groups (Fig. 3.3) suggests that hydrolysis is almost quantitative. The disappearance of stretches due to methyl groups is especially clear in the spectra of hydrolyzed PAH/Bu-PAA films (inset, Fig. 3.3). The presence of the strong amide peak at 1675 cm⁻¹ also shows that amide groups are stable under hydrolysis conditions.

The ellipsometric thicknesses of six-bilayer films range from 200 to 300 Å (Table 3.1). Film thickness results chiefly from the d-PAA deposition step, as the thickness increase after deposition of each PAH layer is only about 10 Å. Heating at 180 °C decreases film thickness by about 15%. This decrease may be due to loss of absorbed water²⁷ as well as dehydration of carboxylate-ammonium salts. Hydrolysis, on the other hand, does not decrease thickness, suggesting that cross-linked films do not collapse after ester cleavage. Hydrolyzed films may also absorb solvent.

3.3.2 Contact Angles. The presence of ester groups in PAH/d-PAA coatings dramatically alters film hydrophobicity. For unheated films, the advancing water contact angles (Table 3.1) increased from 42° for underivatized PAH/PAA to as high as 101° for PAH/Bu-PAA. Contact angles appear to increase with the amount of derivatization as well as the length of alkyl groups. After heating, however, contact angles on PAH/d-PAA films dropped in most cases, probably because polymers are less flexible after cross-linking and hydrophobic groups cannot collect at the air interface. Upon removal of hydrophobic groups through ester cleavage, PAH/d-PAA films become very

hydrophilic. This dramatic change provides further evidence for successful hydrolysis of cross-linked films.

Table 3.1: Thicknesses and advancing water contact angles for 6-bilayer PAH/d-PAA films.

| | thickness (Å) | | | contact angle (deg) ^c | | |
|--------------------|-------------------|------------------|---------------------|----------------------------------|------------------|----------------------------------|
| d-PAA ^a | before heating | after heating | after hydrolysis | before heating | after heating | after hydrolysis ^b |
| PAA | 247 ± 10 | 217 ± 8 | | 42 ± 2 | 68 ± 4 | |
| Et (19%) | 195 ± 9 | 171 ± 9 | 176 ± 6 | 80 ± 2 | 65 ± 5 | <10 |
| Et (67%) | 210 ± 8 | 178 ± 8 | 188 ± 6 | 85 ± 4 | 70 ± 2 | <10 |
| Pr (61%) | 230 ± 12 | 194 ± 11 | 204 ± 7 | 89 ± 2 | 72 ± 3 | <10 |
| Bu (69%) | 295 ± 13 | 269 ± 10 | 281 ± 11 | 101 ± 4 | 91 ± 2 | <10 |
| Ben (52%) | 255 ± 12 | 229 ± 11 | 225 ± 6 | 81 ± 2 | 96 ± 3 | <10 |
| mBu (30%) | 263 ± 10 | 227 ± 7 | 239 ± 12 | 88 ± 4 | 82 ± 3 | <10 |

^a The number in parentheses represents the fraction of -COOH groups that were derivatized as determined by NMR.

^b Water is rapidly adsorbed by hydrolyzed films.

^c Contact angles of PAH/Et(19%)-PAA and PAH/mBu(30%)-PAA are the average of values at four different spots on one film. The other values are the average of eight different spots on two films.

3.3.3 Electrochemical Studies. The presence of ester groups in PAH/d-PAA films greatly decreases their permeability to electrochemically active probe molecules. Peak currents in cyclic voltammograms (CVs) of Ru(NH₃)₆³⁺ at all PAH/d-PAA-coated electrodes are significantly lower than those at PAH/PAA-coated electrodes (Fig. 3.4, top). For films containing 1-propyl, 1-butyl, 2-methy-1-butyl, and benzyl esters, peak currents decreased by about 2 orders of magnitude compared to underivatized PAA/PAH films. (Peak currents at PAH/d-PAA electrodes were calculated after subtracting currents measured at the same electrode in the absence of the redox couple (see inset of Fig. 3.4)). Similar trends occur in CVs of Fe(CN)₆³ (Fig. 3.4, bottom), showing that hydrophobic films are passivating to both cations and anions. The ethyl-derivatized films do not passivate electrodes as well as other PAH/d-PAA films, probably due to the smaller size and lower hydrophobicity of ethyl groups. However, from the CVs at PAH/Et(19)-PAAand PAH/Et(67)-PAA-coated electrodes (Fig. 3.4, top), one finds that a higher percentage of derivatization does result in more electrode passivation. Cross-linking of films does not dramatically affect peak currents in most cyclic voltammograms (it significantly increases passivation due to PAH/PAA and PAH/Et-PAA films because these coatings were initially highly permeable), but it does stabilize films and allow us to perform basepromoted hydrolysis of ester groups.

Hydrolysis results in greatly increased cathodic currents in CVs of Ru(NH₃)₆³⁺ (Fig. 3.5), showing that the previously passivating PAH/d-PAA films become permeable to Ru(NH₃)₆³⁺. Several pieces of evidence suggest that in the case of propyl-derivatized PAA (and to some extent other cases also) much of the cathodic current is due to adsorbed Ru(NH₃)₆³⁺. First, the cathodic peak is shifted to more negative potentials.

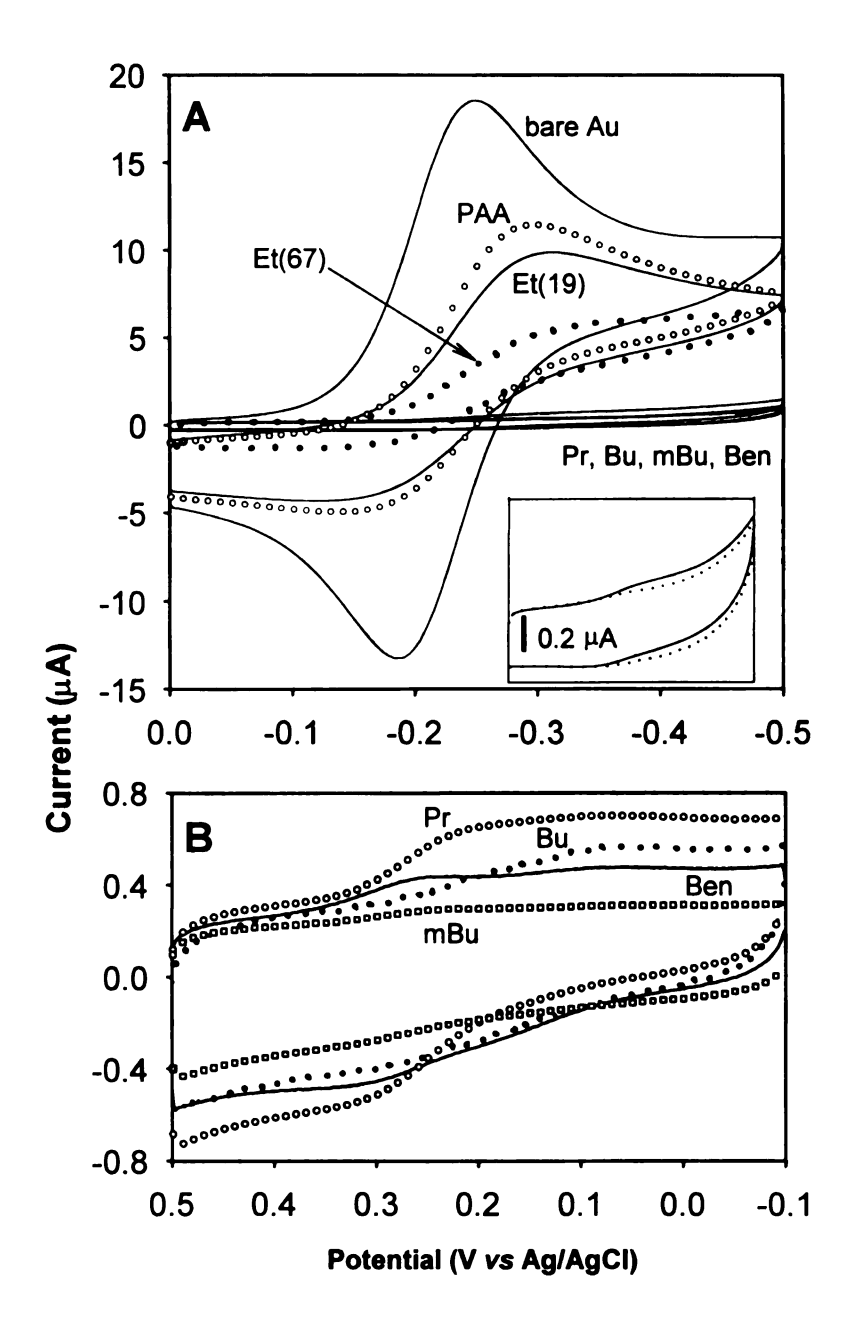


Figure 3.4: Cyclic voltammograms of 1 mM Ru(NH₃)₆Cl₃ (top) and 1 mM $K_3Fe(CN)_6$ (bottom) in 0.5 M Na₂SO₄ at Au electrodes coated with different PAH/d-PAA films (six bilayers). The inset shows enlarged CVs obtained in the presence (solid line) and absence (dotted line) of Ru(NH₃)₆³⁺ at a Au electrode coated with a six bilayer PAH/Bu-PAA film. The scan rate in all CVs was 0.1 V/s, and electrode areas were 0.1 cm².

This likely occurs because the presence of negatively charged -COO groups stabilizes the oxidized form of the couple.²⁸ When 0.1 M tetraethylammonium chloride (NEt₄Cl) was used as supporting electrolyte rather than 0.5 M Na₂SO₄, the cathodic peak shifted another 200 mV negative and the cathodic peak current increased by ca. 40%. This occurs because *NEt₄ cations are large enough that they do not compete with Ru(NH₃)₆³⁺ for adsorption sites. Second, the anodic peak is very small in several cases. The absence of the anodic peak suggests that Ru(NH₃)₆²⁺ produced during the cathodic scan is displaced from the film by the more highly charged Ru(NH₃)₆³⁺. Third, the cathodic peak currents at electrodes coated with hydrolyzed ethyl-, propyl-, and butyl-derivatized films were higher than that at bare gold because of a high concentration of Ru(NH₃)₆³⁺ in the films. Thus the CVs suggest that there is a high density of -COO groups in hydrolyzed films and that these groups are capable of binding ions. Cathodic peak currents at PAH/Et(67)-PAA-coated electrodes are 2-5 times larger than those at PAH/Et(19)-PAAcoated electrodes. This suggests that the amount of adsorption can be varied by controlling the extent of derivatization prior to hydrolysis. These hydrolyzed PAH/d-PAA films behave somewhat like Nafion or Nafion-impregnated membranes where cations residing in the solution phase exchange with cations electrostatically bound to -SO₃ sites in the membrane.^{29,30}

Peak currents in CVs of Fe(CN)₆³⁻ at electrodes coated with hydrolyzed PAH/d-PAA films are about 10-fold lower than those for Ru(NH₃)₆³⁺ at corresponding electrodes (Fig.3.5, inset). The high density of negatively charged -COO⁻ groups likely hinders access of Fe(CN)₆³⁻ to the electrode surface. The negative charges also prevent the adsorption of Fe(CN)₆³⁻.

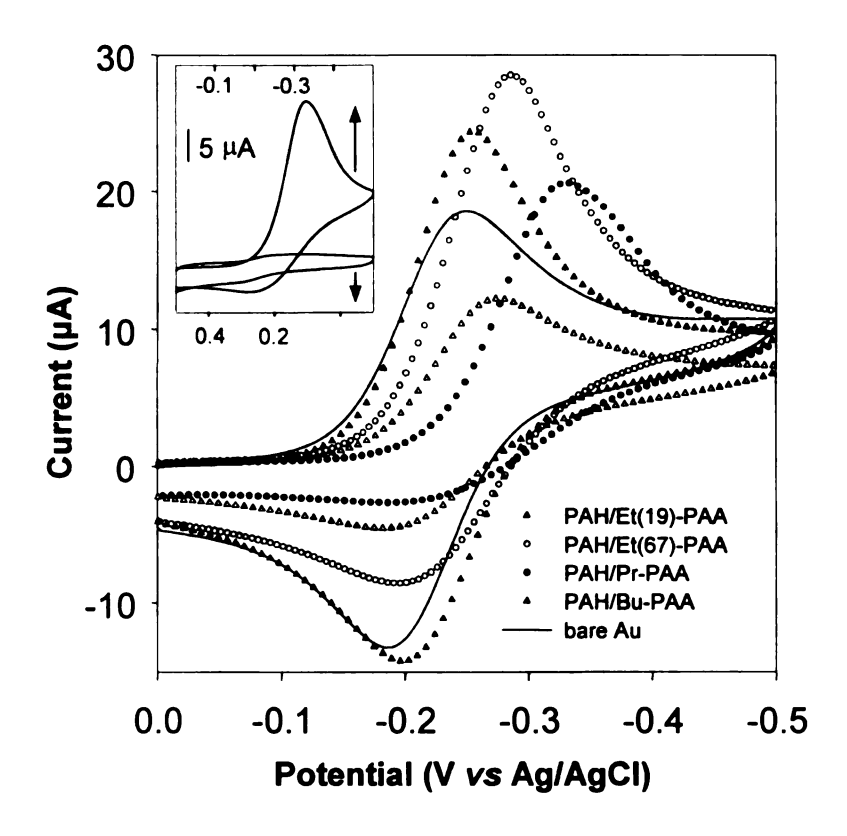


Figure 3.5: Cyclic voltammograms of 1 mM Ru(NH₃)₆Cl₃ in 0.5 M Na₂SO₄ at Au electrodes coated with cross-linked, hydrolyzed PAH/d-PAA films (six bilayers). The inset compares CVs of 1 mM Ru(NH)₆Cl₃ and 1 mM K₃Fe(CN)₆ at a Au electrode coated with cross-linked, hydrolyzed PAH/Pr-PAA. The scan rate in all CVs was 0.1 V/s, and electrode areas were 0.1 cm².

3.3.4 Ion Detection Using Hydrolyzed Films. CVs of Ru(NH₃)₆³⁺ at electrodes coated with hydrolyzed PAH/d-PAA films are affected by low concentrations of other divalent and trivalent metal cations in solution. These effects might allow PAH/d-PAA electrodes to function as sensors for these ions. Figure 3.6 shows CVs of Ru(NH₃)₆³⁺ that were obtained at an electrode coated with PAH/Pr-PAA that was cross-linked and subsequently hydrolyzed. The cathodic peak current and position are affected by concentrations of Ca²⁺ as low as 10⁻⁵ M, even though the measurement is being made in the presence of 0.1 M NaCl. With further addition of Ca²⁺, the peak current continues to drop and peak positions become even more positive. This likely occurs because Ca²⁺ displaces some of the adsorbed Ru(NH₃)₆³⁺ and blocks access to the underlying gold surface. Peak positions shift to more positive potentials as the presence of Ca²⁺ makes the environment around Ru(NH₃)₆³⁺ less negatively charged. After the film is rinsed with 1 mM HCl for 5 min (to remove Ca²⁺ from the film) and then with 1 mM NaOH for 5 min (to deprotonate -COOH groups), the reduction current of Ru(NH₃)₆³⁺ in the absence of Ca²⁺ returns to within 5% of its original value. The electrode responds to Mg²⁺ in a similar way, and selectivities need to be further investigated. We also added AlCl₃ to a 1 mM Ru(NH₃)₆³⁺, 0.1 M NaCl solution and obtained similar results. However, the film does not show a higher sensitivity to Al³⁺ than to Ca²⁺. One might expect the trivalent cation to bind more strongly to -COO groups, but at pH 6, most aluminum ions exist as $Al(OH)^{2+.31}$

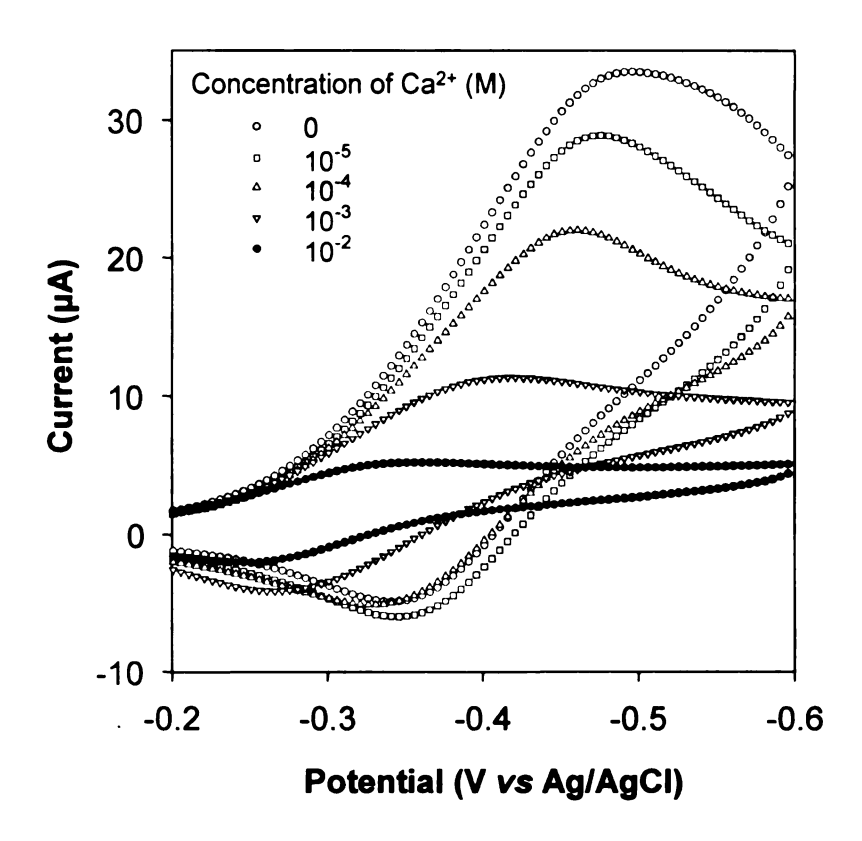


Figure 3.6: Cyclic voltammograms of 1 mM Ru(NH₃)₆Cl₃ in 0.1 M NaCl containing different concentration of Ca²⁺ at a Au electrode coated with six bilayers of cross-linked, hydrolyzed PAH/Pr-PAA. The scan rate was 0.1 V/s, and the electrode area was 0.1 cm².

3.4 Conclusions

Variation of the ester functionalities in PAH/d-PAA films along with subsequent cross-linking and hydrolysis afford control over coating hydrophobicity and charge density. Control of these properties will be important in future applications of layered polyelectrolytes such as ion-separation membranes, sensors, and protective coatings. Esterification with hydrophobic groups can result in advancing water contact angles at least as high as 101°. Cross-linking through amidation strengthens PAH/d-PAA films and allows subsequent modifications. Hydrolysis of ester groups in cross-linked films yields a high density of -COO groups that renders these coatings more permeable to positively charged Ru(NH₃)₆³⁺ than to Fe(CN)₆³⁻. Binding of Ca²⁺ to hydrolyzed PAH/Pr-PAA occurs at concentrations as low as 10⁻⁵ M and results in decreases in peak currents in CVs of Ru(NH₃)₆³⁺. Such effects may prove useful in ion-sensing applications. Taken together, the results in this chapter show the potential of PAH/d-PAA deposition for producing coatings with properties tailored for specific applications.

3.5 References

- 1 Caruso, F.; Rodda, E.; Furlong, D. N.; Niikura, K.; Okahata, Y. *Anal. Chem.* **1997**, *69*, 2043-2049.
- 2 Caruso, F.; Niikura, K.; Furlong, D. N.; Okahata, Y. Langmuir 1997, 13, 3427-3433.
- 3 Shipway, A. N.; Lahav, M.; Blonder, R.; Willner, I. Chem. Mater. 1999, 11, 13-15.
- 4 Krasemann, L.; Tieke, B. Langmuir 2000, 16, 287-290.
- 5 Harris, J. J.; Stair, J. L.; Bruening, M. L. Chem. Mater. 2000, 12, 1941-1946.
- 6 Ackern, F. v.; Krasemann, L.; Tieke, B. *Thin Solid Films* **1998**, *327-329*, 762-766.
- 7 Stroeve, P.; Vasquez, V.; Coelho, M. A. N.; Rabolt, J. F. *Thin Solid Films* **1996**, 708-712.
- 8 Kotov, N. A.; Magonov, S.; Tropsha, E. Chem. Mater. 1998, 10, 886-895.
- 9 Leväsalmi, J.-M.; McCarthy, T. J. Macromolecules 1997, 30, 1752-1757.
- 10 Lukas, J.; Richau, K.; Schwarz, H.-H.; Paul, D. J. Membr. Sci. 1997, 131, 39-47.
- 11 Stair, J. L.; Harris, J. J.; Bruening, M. L. Chem. Mater. 2001, 13, 2641-2648.
- 12 Graul, T. W.; Schlenoff, J. B. Anal. Chem. 1999, 71, 4007-4013.
- 13 Liu, Y. Q.; Ma, H.; Jen, A. K. Y. Chem. Commun. 1998, 2747-2748.
- 14 Wu, A.; Yoo, D.; Lee, J.-K.; Rubner, M. F. J. Am. Chem. Soc. 1999, 121, 4883-4891.
- Dai, J.; Sullivan, D. M.; Bruening, M. L. *Ind. Eng. Chem. Res.* **2000**, *39*, 3528-3535.
- 16 Cochin, D.; Laschewsky, A. *Macromol. Chem. Phys.* **1999**, 200, 609-615.
- 17 Chen, J.; Huang, L.; Ying, L.; Luo, G.; Zhao, X.; Cao, W. *Langmuir* **1999**, *15*, 7208-7212.

- Harris, J. J.; DeRose, P. M.; Bruening, M. L. J. Am. Chem. Soc. 1999, 121, 1978-1979.
- 19 Dubas, S. T.; Schlenoff, J. B. *Macromolecules* **1999**, *32*, 8153-8160.
- 20 Schlenoff, J. B.; Ly, H.; Li, M. J. Am. Chem. Soc. 1998, 120, 7626-7634.
- 21 Lowack, K.; Helm, C. A. *Macromolecules* **1998**, *31*, 823-833.
- 22 Lvov, Y. M.; Lu, Z.; Schenkman, J. B.; Zu, X.; Rusling, J. F. J. Am. Chem. Soc. 1998, 120, 4073-4080.
- 23 Lvov, Y.; Decher, G.; Möhwald, H. Langmuir 1993, 9, 481-486.
- 24 Laurent, D.; Schlenoff, J. B. *Langmuir* **1997**, *13*, 1552-1557.
- Cochin, D.; Passmann, M.; Wilbert, G.; Zentel, R.; Wischerhoff, E.; Laschewsky, A. *Macromolecules* **1997**, *30*, 4775-4779.
- 26 Bryand, W. M. D.; Smith, D. M. J. Am. Chem. Soc. 1936, 58, 1014-1017.
- 27 Lösche, M.; Schmitt, J.; Decher, G.; Bouwman, W. G.; Kjaer, K. *Macromolecules* 1998, 31, 8893-8906.
- Dermody, D. L.; Peez, R. F.; Bergbreiter, D. E.; Crooks, R. M. *Langmuir* **1999**, *15*, 885-890.
- 29 Liu, C.; Martin, C. R. J. Electrochem. Soc. 1990, 137, 510-515.
- Yeager, H. L. In *Perfluorinated Ionomer Membranes*; Yeager, H. L., Eisenberg, A., Eds.; ACS Symposium Series No. 180; American Chemical Society: Washington, DC, 1982, pp 41-63.
- Porterfield, W. W. *Inorganic Chemistry, a United Approach*; Addison-Wesley: Reading, MA, **1984**, page 229.

Chapter 4

Controlling Ion Transport through Multilayer Polyelectrolyte Membranes by Derivatization with Photolabile Functional Groups

4.1 Introduction

Membrane-based separations are attractive because of their operational simplicity and low energy costs, but limitations in membrane flux and/or selectivity restrict many applications of this technology.¹ The most common method for increasing flux is to decrease membrane thickness, and thus commercial membranes are generally prepared with a thin selective skin on a porous support that provides mechanical strength.^{2,3} Methods for forming thin membrane skins include phase inversion,^{4,5} interfacial polymerization,⁶ plasma grafting,^{7,8} casting,⁹ and even deposition of films from the air/water interface.¹⁰ In spite of the success of these methods, synthesizing ultrathin, selective membranes is an ongoing challenge.

Multilayer polyelectrolyte films (MPFs) are potentially attractive materials for synthetic membrane skins because of their convenient synthesis and versatility. Synthesis of these films, first demonstrated by Decher and coworkers, 11,12 simply involves sequential adsorption of polycations and polyanions on an initially charged surface (see chapter 1 of this thesis). The layer-by-layer deposition procedure affords control over film thickness on the nanometer scale, and the minimal total thickness of these films should allow high flux through polyelectrolyte multilayers deposited on highly permeable supports. Moreover, selectivity of polyelectrolyte membranes may be tailored through selection of constituent polyelectrolytes as well as post-deposition cross-linking of films. Separation applications of polyelectrolyte membranes recently

explored by several research groups include gas separations, ¹⁴⁻¹⁷ selective pervaporation from water/organic solvent mixtures, ^{18,19} and ion separations. ^{13,20,21}

This thesis focuses on understanding and controlling ion flux through multilayer polyelectrolyte membranes (MPMs) via control of the composition of these films. In previous studies of ion transport through MPMs, ^{13,20,21} fluxes of monovalent ions were higher than those of divalent ions. Krasemann and Tieke suggested that Donnan exclusion resulting from fixed charge in the membrane is responsible for this selectivity. ²⁰ If Donnan exclusion is the dominant factor in effecting ion-transport selectivity in MPMs, then introduction of more net fixed charge into these membranes should lead to higher monovalent/divalent ion-transport selectivities. The purpose of this work is to explore the relationship between ion-transport selectivity and net fixed-charge density in MPMs. In a similar work from our group, Balanchandra showed that templating with Cu²⁺ also provides a convenient method for introducing net fixed charge and can yield Cl²/SO₄²⁻ selectivities as high as 600. ²²

Although MPFs form due to electrostatic interactions, in the bulk of the film, charges on polyanions are electrically compensated by charges on polyanions and vise versa. ^{23,24} Schlenoff demonstrated that introduction of net fixed charge into MPFs requires post-deposition modification, ²³ and several studies showed that MPFs can be modified after deposition to alter properties such as conductivity ^{25,26} or stability. ^{27,28} We chose to use partially derivatized poly(acrylic acid) (PAA) and poly(allylamine hydrochloride) (PAH) chains as model constituents for controlling charge in MPFs. To introduce net charge into films, we partially derivatized PAA and PAH with photolabile 2-nitrobenzyl (NB) and 2-nitrobenzyloxycarbonyl (NBOC) groups (scheme 4.1). The underivatized –COO

groups in PAA and -NH₃⁺ groups in PAH still allow for film formation through electrostatic adsorption, while UV irradiation of derivatized PAA/PAH films cleaves ester or carbamate bonds and liberates free acid or amine groups. These groups can then protonate/deprotonate to yield net negative (or positive) fixed charges in membranes (Fig. 4.1). The newly formed charges are not electrically compensated by adjacent polyions but by oppositely charged ions from solution.²³ With the introduction of net charge into the membrane, Donnan exclusion should be more pronounced, and monovalent/divalent ion transport selectivity should increase.

$$\begin{array}{c} NO_2 \\ O \\ CH_2 O - C - CI \end{array}$$

$$\begin{array}{c} CH_2 \\ NH \\ NH_2 \\ \end{array}$$

$$\begin{array}{c} CH_2 \\ CH_2 \\ NH_2 + CI \end{array}$$

$$\begin{array}{c} CHO \\ NO_2 \\ CH_2 \\ NH_2 \end{array}$$

$$\begin{array}{c} CHO \\ CHO$$

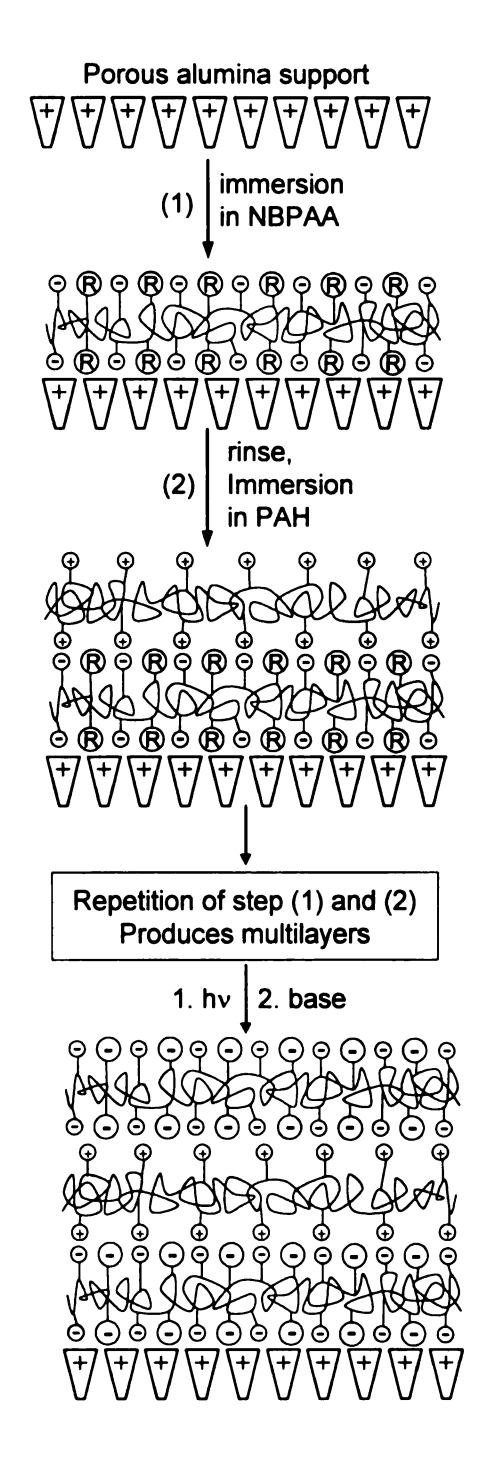


Figure 4.1: Schematic drawing of the formation of a multilayer polyelectrolyte membrane and subsequent introduction of net, fixed charge via photolysis. R represents the 2-nitrobenzyl (NB) photolabile functional group. Interweaving of layers is not shown for figure clarity.

In principle, the simplest way to control net fixed charge in PAA/PAH membranes is to vary the pH of deposition solutions. Rubner showed that deposition of PAA/PAH films at low pH and subsequent immersion in higher pH solutions create ion-exchange sites in the film.²⁹ However, when we attempted depositing PAA/PAH membranes at pH 2.5 and running transport experiments at pH 5-6, we did not observe any increase in selectivity relative to PAA/PAH membranes prepared at pH 5.0. The use of deposition pH to control fixed charge could result in morphological changes in film structure that may decrease selectivity.^{30,31}

In contrast, introduction of fixed charge using photocleavable groups increases the selectivity of PAA/PAH films by an order of magnitude. The use of derivatization with photocleavable groups also allows knowledge of and control over the net, fixed charge in the membrane. Thus, by changing the extent of derivatization, one can control charge density, and hence, tailor ion-transport selectivity. With an estimate of charge density obtained from the extent of derivatization, we utilized a simple model to simulate ion transport through these membranes. The model suggests that both Donnan exclusion and selective diffusion play important roles in effecting selective transport.

4.2 Experimental Section

4.2.1 Materials. PAA ($M_v = 450,000$), PAH ($M_w = 70,000$), 2-nitrobenzyl bromide (99%), 2-nitrobenzyl alcohol (99%), phosgene solution (~20% in toluene), 1,8-diazabicyclo[5.4.0]undec-7-ene (DBU, 98%), and dimethyl sulfoxide (DMSO, reagent) were purchased from Aldrich and used as received. Nitrobenzylchloroformate was synthesized according to a literature procedure.³² Deionized water (18 M Ω -cm, Milli-Q)

was used in preparation of aqueous solutions. Membrane supports (Whatman AnodiscTM membrane filters with a nominal surface pore diameter of $0.02~\mu m$) were purchased from Thomas Scientific.

4.2.2 Synthesis of 2-nitrobenzyl-derivatized PAA (NBPAA). PAA (720 mg, 10 mmol with respect to the repeating unit) was dissolved in 20 mL of DMSO (sonicate for 1h, stir for 2 h at 45 °C to get complete dissolution), and DBU (1.52 g, 10 mmol, in 5 mL DMSO) was added dropwise to this solution while stirring. 1.51 g (7 mmol) 2-nitrobenzyl bromide was then added. The mixture was stirred at 45 °C for 3 h after which 1 mL of acetic acid was added to neutralize DBU, and the solution was stirred for an additional 15 min. Derivatized polymer was then precipitated upon dropwise addition of the mixture into 1500 mL of pH 3 water. The precipitate was collected by filtration, washed thoroughly in water while stirring, and again collected by filtration. The polymer was dried under vacuum at 60 °C for 48 h, and 1.1 g of polymer was obtained (78% yield). H¹ NMR (d-DMSO as solvent) showed that ~50% of the -COOH groups in PAA were derivatized by NB groups (Fig. 4.2). The 23% and 65% NB-derivatized PAA were synthesized in a similar way (56% and 84% yield), except that the quantity of 2nitrobenzyl bromide added was 0.86 g (4 mmol) and 1.73 g (8 mmol) for 23% and 65% derivatization, respectively. 23% NBPAA was precipitated into and washed with ethyl acetate-saturated pH 3 water.

4.2.3 Synthesis of 2-nitrobenzyloxycarbonyl-derivatized PAH (NBPAH). PAH (1.55 g, 17 mmol with respect to the repeating unit) was dissolved in 100 mL of water, and the solution was placed in an ice-bath. After adjusting the pH of the solution to 3.0 with HCl, 1.84 g (8.5 mmol) of 2-nitrobenzylchloroformate in 5 mL dry THF was added

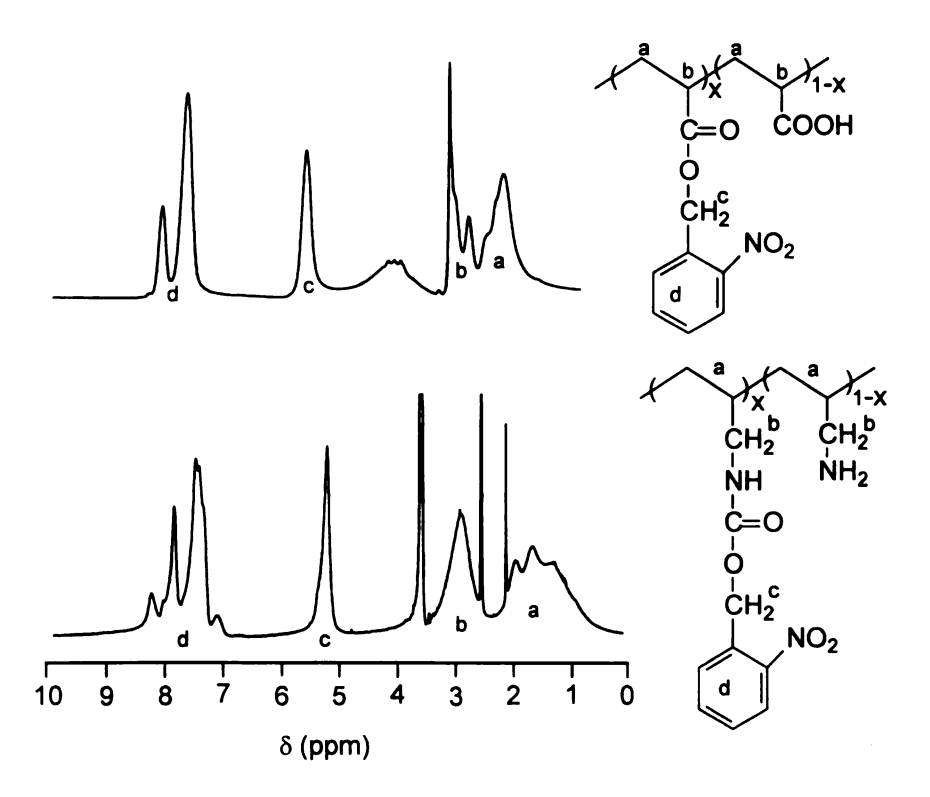


Figure 4.2: ¹H NMR spectra of PAA (top, *d*-DMSO) and PAH (bottom, *d*-DMSO+trace of D₂O) that were 50% derivatized with 2-nitrobenzyl and 2-nitrobenzyloxycarbonyl groups, respectively. The percentage derivatization was calculated from the ratio of the integrated signals due to the benzylic protons and the methylene protons on the polymer backbone. The chemical structures on the right indicate the proton assignments.

dropwise to the solution over a 2 h period while maintaining the solution pH between 3 and 4 through addition of 1 M NaOH. The reaction was then allowed to proceed at room temperature for another 2 h at pH 4. The suspension was collected by centrifugation. The polymer was redissolved in DMSO, precipitated upon addition to a 20% ethyl acetate/80% 2-propanol (v/v) mixture, and dried under vacuum at 50 °C for 72 h to yield 1.77 g of product (71% yield). ¹H NMR showed that ~50% of the amine groups in PAH were derivatized (Fig. 4.2).

4.2.4 Film synthesis and characterization. Before synthesizing MPMs on porous alumina supports, we prepared films on Al-coated wafers (200 nm of Al sputtered on Si(100)) to determine the optimum conditions for deposition. The Al wafer was UV/ozone cleaned for 15 min before immersion in a solution containing a polyanion (PAA or NBPAA). After a 10 min immersion, the wafer was rinsed with water for 1 min, immersed in a solution containing a polycation (PAH or NBPAH) for 10 min, and rinsed with water for 1 min to form the first bilayer. This procedure was repeated until the desired number of bilayers was deposited. (Drying with N₂ occurred only after deposition of the entire film.) The solutions used to form films were: PAA (0.01 M, pH 5.0), PAH (0.02 M, pH 5.0), NBPAA (200 mg in 20 mL DMSO + 80 mL MeOH + 80 mg KOH), NBPAH (0.1 mM, pH 5.0). Concentrations of polymers are given with respect to the repeating unit, and pH values were adjusted with 0.1 M HCl or 0.1 M NaOH. Film thickness was measured with a rotating analyzer ellipsometer (J. A. Woollam model M-44), assuming a film refractive index of 1.5. Reflectance FTIR spectra were obtained with a Nicolet Magna-560 FTIR spectrometer using a Pike grazing angle attachment (80°

angle of incidence). The spectrometer employs a MCT detector. Films were also deposited on porous alumina using the above procedure.

4.2.5 Photolysis. Polyelectrolyte films and membranes were irradiated in air with a medium-pressure mercury arc lamp (Hanovia, 450 W) without a filter at a distance of 30 cm from the source. The irradiation time was 60 min for all samples. Samples were dried with N₂ purging for 2 h before photolysis.

4.2.6 Transport studies. The diffusion dialysis apparatus consists of two cells separated by the membrane, which is contained in the middle of a 2.5 cm-long neck. The source cell was filled with 90 mL of a 0.1 M solution of the desired salt (NaCl, Na₂SO₄, or MgCl₂), while the receiving cell initially contained 90 mL of deionized water. The measured pH values of the unbuffered 0.1 M salt solutions were 5.3 (NaCl), 5.6 (Na₂SO₄), and 5.0 (MgCl₂). The area of the membrane exposed to the solution was 2 cm². The concentration of salt in the receiving cell was monitored at 5 min intervals for 45 min using a conductivity meter (Orion model 115). Solutions in both cells were vigorously stirred to minimize concentration polarization at the membrane surface. Membranes were soaked in water for at least 12 h before use, and three different membranes were prepared and tested for each type of film.

The conductivity in the receiving cell was transformed to concentration using a calibration curve. The flux (J) and selectivity (α) of ion transport were then calculated according to equations 1 and 2

$$J = \frac{\Delta C}{\Delta t} \cdot \frac{V}{A} \tag{1}$$

$$\alpha_{1/2} = \frac{J_1}{J_2} \tag{2}$$

where $\frac{\Delta C}{\Delta t}$ is the concentration change with time calculated from the slope of a plot of concentration versus time, V is the volume of solution in the receiving cell, A is the exposed area of the membrane, and the subscripts I and I represent two different ions.

4.3 Results and Discussion

4.3.1 Derivatization of PAA and PAH. The 2-nitrobenzyl group and its analogues have been intensively employed as photoremovable protecting groups in a variety of synthetic strategies. 33,34 These photolabile groups were also, though less frequently, used to modify polymers.³⁵⁻³⁷ Derivatization of PAA with 2-nitrobenzyl bromide occurs under mild conditions using a method developed by Nishikubo and coworkers for modification of poly(methacrylic acid).³⁶ Derivatization of PAH, however, is more challenging because both PAH and deprotonated poly(allyl amine) are not very soluble in most organic solvents. To overcome this problem, we reacted PAH with 2nitrobenzylchloroformate in aqueous solution while controlling pH. This procedure is similar to the common practice in peptide synthesis of protecting amines with NBOC groups using an aqueous reaction. 33,38 Amines react with 2-nitrobenzylchloroformate at a much faster rate than does water, and thus hydrolysis of 2-nitrobenzylchloroformate is not a problem. In fact at high pH, this reaction occurs so rapidly that polymer immediately begins to precipitate upon addition of nitrobenzylchloroformate. To slow down the reaction and achieve uniform derivatization without precipitation, we ran the reaction at a pH of about 4 so most of the amine groups would be protonated.³⁹ 4.3.2 Film formation and photochemistry. We prepared polyelectrolyte solutions in water in all cases where the polyelectrolyte was sufficiently soluble. Using a deposition

pH of 5, we were able to obtain homogeneous films with reasonable thicknesses (Table 4.1 on page 80). NBPAH was only slightly soluble in water, but concentrations of 10⁻⁴ M were sufficient for film formation. Derivatized PAA, however, did not dissolve in water, so we employed a DMSO/methanol cosolvent for these polymers and added a stoichiometric amount of KOH to deprotonate –COOH groups. To assess whether changing deposition solvent affects film properties, we also prepared underivatized PAA/PAH films using PAA dissolved in DMSO/methanol containing KOH. These films have basically the same IR spectra and ion-transport selectivities as films prepared only in water, but their thickness is ~30% less than for the entirely water-based deposition. These experiments indicate that the enhanced selectivity (*vide infra*) of NBPAA/PAH membranes is not due to deposition from an organic solvent.

Figure 4.3 shows the reflectance FTIR spectra of a 10.5-bilayer 50%NBPAA/PAH film before and after UV irradiation. (The addition of an extra half bilayer results in NBPAA being the top layer in these films.) The strong absorbance at 1740 cm⁻¹ is primarily due to the ester carbonyl groups of derivatized PAA, but underivatized, protonated –COOH groups likely also contribute to this peak. After 60 min of UV irradiation, peaks due to –NO₂ groups (1530 cm⁻¹ and 1345 cm⁻¹) completely disappeared, showing that photolysis was complete. The peak at 1720 cm⁻¹ after irradiation is due largely to –COOH groups produced by photolysis (Scheme 1) and thus decreases significantly (~60%) after deprotonation in pH 9.2 buffer. We also see an increased –COO⁻ absorbance at 1575 cm⁻¹ after deprotonation. Similar results were obtained for PAA/50%NBPAH films (Fig.4.4). The carbamate carbonyl absorbance at 1716 cm⁻¹ and peaks due to –NO₂ groups vanished after 60 min of UV irradiation,

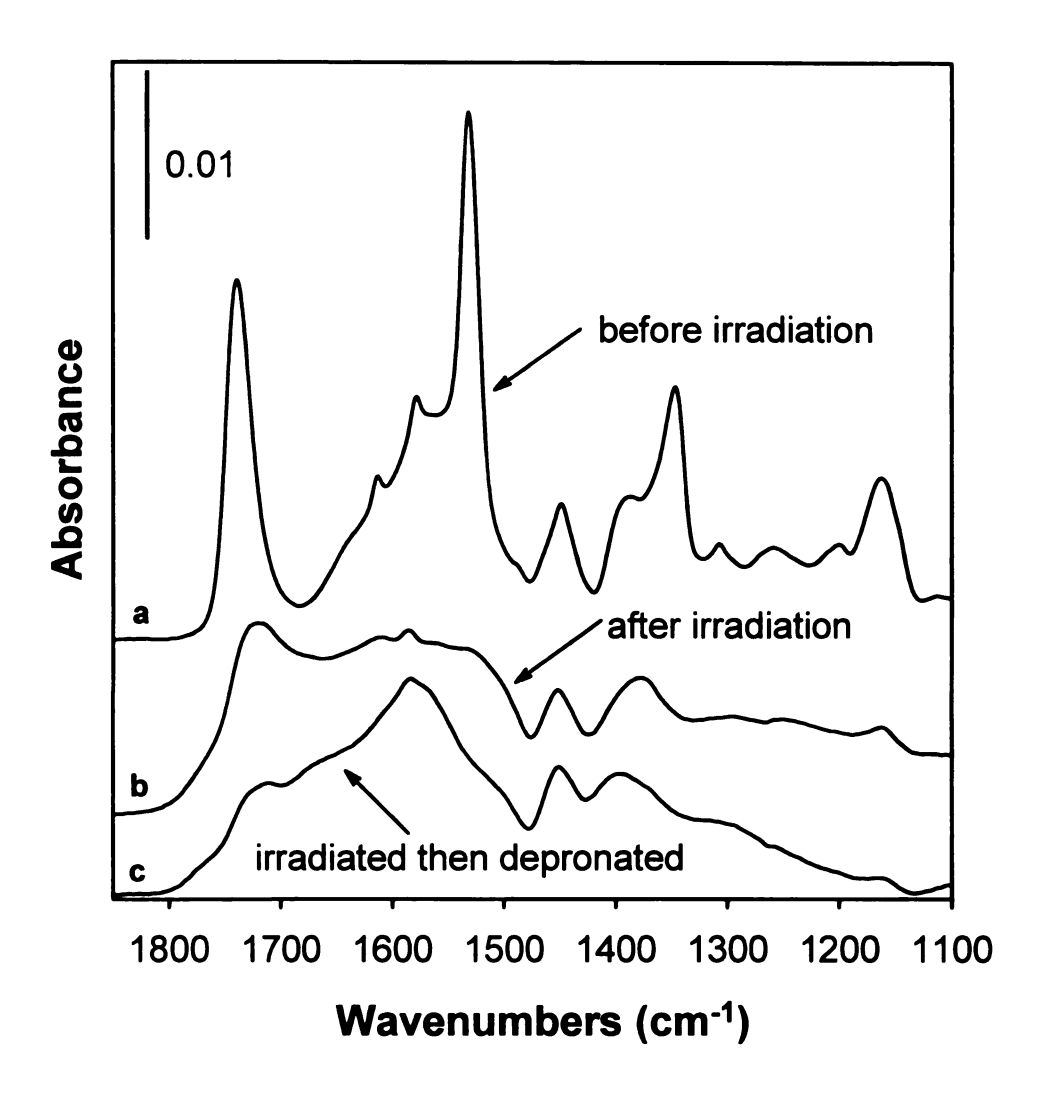


Figure 4.3: Reflection FTIR spectra of a 10.5-bilayer 50%NBPAA/PAH film on an Al-coated wafer before (a) and after (b) UV irradiation.

Spectrum (c) is that of the irradiated film after a 30 min immersion in pH 9.2 buffer solution and rinsing with ethanol.

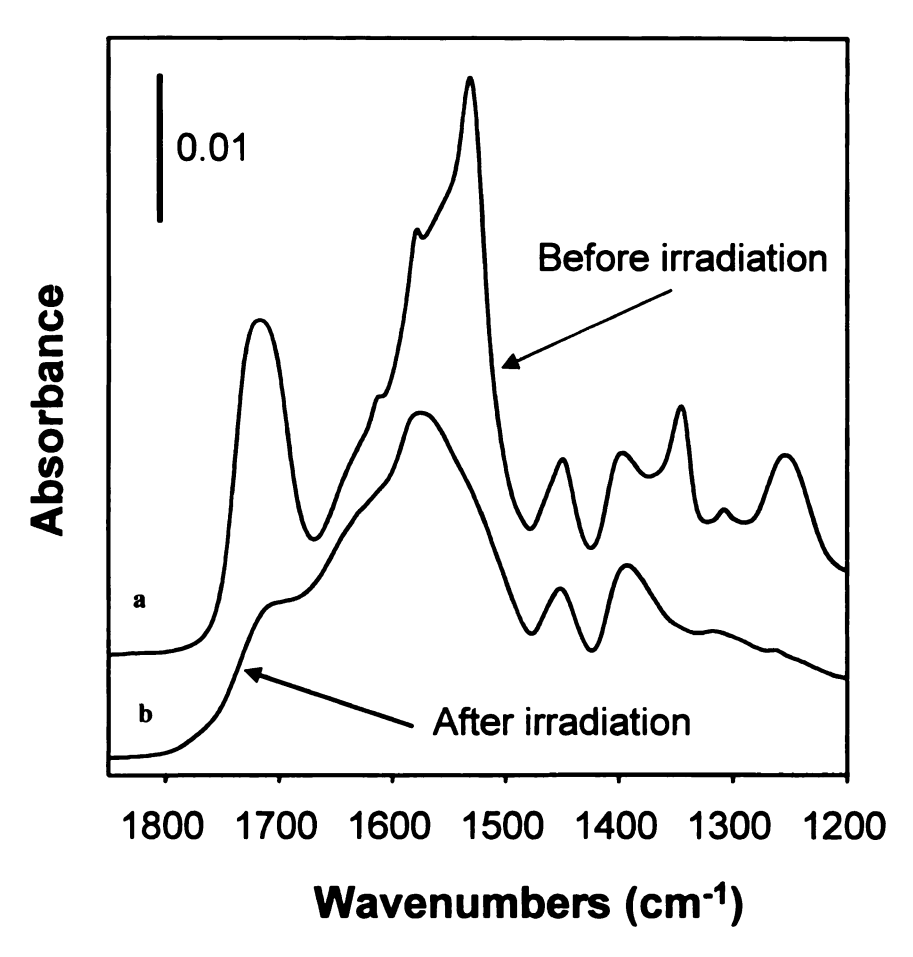


Figure 4.4: Reflection FTIR spectra of a 10.5-bilayer PAA/50%NBPAH film on an Al-coated wafer before (a) and after (b) UV irradiation.

indicating complete photolysis. The mechanism of photocleavage of NB or NBOC groups proceeds via an intramolecular pathway, ^{37,38,44,45} and thus it is efficient in solid films as well as in solution.

4.3.3 Ion-transport studies. Table 4.1 summarizes fluxes and selectivities for several salts in diffusion dialysis experiments with PAA/PAH and derivatized PAA/PAH membranes. The table shows three interesting trends for 10.5-bilayer membranes: (1) photolyzed NBPAA/PAH membranes have 10- to 20-fold higher Cl⁻/SO₄²⁻ selectivities than corresponding underivatized PAA/PAH membranes; (2) Cl⁻/SO₄²⁻ selectivity for photolyzed 10.5-bilayer NBPAA/PAH membranes increases with the extent of derivatization; and (3) photolyzed PAA/NBPAH membranes show increased cation selectivities compared to PAA/PAH membranes (3-4 times) and minimal anion selectivities. NaCl fluxes are about the same for all coated membranes. Thus high selectivity can be achieved without a significant decrease in flux.

As Figure 4.1 schematically shows, the difference between underivatized PAA/PAH membranes and UV-irradiated NBPAA/PAH membranes is that the latter contain net, fixed negative charge in the bulk of the film. Photolysis may also increase net charge at the surface of these films. Higher percentages of PAA derivatization lead to more negative fixed charge in membranes, and hence higher anion-transport selectivity. Similarly, the introduction of net positive charges using photolyzed PAA/NBPAH increases Donnan exclusion of cations, and hence monovalent/divalent cation transport selectivity. However, this selectivity enhancement is not as significant as that displayed for anions by NBPAA/PAH membranes. A possible reason for the lower enhancement may be incomplete conversion of carbamates to amines during photocleavage. Although

Table 4.1. Fluxes and selectivities through membranes prepared from PAA, PAH, NBPAA, and NBPAH deposited on porous alumina.

| Type of membrane ^{a,b} | Thickness | Flux | (×10 ⁹ mole/ | selectivity ^d | | |
|---------------------------------|--------------------|-------|---------------------------------|--------------------------|--|----------------|
| | $(\mathring{A})^c$ | NaCl | Na ₂ SO ₄ | $MgCl_2$ | Cl ⁻ /SO ₄ ²⁻ | Na^+/Mg^{2+} |
| Bare porous alumina | | 43± 2 | 32±1 | 32±1 | 1.3±0.1 | 1.3±0.1 |
| PAA/PAH (10) | 420±16 | 22±1 | 3.6±0.3 | 1.9±0.3 | 6.0±0.8 | 12±1 |
| 50%NBPAA/PAH (10) | 260±20 | 18±1 | 0.15±0.01 | 2.0±0.1 | 120±10 | 9.1±0.5 |
| PAA/50%NBPAH (10) | 400±35 | 14±2 | 15±1 | 0.35 ±0.1 | 1.0±0.1 | 43±7 |
| 50%NBPAA/50%NBPAH (10) | 320±20 | 22±2 | 1.8±0.3 | 2.0±0.2 | 12±1 | 11±1 |
| PAA/PAH (10.5) | 450±30 | 20±1 | 2.2±0.2 | 2.1±0.2 | 9.3±0.6 | 10±1 |
| 23%NBPAA/PAH (10.5) | 330±15 | 18±2 | 0.19±0.02 | 2.1±0.2 | 100±4 | 8.7±0.1 |
| 50%NBPAA/PAH (10.5) | 270±15 | 16±2 | 0.11±0.02 | 2.0±0.1 | 150±10 | 8.1±1.1 |
| 65%NBPAA/PAH (10.5) | 275±15 | 17±2 | 0.10±0.01 | 2.1±0.2 | 170±20 | 8.0±0.7 |
| PAA/50%NBPAH (10.5) | 410±35 | 15±2 | 13±1 | 0.4±0.1 | 1.2±0.1 | 38±8 |

^a The number in parentheses represents the number of bilayers deposited.

^b The percentage values represent the degree of derivatization of the particular polymer as calculated from NMR spectra.

^c Post-UV irradiation thickness of films prepared on Al-coated wafers. Thicknesses before irradiation were 10-25% higher.

^d Selectivities were calculated as the average of selectivity values from different membranes and not simply as a ratio of average flux values.

removal of the nitrobenzyloxycarbonyl group is quantitative, side reactions may result in lower yields of amines. Patchornik and coworkers reported a 25% yield of amines when photocleaving nitrobenzyloxycarbonyl-protected amino acids. This may also explain why the Cl⁻/SO₄²⁻ selectivity of 10-bilayer 50%NBPAA/50%NBPAH membranes is twice as large as that of 10-bilayer PAA/PAH membranes. If derivatized PAH introduces less charge than does derivatized PAA, 50%NBPAA/50%NBPAH membranes would have a net negative charge and hence an increased Cl⁻/SO₄²⁻ selectivity relative to PAA/PAH.

Because Donnan exclusion can result from charges at both the surface and the interior of a film, changing the outer layer of a membrane from a polyanion to a polycation should affect selectivity. ^{13,21,23,41} Table 4.1 shows some effect of changing the sign of surface charge, but the change in selectivity is not very large. Capping a membrane with a PAA or NBPAA top layer (10.5 bilayer membranes) increases anion selectivity by 20-50%, while capping with PAH (or NBPAH) (10 bilayer membranes) may slightly increase cation selectivity. In previous studies, however, CI/SO₄²⁻ selectivity increased by as much as two orders of magnitude when the outer layer of the film was a polyanion rather than a polycation. ¹³ The reason for the small effect in the present case is probably that films were prepared in the absence of supporting electrolyte. Preparation under these conditions reduces the net charge on the membrane surface, ^{23,46,47} and hence the bulk of the membrane will play a much larger role in determining selectivity.

4.3.4 Modeling of Ion Transport. To estimate the contributions of Donnan exclusion and selective diffusion to ion-transport selectivity, we utilized a simple model for ion transport based on previous simulations of ion-exchange membranes^{48,49} and MPMs.^{20,50}

The model includes Donnan equilibria at the feed/membrane interface and at the alumina/polyelectrolyte film boundary (Fig.4.5) as well as Nernst-Planck transport within the membrane. Figure 4.5 portrays the concentration profile in the membrane. We did not include a charged surface layer because reversing the charge in the top layer of the membrane had only a small effect on selectivity. To calculate diffusion coefficients in the membrane, we performed the procedure given in the appendix.

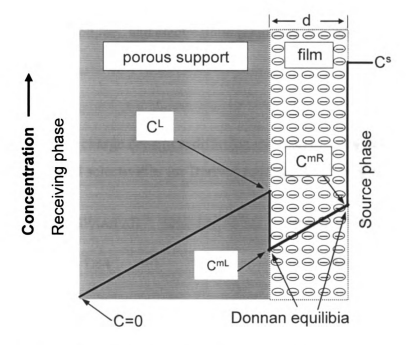


Figure 4.5: Schematic diagram of a model for ion transport through a multilayer polyelectrolyte membrane. The line represents the concentration profile of the excluded ion. Symbols are defined in the text.

cal

N

co

fra

W Wi

lis

Ta

(x

• S

wa (re

The transport model requires knowledge of the charge density, C_x , in MPMs. For our calculation, we assumed that all fixed charges resulted from photolysis of NBPAA or NBPAH. Pure PAA contains ~16 M -COOH groups. Assuming an equal volume fraction for PAA and PAH components, and considering 50% derivatization, the concentration of net charge in 50%NBPAA/PAH films would be approximately 4M. With this estimation, we calculated diffusion coefficients in different membranes along with values for diffusion, α_D , and electrostatic (Donnan), α_E , selectivities. The results are listed in Table 4.2.

Table 4.2: Estimated charge densities, diffusion coefficients, Donnan selectivities, and diffusional selectivities for Derivatized PAA/PAH membranes.

| Membrane | 23%NBP | AA/PAH | AH 50%NBPAA/PAI | | 65%NBPAA/PAH | | PAA/50%NBPAH ^b | |
|---|--------|-------------------------------|-----------------|-------------------------------|-----------------|-------------------------------|---------------------------|------------------|
| $Z_{x}C_{x}(M)$ | -1.84 | | -4.0 | | -4.6 | | 1.0 | |
| $^{D}_{(\times 10^{10} \text{ cm}^2/\text{s})}$ | Cl | SO ₄ ²⁻ | Cl ⁻ | SO ₄ ²⁻ | Cl ⁻ | SO ₄ ²⁻ | Na ⁺ | Mg ²⁺ |
| | 135 | 5 | 204 | 12 | 255 | 15 | 65 | 3.5 |
| $\alpha_{\mathrm{D}}^{}^{}}}$ | 27 | | 17 | | 17 | | 19 | |
| α_E^{a} | 3.7 | | 8.8 | | 10 | | 2.3 | |

^a See equation 8 in the Appendix for the definition of α_D , α_E , and ΔC .

^b To obtain fixed charge density in this film, the initial estimate of amine concentration was divided by 4 to reflect a low yield of amine groups from photocleavage (reference 38).

Calculations with this simple model suggest that ion-transport selectivity is only partially due to Donnan exclusion, and that diffusive selectivity is a larger factor than Donnan exclusion. However, the contribution of Donnan exclusion to selectivity does increase with increasing charge density in the membrane as would be expected. Diffusive selectivity is consistent with the fact that the calculated diffusion coefficients (ranging from 5.2×10^{-10} to 2.5×10^{-8} cm²/s) in MPFs are very small.

The slow diffusion and the difference in diffusion coefficients could result from steric hindrance and/or electrostatic interactions. Farhat and Schlenoff suggest that transport through polyelectrolyte multilayers occurs by hopping of ions between transient ion-exchange sites. ⁴⁷ Because more highly charged ions require more ion-exchange sites, their movement through MPMs may be slower than that of monovalent ions. Yeager reported that the diffusion coefficient of Cl⁻ could be 14 times larger than that of SO₄²⁻ in perfluorinated carboxylate membranes. ⁵¹ Even for similarly charged ions such as Na⁺ and Cs⁺, diffusion coefficients can differ by a factor of four in Nafion™ membranes. ⁵² By modeling Donnan dialysis data for ion transport through cation-exchange membranes, Miyoshi obtained effective diffusion coefficients of 6.33×10⁻8 and 1.34×10⁻8 cm²/s, for Na⁺ and Mg²⁺, respectively. ⁵³ Thus the low diffusion coefficients and the diffusional selectivities resulting from these simple simulations are within reasonable limits.

The limitations of the ion-transport model must be kept in mind, however. The simulation does not consider activity coefficients and possible differences in solubilities of different ions in MPMs.^{54,55} This could account for the fact that calculated diffusivity selectivities in derivatized membranes are about 2-fold larger than total selectivities for pure PAA/PAH membranes. Additionally, charge densities are only approximate.

However, even with these limitations, the modeling results and data for transport through underivatized membranes suggest that Donnan exclusion is only partially responsible for selectivities. Future work on determining partition coefficients would be helpful for a better understanding of transport, but such studies will be challenging given the minimal thickness of MPFs.

4.4 Conclusions

Introduction of net, fixed charge into MPMs through derivatization and photolysis is straightforward and quantitatively controllable. The presence of ion-exchange sites in the membrane significantly increases ion-transport selectivities, and this increase correlates with the charge density introduced into the membrane. Simulations suggest that the enhancement of selectivity is due to both Donnan exclusion and diffusivity differences among ions. In addition, the methods for derivatizing poly(acrylic acid) and poly(allyl amine) may provide a general way to modify the properties of MPFs.

4.5 Appendix

To calculate diffusion coefficients in MPMs, we applied the following procedure. The ion concentration on the left side of the porous support/polyelectrolyte membrane interface, C_i^L , was calculated using equation 3

$$C_i^L = \frac{J_{coated}}{J_{bare}} \times C_i^S \tag{3}$$

where J_{coated} and J_{bare} are fluxes through coated and bare porous alumina supports, respectively, and C_i^S is the concentration of ion in the source-phase solution (0.1M). This equation assumes that ion concentrations in the receiving phase are negligible and that flux through the alumina is proportional to a linear concentration gradient. The concentration of excluded ion just inside the left end of the coated polyelectrolyte film (Figure 4.5), C^{mL} , was calculated assuming Donnan equilibrium. For a salt $A_x B_y$ with counterion charge Z_A and excluded ion charge Z_B , C_B^{mL} can be expressed by equation 4

$$C_{B}^{mL} = C_{B}^{L} \left(-\frac{Z_{B}C_{B}^{mL} + Z_{x}C_{x}}{Z_{A}C_{A}^{L}} \right)^{\frac{Z_{B}}{Z_{A}}}$$
(4)

where Z_x and C_x are the sign and concentration of the fixed charge in the membrane.

Next, we employed the Nernst-Planck equation, (5), to calculate the excluded ion concentration, C_R^{mR} , at the right side of the polyelectrolyte film.

$$J_{i} = -D_{i} \frac{dC_{i}}{dx} - \frac{Z_{i}FD_{i}C_{i}}{RT} \frac{d\phi}{dx}$$
 (5)

In this equation, D is the diffusion constant, ϕ is the electrical potential, x is the distance in membrane, and F, R, and T are the Faraday constant, the gas constant, and the temperature, respectively. Subscript i indicates the ith ion. Because the concentration of

the excluded ion in the membrane is low, the migration term in the Nernst-Planck equation is negligible compared to the diffusion term for this ion. Assuming constant flux, equation 5 for the excluded ion can then be simplified to equation 6

$$J_B = -D_B \left(\frac{C_B^{mR} - C_B^{mL}}{d} \right) \tag{6}$$

where d is the thickness of the polyelectrolyte film. Rearrangement of equation 6 allows calculation of C_B^{mR} once C_B^{mL} is calculated. Finally, using equation 7, the concentration of the excluded ion in the source phase, C_B^S , could be calculated.

$$C_{B}^{S} = C_{B}^{mR} \left(-\frac{Z_{B}C_{B}^{mR} + Z_{x}C_{x}}{Z_{A}C_{A}^{S}} \right)^{-\frac{Z_{B}}{Z_{A}}} \tag{7}$$

We performed the entire calculation iteratively, using the experimental flux and varying the diffusion coefficient of the excluded ion until the calculated excluded ion concentration in the source phase matched that used experimentally (0.1 M). Selectivity for species 1 (e. g., Cl⁻) over species 2 (e. g., SO₄²⁻) is given by equation 8

$$\alpha_{B_1/B_2} = \frac{J_{B_1}}{J_{B_2}} = \frac{D_{B_1}}{D_{B_2}} \times \frac{\Delta C_{B_1}^m}{\Delta C_{B_2}^m} = \alpha_D \times \alpha_E \quad (8)$$

where $\Delta C_B^m = C_B^{mR} - C_B^{mL}$ (Figure 4.5), and α_D and α_E denote selectivities arising from selective diffusion of ions and electrostatic exclusion, respectively.

4.6 References and Notes

- 1 Liu, C.; Martin, C. R. Nature London 1991, 352, 50-52.
- 2 Kesting, R. E.; Fritzche, A. K. *Polymeric Gas Separation Membranes*; John Wiley & Sons: New York, **1993**.
- 3 Brandt, D. C.; Leitner, G. F.; Leitner, W. E. In Reverse Osmosis Membrane Technology, Water, Chemistry, and Industrial Applications; Amjad, Z., Ed.; Van Nostrand Reinhold: New York, 1993, pp 1-36.
- 4 Niwa, M.; Kawakami, H.; Nagaoka, S.; Kanamori, T.; Shinbo, T. J. Membr. Sci. 2000, 171, 253-261.
- 5 Shieh, J.-J.; Chung, T.-S. Ind. Eng. Chem. Res. 1999, 38, 2650-2658.
- 6 Parthasarathy, A.; Brumlik, C. J.; Martin, C. R.; Collins, G. E. J. Membr. Sci. 1994, 94, 249-254.
- 7 Chen, H.; Belfort, G. J. Appl. Polym. Sci. 1999, 72, 1699-1711.
- 8 Kilduff, J. E.; Mattaraj, S.; Pieracci, J. P.; Belfort, G. *Desalination* **2000**, *132*, 133-142.
- 9 Linder, C.; Kedem, O. J. Membr. Sci. 2001, 181, 39-56.
- Zhang, L.-H.; Hendel, R. A.; Cozzi, P. G.; Regen, S. L. J. Am. Chem. Soc. 1999, 121, 1621-1622.
- 11 Decher, G.; Hong, J. D. Macromol. Chem., Macromol. Symp. 1991, 46, 321-327.
- 12 Decher, G.; Hong, J. D. Ber. Bunsenges. Phys. Chem. 1991, 95, 1430-1434.
- 13 Stair, J. L.; Harris, J. J.; Bruening, M. L. Chem. Mater. 2001, 13, 2641-2648.
- 14 Ackern, F. v.; Krasemann, L.; Tieke, B. *Thin Solid Films* **1998**, *327-329*, 762-766.
- Stroeve, P.; Vasquez, V.; Coelho, M. A. N.; Rabolt, J. F. *Thin Solid Films* **1996**, 708-712.
- 16 Kotov, N. A.; Magonov, S.; Tropsha, E. Chem. Mater. 1998, 10, 886-895.
- 17 Leväsalmi, J.-M.; McCarthy, T. J. *Macromolecules* **1997**, *30*, 1752-1757.
- 18 Krasemann, L.; Toutianoush, A.; Tieke, B. J. Membr. Sci. 2001, 181, 221-228.

- 19 Meier-Haack, J.; Lenk, W.; Lehmann, D.; Lunkwitz, K. J. Membr. Sci. 2001, 184, 233-243.
- 20 Krasemann, L.; Tieke, B. Langmuir 2000, 16, 287-290.
- 21 Harris, J. J.; Stair, J. L.; Bruening, M. L. Chem. Mater. 2000, 12, 1941-1946.
- 22 Balanchandra, A. M.; Dai, J.; Bruening, M. L. *Macromolecules* **2001**, *35*, 3171-3178.
- 23 Schlenoff, J. B.; Ly, H.; Li, M. J. Am. Chem. Soc. 1998, 120, 7626-7634.
- 24 Laurent, D.; Schlenoff, J. B. Langmuir 1997, 13, 1552-1557.
- 25 Kotov, N. A.; Dekany, I.; Fendler, J. H. Adv. Mater. 1996, 8, 637-641.
- Joly, S.; Kane, R.; Radzilowski, L.; Wang, T.; Wu, A.; Cohen, R. E.; Thomas, E. L.; Rubner, M. F. *Langmuir* **2000**, *16*, 1354-1359.
- 27 Chen, J.; Huang, L.; Ying, L.; Luo, G.; Zhao, X.; Cao, W. *Langmuir* **1999**, *15*, 7208-7212.
- 28 Harris, J. J.; DeRose, P. M.; Bruening, M. L. J. Am. Chem. Soc. 1999, 121, 1978-1979.
- 29 Yoo, D.; Shiratori, S. S.; Rubner, M. F. *Macromolecules* **1998**, *31*, 4309-4318.
- 30 Fery, A.; Scholer, B.; Cassagneau, T.; Caruso, F. *Langmuir* **2001**, *17*, 3779-3783.
- 31 Mendelsohn, J. D.; Barrett, C. J.; Chan, V. V.; Pal, A. J.; Mayes, A. M.; Rubner, M. F. *Langmuir* **2000**, *16*, 5017-5023.
- 32 Dyer, R. G.; Turnbull, K. D. J. Org. Chem. 1999, 64, 7988-7995.
- Corrie, J. E. T.; Trentham, D. R. In *Bioorganic Photochemistry*; Morrison, H., Ed.; John Wiley: New York, 1993; Vol. 2, pp 243-305.
- Pillai, V. N. R. In *Organic Photochemistry*; Padwa, A., Ed.; Marcel Dekker: New York, 1987; Vol. 9, pp 225-323.
- 35 Matuszczak, S.; Cameron, J. F.; Fréchet, J. M. J.; Wilson, C. G. *J. Mater. Chem.* **1991**, *I*, 1045-1050.
- 36 Nishikubo, T.; Ilzawa, T.; Takahashi, A.; Shimokawa, T. J. Polym. Sci. A: Polym. Chem. 1990, 28, 105-117.

- 37 Beecher, J. E.; Cameron, J. F.; Fréchet, J. M. J. J. Mater. Chem. 1992, 2, 811-816.
- 38 Patchornik, A.; Amit, B.; Woodward, R. B. J. Am. Chem. Soc. 1970, 92, 6333-6335.
- 39 Yoshikawa, Y.; Matsuoka, H.; Ise, N. *Br. Polym. J.* **1986**, *18*, 242-246.
- 40 Shiratori, S. S.; Rubner, M. F. *Macromolecules* **2000**, *33*, 4213-4219.
- 41 Dubas, S. T.; Schlenoff, J. B. *Macromolecules* **1999**, *32*, 8153-8160.
- Dai, J.; Jensen, A. W.; Mohanty, D. K.; Erndt, J.; Bruening, M. L. *Langmuir* **2001**, 17, 931-937.
- Cochin, D.; Passmann, M.; Wilbert, G.; Zentel, R.; Wischerhoff, E.; Laschewsky, A. *Macromolecules* **1997**, *30*, 4775-4779.
- 44 Gravel, D.; Giasson, R.; Blanchet, D.; Yip, R. W.; Sharma, D. K. Can. J. Chem. 1991, 69, 1193-1200.
- 45 DeMayo, P. Adv. Org. Chem. 1960, 2, 367-425.
- 46 Schlenoff, J. B.; Dubas, S. T. *Macromolecules* **2001**, *34*, 592-598.
- 47 Farhat, T. R.; Schlenoff, J. B. *Langmuir* **2001**, *17*, 1184-1192.
- 48 Meyer, K. H.; Sievers, J.-F. Helv. Chim. Acta 1936, 19, 649-664.
- Teorell, T. In *Progress in Biophysics and Biophysical Chemistry*; Buter, J. A. V., Randall, J. T., Eds.; Academic Press: New York, 1953; Vol. 3, pp 305-369.
- 50 Lebedev, K.; Ramirez, P.; Mafé, S.; Pellicer, J. Langmuir 2000, 16, 9941-9943.
- 51 Herrera, A.; Yeager, H. L. J. Electrochem. Soc. 1987, 134, 2446-2451.
- 52 Rollet, A.-L.; Simonin, J.-P.; Turq, P. Phys. Chem. Chem. Phys. 2000, 2, 1029-1034.
- 53 Miyoshi, H. J. Membr. Sci. **1998**, 141, 101-110.
- 54 Paula, S.; Volkov, A. A.; Deamer, D. W. *Biophys. J.* **1998**, 74, 319-329.
- 55 Makino, K.; Oshima, H.; Kondo, T. Colloid Polym. Sci. 1987, 265, 911-915.

Chapter 5

Metal Nanoparticles/Polyelectrolyte Multilayer films: Synthesis and Catalytic Applications

5.1 Introduction

Due to their small size, metal nanoparticles often have properties that are different from those of bulk metals.^{1,2} These novel properties may find applications in areas such as photoelectronics, ^{3,4} catalysis, ^{5,6} magnetism, ^{7,8} and sensing. ^{9,10} In many cases, the particles will be most useful in the form of thin films, but preparation of tunable, homogeneous films that contain nanoparticles is an on-going challenge. Several technologies have been exploited to fabricate such films. Mechanical mixing of metal particles with polymers is simple and straightforward but often yields heterogeneous films.¹¹ Spin-coating or smearing of polymer-metal ion mixtures followed by reduction may result in homogenous coatings, but deposition of ultrathin films can be difficult, and coverage of substrates with unusual geometries is not possible. ¹²⁻¹⁴

Layer-by-layer deposition of nanoparticles allows fine control over film thickness and formation of films on a wide variety of surfaces. Interactions used to form such films include ligand-metal ion-ligand bridges¹⁵ and covalent bonding.^{16,17} The most convenient and versatile technique for layer-by-layer deposition, however, is probably the alternating adsorption of oppositely charged polyelectrolytes.¹⁸ Control of film thickness on the nanometer scale results simply from controlling deposition conditions such as the number of layers, pH, and the supporting electrolyte concentration present during adsorption.^{19,20} This method has been used extensively to construct composite films containing inorganic colloid (e.g., sulfides, selenides, tellurides, and oxides of Cd, Pb, Ti, Zn, Si, Fe, and

Mn). ^{21,22} ^{23,24} A few groups synthesized colloid/polyelectrolyte films by utilizing dendrimer-, ²⁵ citrate-, ^{26,27} or polyelectrolyte-stabilized gold nanoparticles. The common and crucial feature in all of these studies is to prepare properly charged, stabilized metal nanoclusters before film construction. Alternating adsorption of colloids and polymeric electrolytes then results in film formation.

This chapter of the thesis reports the synthesis of nanoparticle-containing films through formation of a polyelectrolyte-metal ion complex, layer-by-layer adsorption of this complex and a polyanion, and finally post-deposition reduction of the metal ions (Scheme 5.1). The diameters of the nanoparticles depend on the concentration of metal ions in the film. This method has several assets. First, because the metal ions are well distributed along the polymer chains, nanoparticles are dispersed throughout the film. Second, the surrounding polymer limits particle aggregation and thus yields a small particle size. Finally, the process circumvents the need to develop methods to synthesize and isolate uniform, stabilized colloids in solution.

Rubner and coworkers reported the synthesis of poly(acrylic acid)
Ag(0)/poly(allylamine hydrochloride) (PAH) films by a related method.²⁹ They

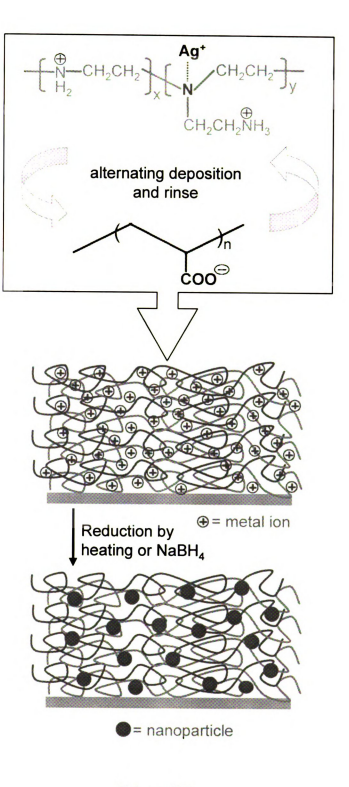
immersed a preformed poly(acrylic acid) (PAA)/PAH film into a solution containing Ag⁺

to trap the metal ion in the film by ion exchange. Reduction of the Ag⁺ with H₂ resulted

in Ag nanoparticles. This ion-exchange method was also used to construct

semiconductor nanocomposites by first adsorbing a metal ion into a polyelectrolyte film

and subsequently treating the film with H₂S.^{30,31}



Scheme 5.1

By comparison, the method described herein involves formation of the metal complex before film deposition. This affords a convenient method for controlling the amount of metal ion in the film, which in turn allows control over particle size after reduction.

Transmission electron microscopy (TEM) shows that particle size can be tuned from 4 to 30 nm, and initial studies of these particle-containing films show them to be active as both catalysts and antimicrobial coatings.

5.2 Experimental Section

Materials. Polyethyleneimne (PEI) ($M_w = 25,000$), poly(acrylic acid) (25 wt% in water, $M_w = 90,000$), tetraamineplatinum(II) chloride hydrate, and sodium perchlorate hydrate were purchased from Aldrich. Silver nitrate and methylene bromide were purchased from E. Merck and J. T. Baker, respectively. Films were prepared on quartz slides, Aucoated Si (200 nm sputtered Au on 20 nm Cr on Si(100)), and copper-coated carbon TEM grids. Prior to deposition, Au-coated Si and TEM grids were cleaned with UV/ozone for 15 min, while quartz slides were cleaned in hot piranha solution (H₂SO₄:H₂O₂, 3:1) for 30 min and copiously rinsed with water. Caution: Pirhana solution reacts violently with organic compounds and should be used with care. Waste piranha should be stored in loosely capped bottles. To deposit one PEI-Ag⁺/PAA bilayer, substrates were immersed in PEI-Ag⁺ solution (0.1, 0.5, or 3.0 mM AgNO₃, 1 mg/mL PEI; pH adjusted to 7.0 with 0.1 M HNO₃) for 5 min, rinsed with water for 1 min, immersed in a 3 mg/mL PAA solution (pH adjusted to 5.0 with 0.1 M NaOH) for 5 min, and rinsed again with water for 1 min. Bilayers containing other metal ions were prepared in the same fashion. Mutilayers were obtained by repetitive deposition of PEI-Ag⁺ and PAA. Reduction of

ions was effected by heating at 150 °C for 2 h under the protection of N₂, or by immersing the film in a freshly prepared 1 mM NaBH₄ solution for 30 min.

UV-visible spectra were recorded using a Perkin-Elmer Lamda 40 spectrometer. TEM was performed on a JEOL 100CX microscope operating at 100 kV, and cyclic voltammograms were obtained with a CH Instruments electrochemical analyzer (model 604). Measurements were made using a Ag/AgCl (3 M KCl) reference electrode and a platinum wire counter electrode. Working electrodes were gold-coated silicon wafers placed in an O-ring cell that exposed 0.1 cm² of area. In the antimicrobial test, one seed colony of *E.Coli* (INFalphaF, Invitrogen) was inserted into the test tube and allowed to grow overnight at 37 °C in *Luria-Bertani* broth.

5.3 Results and discussion

5.3.1 Synthesis of metal nanoparticles. Branched polyethyleneimine (PEI) contains primary, secondary, and tertiary amino groups and thus is an attractive polymer for metal-ion complexation.³² Initially, we tried to prepare PEI-stabilized Ag colloids in solution and subsequently form films by alternating adsorption of PAA and the PEI-stabilized colloids. A brownish solution formed immediately after adding 1 mL of 0.1 M NaBH₄ to a 20 mL mixture of PEI (1 mg/mL) and 0.5 mM AgNO₃. The brown color gradually faded to yellow over a 10 h period, and this clear yellow color did not change for 3 months. No precipitation was observed. UV-visible spectra and TEM confirmed the initial formation and growth of silver clusters (Fig. 5.1). Particle size increased from a value of 8 nm (1 hour after addition of NaBH₄) to 21 nm nine hours later.

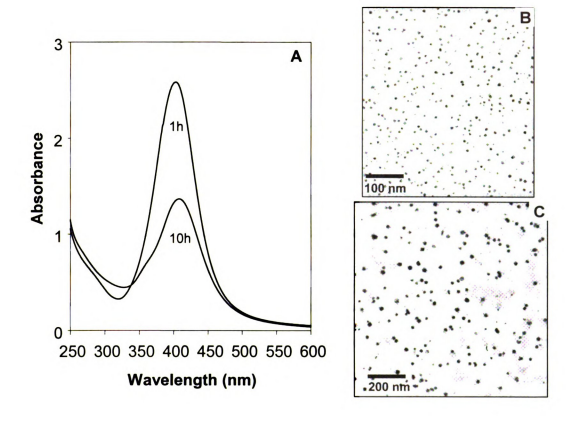


Figure 5.1: UV-visible spectra (A) and TEMs (B,C) of PEI-protected silver colloids reduced with NaBH₄. The absorbance decreased 50% in the first 10 hours, and average particle size increased from 8 nm at 1h (B) to 21 nm at 10 h (c). [Ag^{+}]=0.5 mM, [PEI]=1 mg/mL.

The surface plasmon absorbance decreased ~50% with a red shift of 8 nm over the same time period. These results indicate that PEI stabilizes silver nanoparticles temporarily and prevents precipitation over longer time periods. However, PEI does not inhibit gradual particle aggregation. Mayer and coworkers investigated various polyelectrolytes as colloid stabilizers in solution and found that many simple polyelectrolytes are not satisfactory.³³

Interestingly, in multilayered polyelectrolyte films prepared using solutions of PEI-Ag(0) colloids and PAA, surface plasmon absorbance was very weak even after deposition of 10 bilayers. This suggests that the silver nanoparticles did not transfer into the film along with the PEI. During film formation, adsorbed PEI may release colloids to maximize electrostatic interactions. In contrast, NaBH₄ reduction of silver ions within PEI-Ag⁺/PAA films (Scheme 5.1) easily yields stable nanoparticles. The surface plasmon absorbance that results from these Ag(0) particles increases with the number of layers in the film as would be expected (Fig. 5.2). Additionally, this absorbance dropped less than 10% after aging a film for 16 days, suggesting that when silver ions are reduced within PEI/PAA films, movement of the resulting nanoparticles is restricted, and hence particle aggregation is very slow. The TEM image in Figure 5.1 shows that the particles produced by NaBH₄ reduction are relatively monodisperse (diameters of 4.0 ± 0.6 nm). Similar particles can be formed by including Pt(II) in PEI/PAA films (Fig. 5.3).

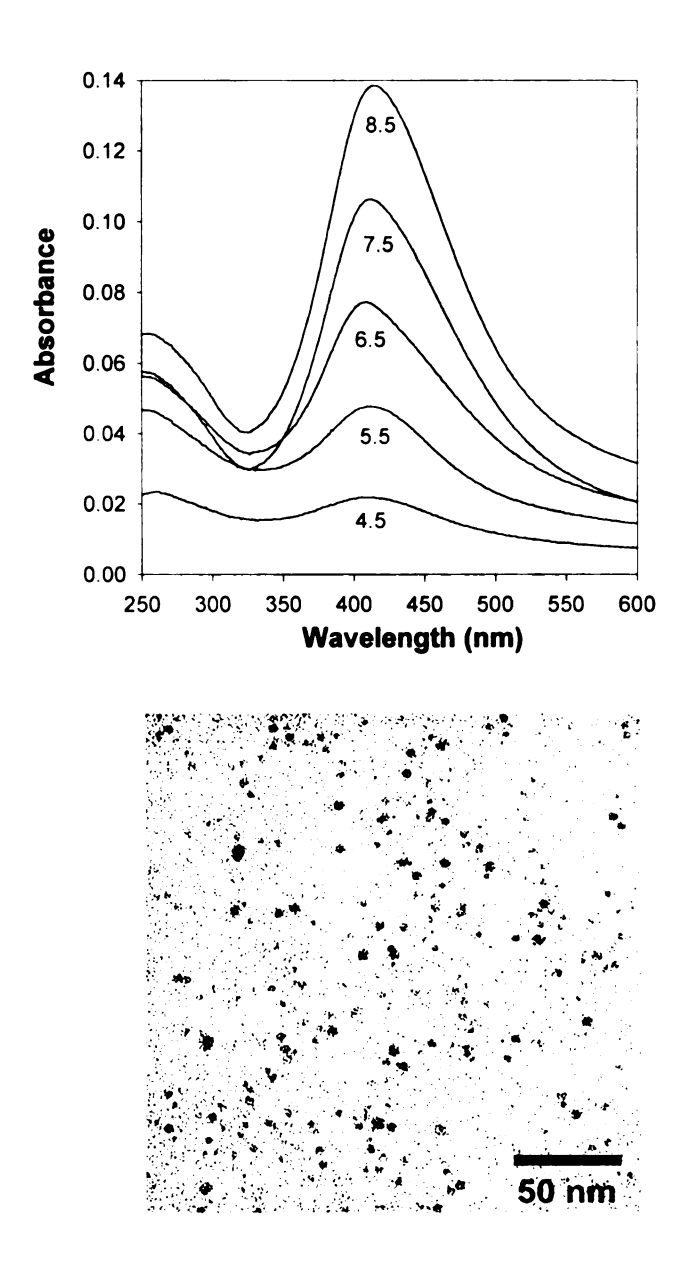


Figure 5.2: (Top) UV-visible spectra of NaBH₄-reduced PEI-Ag(0)/PAA films. Numbers on the plot refer to the number of bilayers in the film. (Bottom) TEM image of a NaBH₄-reduced PEI-Ag(0)/PAA film (5.5 bilayers, the additional half bilayer results in PEI-Ag(0) being the top layer in the film). Silver particle size is 4.0 ± 0.6 nm, and 0.5 mM AgNO₃ was used in film deposition.



Figure 5.3: TEM image of a 5.5-bilayer PEI-Pt(0)/PAA (NaBH₄ reduced) film. Platinum nanoparticle size: 10 ± 4 nm. 0.5 mM Pt(NH₃)₄Cl₂ was used in the film deposition, and other conditions were the same as the synthesis of PEI-Ag(0)/PAA film.

Heat-induced reduction also creates silver nanoparticles in PEI-Ag $^{+}$ /PAA films. For films synthesized under the same conditions (0.5 mM Ag $^{+}$), the diameters of thermally reduced particles are ~2.5 times as large as those of chemically reduced particles (compare TEMs in Fig. 5.2 and Fig. 5.4B). This is probably because heating (150 °C) promotes aggregation of Ag atoms. The TEM images in Figure 5.4 also show that particle size depends on the Ag $^{+}$ /PEI ratio in deposition solutions. The average particle sizes when using 0.1 mM, 0.5 mM, and 3.0 mM Ag $^{+}$ during deposition were 6, 10, and 26 nm, respectively. Control of particle size should provide a convenient means for tuning film properties.

Reduction of Ag^+ by heating should also result in cross-linking of PEI- Ag^+ /PAA systems via heat-induced amide formation from carboxylate-ammonium complexes. ³⁴ The appearance of an amide peak in the external reflection FTIR spectra of heated PEI- Ag^+ /PAA films (Fig. 5.5) confirms that some cross-linking occurs. Cross-linking should strengthen the film, and control of the cross-linking density may allow tailoring of film permeability. Such control could find application in selective catalysis.

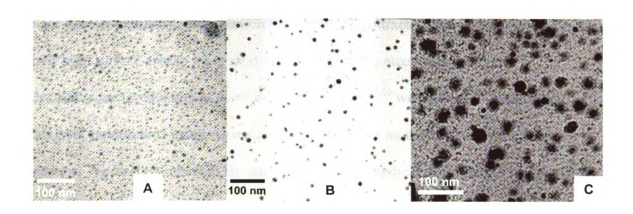


Figure 5.4: TEM images of thermally reduced (heating for 2 h at 150 °C under N_2) 5.5-bilayer PEI-Ag(0)/PAA films prepared using different concentrations of Ag^+ during PEI adsorption. (A) $[Ag^+] = 0.1$ mM, particle size = 6 ± 1 nm; (B) $[Ag^+] = 0.5$ mM, particle size = 10 ± 2 nm; (C) $[Ag^+] = 3.0$ mM, particle size = 10 ± 2 nm; (C) $[Ag^+] = 3.0$ mM, particle size = 10 ± 2 nm; (C) $[Ag^+] = 3.0$ mM, particle size = 10 ± 2 nm; (D) $[Ag^+] = 3.0$ mM, particle size

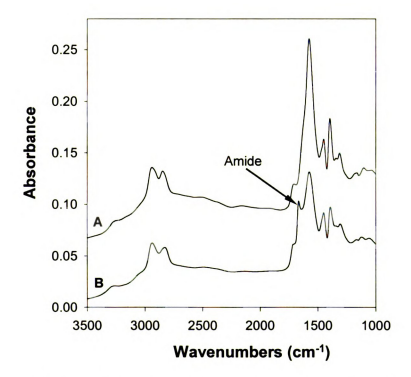


Figure 5.5: Reflectance FTIR spectra of a 5.5-bilayer PEI-Ag³/PAA film on Al before (A) and after (B) heating at 150 °C for 2h under N₂. Appearance of the amide peak indicates partial cross-linking.

5.3.2 Electrocatalysis. Nanoparticles are especially attractive for catalysis because of their high surface area to mass ratio. Because bulk Ag electrodes catalyze electrochemical reduction of some organic halogens, ^{35,36} we performed preliminary catalysis experiments using Ag nanoparticles to reduce methylene bromide. In this reaction, Ag likely binds with Br and a carbene intermediate to facilitate breaking of the C-Br bond. The main products of the reduction are ethylene and methane.³⁶ In cyclic voltammograms using Au electrodes coated with PEI-Ag(0) /PAA films (5.5 bilayers, NaBH₄ reduced), the methylene bromide reduction peak occurred at 0.77 V (vs Ag/AgCl), while at bare or PEI/PAA-coated Au electrodes, no reduction peak was observed in this region (Fig. 5.6A). Thus the nanoparticles are catalytic. The reduction peak potential at the PEI-Ag(0)/PAA-coated Au electrode was, however, 0.12 V negative of that at a bare Ag electrode. This could be due to electrical resistance in the film, hindered access of reagent to the nanoparticles, or a lower intrinsic catalytic activity of the nanoparticles. Although the composite nanoparticle film is less effective per apparent surface area than the silver wire, one has to consider that composite films can contain a much lower mass of precious metal than bulk electrodes.

PEI-Pt(0)/PAA films also exhibit electrocatalytic properties. Figure 5.6B shows cyclic voltammograms at bare, PEI/PAA-, and PEI-Pt(0)/PAA-coated gold electrodes in oxygen-saturated 1.0 M H₂SO₄. Oxygen reduction begins at ~0.15 V (vs Ag/AgCl) for the electrode coated with PEI-Pt(0)/PAA, while no reduction currents appear for bare gold and PEI-PAA-coated gold electrodes from 0.6 to -0.1 V.³⁷ The studies with both Ag and Pt nanoparticles show that at least a portion of the nanoparticles are in electrical contact

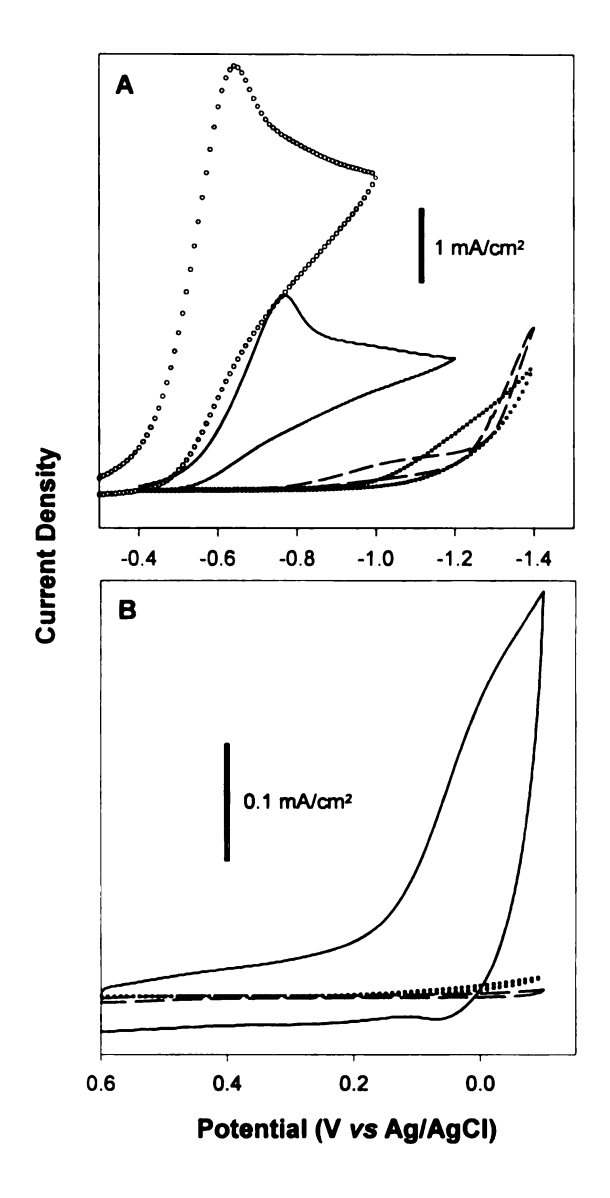


Figure 5.6: (A) Cyclic voltammograms of CH₂Br₂ (25 mM) at bare (filled circles), PEI/PAA-coated (dashed line), and PEI-Ag(0)/PAA-coated (solid line) Au electrodes, and at a bulk Ag electrode (open circles). The supporting electrolyte was 1.0 M NaClO₄, the scan rate was 100 mV/s, and films contained 5.5 bilayers of polyelectrolyte. (B) Cyclic voltammograms at bare (filled circles), PEI/PAA-coated (dashed line), and PEI-Pt(0)/PAA-coated (solid line) Au electrodes in O₂-saturated 1.0 M H₂SO₄. Films contained 9.5 bilayers of polyelectrolyte, and the scan rate was 50 mV/s.

with the gold substrate, and these particles can be accessed by analyte molecules in solution.

5.3.3 Inhibition of bacteria growth. For centuries silver metal and silver salts have been used to treat burn wounds.^{38,39} Although these compounds are effective antimicrobial agents, their use likely results in unwanted adsorption of silver ions in epidermis cells and sweat glands.³⁸ To reduce the likelihood of silver-ion adsorption, membranes containing metallic silver, *e.g.*, silver-coated nylon,³⁹ are being investigated as anti-microbial agents. Because polyelectrolyte films can form on various substrates including natural and synthetic polymers,⁴⁰ PEI-Ag(0) films could potentially be used to construct antibacterial membranes for wound treatment.

To investigate the inhibition of bacterial growth by PEI-Ag(0)/PAA films, we compared the growth of *E. Coli* in bare glass test tubes and test tubes coated with PEI-Ag(0)/PAA (Fig. 5.7). *E. Coli*-seeded solutions in both bare and 5.5-bilayer PEI/PAA-coated test tubes became turbid after 12 h of incubation at 37 °C. Under the same conditions, tubes coated with 5.5-bilayers of PEI-Ag⁺/PAA or PEI-Ag(0)/PAA (NaBH₄ reduced) remained clear, showing that the latter two films inhibited the growth of bacteria. Optical density measurements quantitatively show the differences in turbidity as the absorbance at 600 nm is proportional to the number of bacteria. For the blank tube and the tube coated with a PEI/PAA film, absorbances at 600 nm were 0.66 and 0.56, respectively (Fig. 5.7), while absorbance values for PEI-Ag⁺/PAA- and PEI-Ag(0)/PAA-coated tubes were nearly zero (0.010 and 0.012, respectively). Significantly, the silver nanoparticle-included films have the same antibacterial effect as films containing silver

ions. The nanoparticle films may be more desirable because they should minimize the amount of Ag^{\dagger} absorbed in the body.

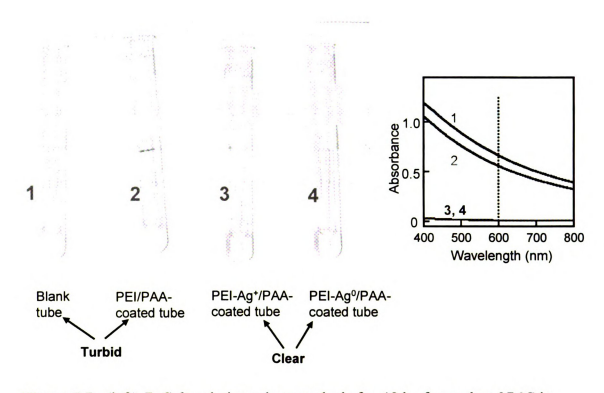


Figure 5.7: (left) E. Coli. solutions photographed after 12 h of growth at 37 °C in LB broth. The test tubes were coated with different films as noted on the picture. (right) Visible spectra of the solutions in the four test tubes. Solutions were diluted 3-fold before acquiring the spectra.

5.4 Conclusions. The ability of PEI to form complexes with Ag⁺ and Pt(II) (and presumably a wide variety of metal ions) allows the formation of nanoparticles by reduction of metal ions in PEI/PAA films. The size of the nanoparticles can be varied easily by changing the concentration of metal ions present during PEI/PAA deposition. Silver and Pt nanoparticles in PEI/PAA films are electrocatalytically active, showing that the nanoparticles are accessible to analyte molecules and electrically connected with the electrode. Additionally, PEI-Ag(0)/PAA films are effective in inhibiting bacterial growth. The use of PEI-metal ion complexes and alternating polyelectrolyte deposition followed by reduction appears to be a general method for forming nanoparticles, and should also be applicable to forming bimetallic particles.

5.5 References and notes:

- 1 Fendler, J. H. Nanoparticles and Nanostructured Films: Preparation, Characterization and Applications; Wiley-VCH: Weinhein, 1998.
- 2 Schmid, G. In *Natoscale materials in chemistry*; Klabunde, K. J., Ed.; Wiley-Interscience: New York, **2001**, pp 15-59.
- 3 Sudeep, P. K.; Ipe, B. I.; Thomas, K. G.; George, M. V.; Barazzouk, S.; Hotchandani, S.; Kamat, P. V. Nano Lett. 2002, 2, 29-35.
- 4 Merschdorf, M.; Pfeiffer, W.; Thon, A.; Voll, S.; Gerber, G. Appl. Phys. A 2000, 71, 547-552.
- 5 Zhong, C.-J.; Maye, M. M. Adv. Mater. 2001, 13, 1507-1511.
- 6 Gates, B. C. Chem. Rev. 1995, 95, 511-522.
- 7 Li, X. G.; Takahashi, S.; Watanabe, K.; Kikuchi, Y.; Koishi, M. *Nano Lett.* **2001**, *1*, 475-480.
- 8 Sun, X.; Gutierrez, A.; Yacaman, M. J.; Dong, X.; Jin, S. *Mater. Sci. Eng., A* **2000**, 286, 157-160.
- 9 Kim, Y.; Johnson, R. C.; Hupp, J. T. Nano Lett. 2001, 1, 165-167.
- 10 Ruiz, A.; Arbiol, J.; Cirera, A.; Cornet, A.; Morante, J. R. *Mater. Sci. Eng. C* **2002**, *19*, 105-109.
- 11 Ghosh, K.; Maiti, S. N. J. Appl. Polym. Sci. 1996, 60, 323-331.
- 12 Liu, C.; Xu, Y.; Liao, S.; Yu, D. Appl. Catal., A 1998, 172, 23-29.
- Fritzsche, W.; Porwol, H.; Wiegand, A.; Bornmann, S.; Kohler, J. M. Nanostruct. Mater. 1998, 10, 89-97.
- 14 Zhang, Z.; Zhang, L.; Wang, S.; Chen, W.; Lei, Y. *Polymer* **2001**, *42*, 8315-8318.
- Zamborini, F. P.; Hicks, J. F.; Murray, R. W. J. Am. Chem. Soc. 2000, 122, 4514-4515.
- 16 Sarathy, K. V.; Thomas, P. J.; Kulkarni, G. U.; Rao, C. N. R. J. Phys. Chem. B 1999, 103, 399-401.
- 17 Musick, M. D.; Keating, C. D.; Keefe, M. H.; Natan, M. J. *Chem. Mater.* **1997**, *9*, 1499-1501.

- 18 Decher, G. Science 1997, 277, 1232-1237.
- 19 Dubas, S. T.; Schlenoff, J. B. *Macromolecules* **1999**, *32*, 8153-8160.
- 20 Shiratori, S. S.; Rubner, M. F. *Macromolecules* **2000**, *33*, 4213-4219.
- 21 Mamedov, A. A.; Belov, A.; Giersig, M.; Mamedova, N. N.; Kotov, N. A. J. Am. Chem. Soc. 2001, 123, 7738-7739.
- 22 Lvov, Y.; Munge, B.; Giraldo, O.; Ichinose, I.; Suib, S. L.; Rusling, J. F. *Langmuir* **2000**, *16*, 8850-8857.
- 23 Liu, Y.; Wang, A.; Claus, R. O. Appl. Phys. Lett. 1997, 71, 2265-2267.
- Ostrander, J. W.; Mamedov, A. A.; Kotov, N. A. J. Am. Chem. Soc. 2001, 123, 1101-1110.
- He, J.-A.; Valluzzi, R.; Yang, K.; Dolukhanyan, T.; Sung, C.; Kumar, J.; Tripathy, S. K.; Samuelson, L.; Balogh, L.; Tomalia, D. A. Chem. Mater. 1999, 11, 3268-3274.
- 26 Schrof, W.; Rozouvan, S.; Van Keuren, E.; Horn, D.; Schmitt, J.; Decher, G. Adv. Mater. 1998, 10, 338-341.
- 27 Feldheim, D. L.; Grabar, K. C.; Natan, M. J.; Mallouk, T. E. J. Am. Chem. Soc. 1996, 118, 7640-7641.
- 28 Liu, Y.; Wang, Y.; Claus, R. O. Chem. Phys. Lett. 1998, 298, 315-319.
- 29 Joly, S.; Kane, R.; Radzilowski, L.; Wang, T.; Wu, A.; Cohen, R. E.; Thomas, E. L.; Rubner, M. F. *Langmuir* 2000, 16, 1354-1359.
- 30 Xiong, H.; Cheng, M.; Zhou, Z.; Zhang, X.; Shen, J. Adv. Mater. 1998, 10, 529-532.
- 31 Dante, S.; Hou, Z.; Risbud, S.; Stroeve, P. *Langmuir* **1999**, *15*, 2176-2182.
- 32 Belfiore, L. A.; Indra, E. M. J. Ploym. Sci. B 2000, 38, 552-561.
- 33 Mayer, A. B. R.; Hausner, S. H.; Mark, J. E. Polym. J. 2000, 32, 15-22.
- 34 Harris, J. J.; DeRose, P. M.; Bruening, M. L. J. Am. Chem. Soc. 1999, 121, 1978-1978.
- 35 Guerrini, M.; Mussini, P.; Rondinini, S.; Torri, G.; Vismara, E. *Chem. Commun.* **1998**, 1575-1576.

- 36 Fedurco, M.; Satoretti, C. J.; Augustynski, J. Langmuir 2001, 17, 2380-2387.
- As with Ag, the Pt nanoparticles in film are less catalytically active than a bare Pt electrode. At a freshly cleaned (with concentrated HNO₃) Pt wire, reduction of oxygen begins at around 0.4 V (vs Ag/AgCl).
- 38 Klasen, H. J. Burns **2000**, 26, 117-138.
- 39 Balogh, L.; Swanson, D. R.; Tomalia, D. A.; Hagnauer, G. L.; McManus, A. T. *Nano Lett.* **2001**, *1*, 18-21.
- 40 Phuvanartnuruks, V.; McCarthy, T. J. Macromolecules 1998, 31, 1705 2018.
- Brown, T. A. Essential Molecular Biology: a Practical Approach; Oxford University Press: New York, 1991; Vol. 1, pp22-26.

Chapter 6

Selective Hydrogenation Using Nanoparticle-Containing Polyelectrolyte Films

6.1. Introduction

Metal nanoparticles are attractive for catalysis because their large surface area to volume ratio results in a high catalytic efficiency per amount of precious metal empolyed. Additionally, reaction rates at a particular metal can vary with nanoparticle size, allowing optimization of catalytic properties. Unfortunately, however, aggregation of naked nanoparticles often prohibits control over particle size. To overcome this problem, catalytic nanoparticles are either immobilized on solid supports (e.g., carbon, metal oxides, and zeolites) or stabilized by capping the colloids with ligands ranging from small organic molecules to large polymers. Recently, dendrimers, block copolymer nanospheres, and cross-linked lyotropic liquid crystals were employed to encapsulate metal nanoparticles.

In addition to protecting nanoparticles from aggregation, encapsulating materials and ligand stabilizers can sometimes impart selectivity to catalysis. For example, hydrogenation of 2-hexyne catalyzed by 2-n-butylphenanthroline-protected palladium particles yields exclusively *cis*-2-hexene, ¹¹ and hydrogenation of allyl alcohol is 11-fold faster than hydrogenation of 3-methyl-1-penten-3-ol when using dendrimer-encapsulated palladium particles as catalysts. ¹² Triblock copolymers that encapsulate Pd nanospheres also function as nanofilters that allow preferential hydrogenation of methyl methacrylate in the presence of ethylene glycol dimethacrylate. ⁹ Thus, variation of the matrix around

catalytic nanoparticles should allow tuning of catalyst properties while helping to stabilize particles and decrease leaching of catalyst.

Multilayer polyelectrolyte films should provide an especially convenient and versatile matrix for encapsulating nanoparticles. Several studies show that adsorption of multilayer polyelectrolytes and inorganic colloids provides a controlled method for depositing nanoparticle-containing films. 13-17 Such methods are convenient because film deposition occurs simply by alternating immersion of a charged substrate in solutions containing polyelectrolytes and colloids. 18,19 However, stabilized colloids must be prepared prior to film deposition. To overcome this limitation, Rubner^{20,21} and Stroeve^{22,23} utilized ion-exchange to insert metal ions into multilayer polyelectrolyte films after deposition. Subsequent reactions of the metal ions yielded nanoparticlecontaining films. We recently reported a variation of this method.²⁴ The procedure involves alternating adsorption of polymeric metal-ion complexes and polyanions followed by reduction of the metal ions. Control over the concentration of metal ions present in the polycation deposition solution allows control over particle size, and cyclic voltammetry shows that nanoparticles in these films are accessible to analytes and electrocatalytically active.

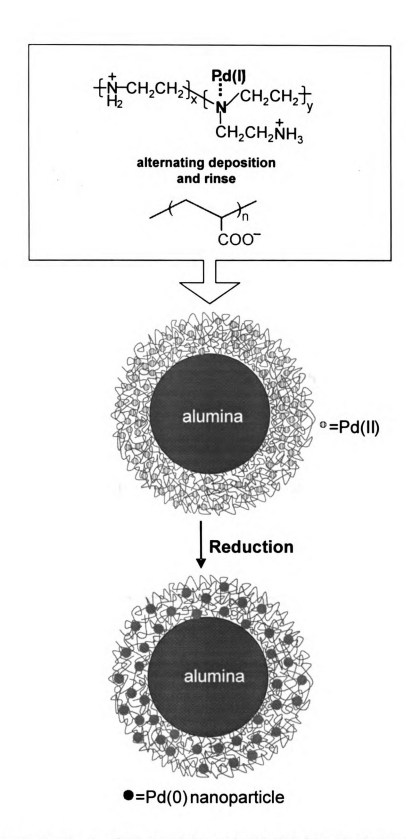
In other studies, we showed that control over the composition of multilayer polyelectrolyte membranes can yield remarkably ion-transport (Cl⁻/SO₄²⁻=1000) or gas transport (CO₂/CH₄=68) selectivities.^{25,26} Preliminary studies of the transport of neutral organic molecules through multilayer polyelectrolyte films indicate that even in simple poly(acrylic acid) (PAA)/poly(allylamine hydrochloride) (PAH) films, methanol diffusion is ten times faster than isopropanol diffusion. We therefore surmised that

polyelectrolyte films might function as highly selective filters for catalysis by encapsulated nanoparticles.

This chapter reports our initial investigations of selective hydrogenation by polyelectrolyte-encapsulated Pd nanoparticles (PEPdNs). To increase film surface area and enhance reaction rate, we deposited PEPdNs on 150-µm-diameter alumina particles (Scheme 6.1). The alumina particles are small enough that they can be suspended in solution by vigorous stirring, but large enough so that simple filtration allows catalyst recovery. To demonstrate selectivity, we investigated the hydrogenation of five different water-soluble unsaturated alcohols (Scheme 6.2). Although these alcohols have very similar reactivity on 'naked' Pd catalysts, reaction rates at PEPdNs differ by up to a factor of 31. Selectivity is enhanced by both capping of particle-containing films with a more selective polycation/polyanion pair and heat-induced cross-linking. We expect that even higher selectivities can be obtained by carefully controlling the composition and chemistry of multilayer polyelectrolyte films.

6.2 Experimental

6.2.1 Materials. Polyethyleneimine (PEI) ($M_w = 25,000$), poly(acrylic acid) (25 wt% in water, $M_w = 90,000$), palladium (5 wt% on alumina powder), α -alumina (100 mesh), allyl alcohol (99%), 1-penten-3-ol (99%), 3-methyl-1-penten-3-ol (99%), 3-methyl-2-buten-1-ol (99%), and crotyl alcohol (97%, mixture of isomers) were purchased from Aldrich, while potassium tetrachloropalladate(II) (99.99%) was obtained from Alfa Aesar. All reagents were used as received except crotyl alcohol, which was vacuum distilled before



Scheme 1. Synthesis of Pd-containing poly(ethyleneimne)/poly(acrylic acid)

Scheme 2. Substrates for catalytic hydrogenations.

use. Prior to synthesis of films, alumina was washed 4 times (suspension in water followed by centrifugation and decantation). All solutions were prepared with 18 $M\Omega$ cm Milli-Q water.

6.2.2 Synthesis of polyelectrolyte films containing Pd nanoparticles. Synthesis followed the general layer-by-layer adsorption method shown in scheme 6.1. First, 15 g of α-alumina was added to a 100 mL PEI-Pd(II) solution (1mg/mL PEI, 2.0 mM K₂PdCl₄, pH adjusted to 9.0 with 0.1 M HCl), which was stirred vigorously for 10 min.

Subsequently, the alumina was precipitated by centrifugation for 2 min. The supernatant was saved for the next polycation deposition, and the precipitated alumina was washed with 3 cycles of stirring in fresh water and centrifugation. To deposit a polyanion layer, 100 mL of 20.0 mM PAA (pH adjusted to 4.0 with 0.1 M NaOH, molarity of PAA given with respect to the repeating unit) was added to the PEI-Pd(II)-coated alumina, and the particles were precipitated and washed as described above to yield 1 adsorbed bilayer of PEI-Pd(II)/PAA. This procedure was repeated until 7 bilayers of PEI-Pd(II)/PAA were deposited. Reduction of the Pd(II) in the films by exposure to 100 mL of fresh 1.0 mM NaBH₄ for 30 min (with stirring) provided PEI-Pd(0)/PAA-coated alumina. Particles were washed three times after exposure to NaBH₄.

For the convenience of characterization, we also synthesized PEPdN films on Alcoated slides (200 nm of Al sputtered on Si(100)) using a similar dip-and-rinse procedure. Reflection FTIR (Nicolet Magna-560) and ellipsometry (J. A. Woolam M-44) were used to monitor the film formation. Films (5 bilayers) were also deposited on copper-coated carbon grids for TEM measurements. TEM was performed on a JEOL 100CX microscope operating at 100kV. The Al-coated slides and TEM grids were UV/ozone cleaned for 15 min before deposition.

6.2.3 Hydrogenation. Catalytic hydrogenations were run in a 100mL 3-neck, pearshaped flask. H₂ was bubbled through a frit at the bottom of the solution at a rate of 5 mL/min (atmospheric pressure), and the solution was vigorously stirred throughout the reaction. In most instances, the hydrogenation solution initially contained 1.0 mmol of substrate (or total 1 mmol of substrates with eqimolar of each component in competitive hydrogenation) and either 10 mg of commercial 5%-Pd-on-alumina or 250 mg of alumina coated with PEPdNs in 50 mL water. For 3-methyl-2-buten-1-ol hydrogenation with the commercial catalyst, 2 mmol of substrate and 5 mg catalyst were used so that low conversion of the alcohol could be effectively studied. Solutions of catalyst and solvent (H₂O) were bubbled with H₂ for 15 min before adding the substrates, all of which were liquids. Gas chromatography (GC) (Shimadzu GC-17A equipped with a RTx-BAC1 column) was used to monitor the reactions. The sensitivity of the flame-ionization detector was assumed to be the same for products and reactants because they contain the same number of carbon atoms. For reactions with more than one product, GC-MS and ¹H NMR (Fig. 6.3, appendix) were used to identify the products.

To calculate turnover frequencies, the amount of Pd in the catalyst must be known. For both the commercial and synthesized catalysts, the percentage of palladium in the material was determined by atomic emission spectrometry. The standard solutions (0.1 to 0.5 mM) were prepared by dissolving K₂PdCl₄ in 0.1 M of HNO₃, and sample solutions were prepared by stirring 250 mg of catalyst in 2 mL of *aqua regia* for 15 min. The solution was diluted to 12.5 mL and centrifuged (the α-alumina support does not dissolve in *aqua regia*), and the supernatant was analyzed. To see if the dissolved polymer or a small amount of dissolved alumina interfered with the Pd measurement, we also prepared blank solutions by dissolving 7-bilayer PEI/PAA films (without Pd), and did not observe emission at 633 nm. The determined Pd quantities in 250 mg of 7-bilayer PEI(0)/PAA-on-alumina and 10 mg of 5% Pd-on-alumina were 2.14x10⁻⁶ mole and 5.29x10⁻⁶ mole, respectively. The value for the commercial catalyst corresponds to about 6% by wt, showing that the analyses are reasonable.

6.3 Results and Discussion

6.3.1 Synthesis of PEPdNs. We previously reported the synthesis of Ag and Pt nanoparticles by reduction of metal ions in multilayered polyelectrolyte films.²⁴

Catalysis of many organic reactions, however, requires Pd nanoparticles. The TEM image (Fig. 1) confirms that Pd nanoparticles can also be produced by reduction of Pd(II) ions in PEI/PAA films. The particles have diameters of 1-3 nm and are well distributed throughout the film. Ellipsometry shows that 7-bilayer PEI-Pd(0)/PAA films on Alcoated wafers have thicknesses of 350±30 Å.



Figure 6.1: TEM image of 5 bilayers of PEI-Pd(0)/PAA on a carbon-coated copper grid.

6.3.2 Hydrogenation. To show that encapsulation of Pd nanoparticles in polyelectrolyte films can result in selective catalysis, we hydrogenated a series of unsaturated alcohols (Scheme 6.2) using PEPdN films on alumina as well as a commercial Pd-on-alumina catalyst. Pseudo zero-order kinetics were observed for all hydrogenations at low conversions (up to 80% as shown in Figure 6.2 as well as Figures 6.1 and 6.2 in the Appendix.) Turnover frequencies (TOFs) were calculated from the slopes in these plots (measured in the linear range).

Table 1 summarizes the TOFs for hydrogenation of the two series of molecules. The first series consists of allyl alcohol (1), 1-penten-3-ol (2), and 3-methyl-1-penten-3-ol (3), and members in this group differ in the substituents at the α -carbon of the double bond. Group 2 consists of allyl alcohol, crotyl alcohol (4), and 3-methyl-buten-1-ol (5), and these molecules differ in the number of methyl groups attached to the terminal carbon of the double bond.

On 'naked' 5%-Pd-on-alumina catalyst, the reaction rates for substrates of group 1 are very close ($1/2\approx1/3=0.87$), showing that the bulky alkyl groups at the α -carbon do not have a significant effect on reactivity. The data for group 2 are a little more complicated. The TOF of **4** is somewhat lower than that of **1**, probably because of steric hindrance due to the extra methyl group.²⁷ For similar reasons, the TOF of **5** should be even lower, but a higher (Table 6.1) TOF was observed. However, plots of conversion versus time for **5** show two linear regions (Fig. 6.2,appendix). The linear region at low conversions (up to \sim 20%) has a 3-fold greater slope than the region at higher conversions. Table 6.1 lists TOFs calculated based on both regions. No matter which TOF we choose for **5**, however, rate differences among the molecules in group 2 are still small (1/4=1.43, 1/5=0.52 or 1.63, Table 6.1).

In contrast, PEPdNs afford significantly different hydrogenation rates for the various molecules. The TOF of 1 on PEI-Pd(0)/PAA-on-alumina is only about 30% lower than that on the commercial Pd-on-alumina catalyst, showing that the catalytic efficiency of PEPdNs is not severely decreased by the presence of the polyelectrolyte film. However, the ratios of hydrogenation rates for 1/2 and 1/3 were 2.6 and 5.7, respectively, for the PEI-Pd(0)/PAA catalyst. This difference in reaction rates likely reflects differences in the sizes of the substrates.

This effect of substituents on reaction rate is more pronounced for substrates in group 2 (1, 4, 5). The hydrogenation rates of 4 and 5 were 6 and 31 times lower, respectively than that of 1. The methyl groups attached to the double-bonded carbon likely provide greater steric hindrance to adsorption on polyelectrolyte-protected catalytic sites than do substituents at the α -carbon.

Table 6.1. Rates of hydrogenation for structurally related unsaturated alcohols using commercial 5%-Pd-on-alumina or PEI-Pd(0)/PAA on alumina as catalysts.^a

| | | TOF (mol hydrogenation per mol Pd per h) | | | |
|------------|--------|--|-------------------------|-----------------------------------|---|
| Substrates | | 5% Pd | 7-bilayer PEI-Pd/PAA | Capped PEI-Pd/PAA ^h | Cross-linked PEI-Pd/PAA ^c |
| 1 | OH | 1300±150 | 1030 | 752 | 364 |
| 2 | OH | 1500±120 | 400±30 | 140 | 79 |
| 3 | ОН | 1500±100 | 182 | 56 | 35 |
| 4 | OH + | 910±50 | 184 | | |
| 5 | >=_OH | 2500±150 (~800) ^d | 33 | | |

^a Hydrogenations on commercial catalyst were repeated 3 times. On synthesized catalysts, we chose 2 as a representative example and repeated hydrogenation 3 times. Other hydrogenations were run only once.

^b 7 bilayers of PEI-Pd(0)/PAA capped with 1 bilayer of PAH/PAA.

^c Cross-linking was carried out by heating PEI-Pd(0)/PAA-coated (7 bilayers) alumina at 150 °C for 2h under a N₂ atmosphere.

^d Calculated based on reaction rate at high (above 20%) conversion.

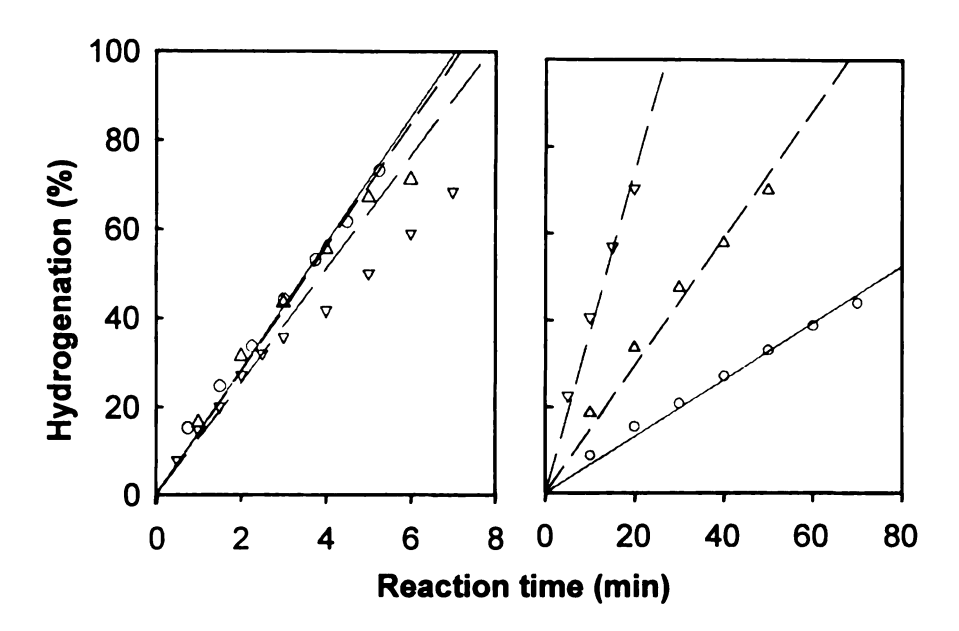


Figure 6.2: Percent of substrates hydrogenated *vs* reaction time for allyl alcohol (inverted triangles), 1-penten-3-ol (triangles), and 3-methyl-1-penten-3-ol (circles) on a commercial 5%-Pd-on-alumina catalyst (left) and on a 7-bilayer PEI-Pd(0)/PAA-coated alumina catalyst. Percent hydrogenation was obtained from the integration of product and reactant peaks in a GC spectrum.

Hydrogenation rates for PEPdNs can be tuned by depositing a capping bilayer of polyelectrolyte on the film. For example, capping 7 bilayers of PEI-Pd(0)/PAA-on-alumina with 1 bilayer of PAH/PAA (no additional Pd) decreased the reactivity of substrates 1, 2, and 3 to different degrees, and yielded reactivity ratios of 1/2 = 5.4 and 1/3 = 13. This represents an approximately 2-fold increase over similar ratios for 7-bilayer PEI-Pd(0)/PAA films.

Cross-linking of polyelectrolyte films via heat-induced amide formation from carboxylate and ammonium groups also increases the selectivity among hydrogenation rates. Selectivities (1/2 = 5 and 1/3 = 10) obtained by heating the catalysts at 150 °C for 2h under N_2 are similar to those achieved by depositing a capping layer. As might be

expected, the increases in selectivity for both capped and cross-linked film are accompanied by a decrease in rate. This likely results from slower diffusion of substrates to nanoparticles.

6.3.3 Competitive hydrogenation. In practical applications of selective catalysts, such as minimizing the number of purification steps involved in organic reactions, one substrate must be hydrogenated in the presence of several impurities.²⁸ The two examples in Figure 6.3 demonstrate the selectivity of PEPdNs in competitive hydrogenation. In an equimolar mixture of 1 and 2, use of the commercial 5%-Pd-onalumina catalyst results in 94 % conversion of 2 when 1 is 99% converted to either the hydrogenated product or isomer (Figure 6.3, left). However, when using the 7-PEI-Pd/PAA-on-alumina catalyst, the conversion of 2 decreased to 57% when 1 was 99% converted. Conversion of 2 dropped to only 40% with the addition of a PAH/PAA capping layer on the polyelectrolyte film. Selectivity improvements are more dramatic for the hydrogenation of a mixture of 1 and 3 (Figure 6.3, right), where the conversion of 3 is 75% for 5%-Pd-on-alumina, 29% for 7-bilayer PEI-Pd/PAA-on-alumina, and 17% for PAH/PAA-capped 7-bilayer PEI-Pd/PAA-on-alumina when 1 has been 99% converted. These selectivities appear to be lower than the ratios of TOFs shown in Table 6.1, and may represent the fact that rate of hydrogenation of 1 will decrease at high conversions.

Relative to commercial catalyst, PEPdNs also exhibited enhanced selectivity in competitive hydrogenation of a mixture of the three components in group 2 (Figure 6.4). Using 5%-Pd-on-alumina, when 1 was 99% converted to products, the conversions of 4

and 5 were 50% and 20%, respectively. For 7-bilayer PEI-Pd(0)/PAA-on-alumina catalyst, conversions of 4 and 5 decreased to 20% and 5%.

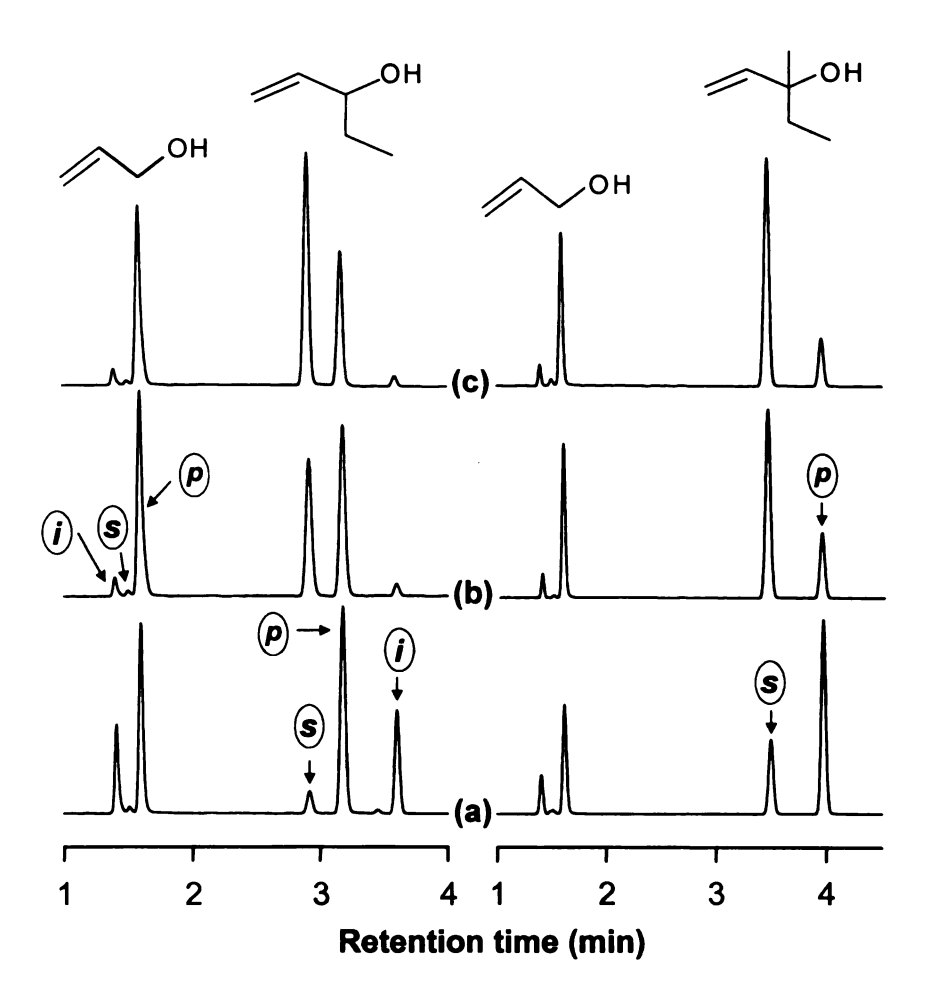


Figure 6.3: Gas chromatograms of reaction mixtures from competitive hydrogenations of allyl alcohol and 1-penten-1-ol (left), and allyl alcohol and 3-methyl-1-penten-3-ol (right). Catalysts used for reactions were (a) 5% Pd-on-alumina, (b) 7-bilayer PEI-Pd(0)/PAH-on-alumina, and (c) 1-bilayer PAH/PAA capped 7-bilayer PEI-Pd(0)/PAH-on-alumina. The circled s, p, and i represent substrate, hydrogenation product, and isomerization product, respectively.

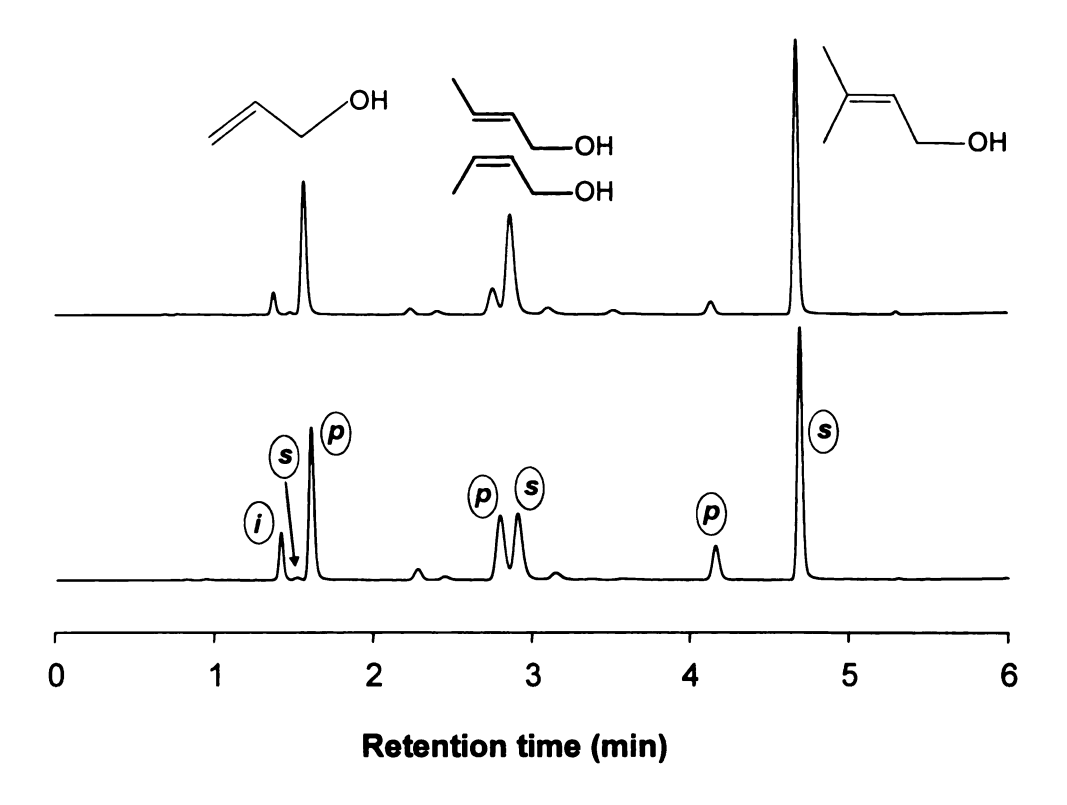


Figure 6.4: Gas chromatograms from competitive hydrogenations of allyl alcohol (left), crotyl alcohol (middle), and 3-methyl-1-buten-1-ol (right) on 5%-Pd/alumina (bottom) and on 7-PEI-Pd/PAA/alumina (top). Polyelectrolyte film-immobilized Pd catalysts significantly improved hydrogenation selectivity. The circled *s*, *p*, and *i* represent substrate, hydrogenation product, and isomerization product.

6.3.4 Suppression of isomerization. Substrate isomerization is a common but unwanted process in hydrogenation, and in some cases, this side reaction is even dominant over hydrogenation.²⁹ Minimization of isomerization is thus desirable to improve the yield of hydrogenation reactions. PEPdNs significantly inhibited substrate isomerization, as shown in Figure 6.5. When the substrate is 99% converted on the 5%-Pd commercial catalyst, the peaks due to the isomerization of allyl alcohol (to propanal) and 1-penten-3-ol (to 3-pentanone) are significant compared to product peaks, 31% and 25%, respectively. In contrast, when using the 7-PEI-Pd/PAA-on-alumina catalyst, the isomer peaks decrease to <10% of the product peak. The fraction of isomer decreases to less than 5% when using PAH/PAA-capped 7-bilayer PEI-Pd(0)/PAA-on-alumina.

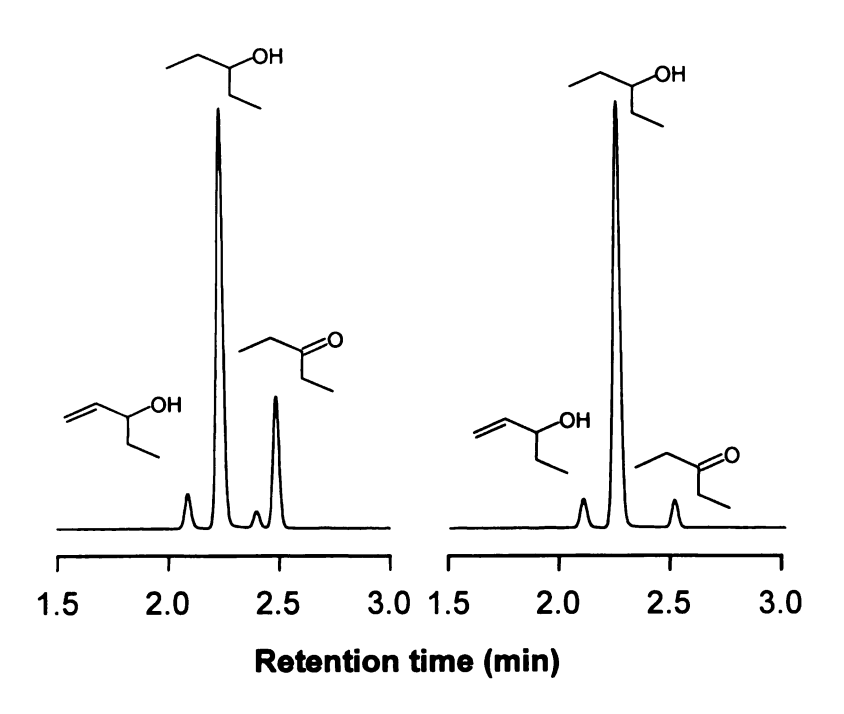


Figure 6.5: Gas chromatograms of the reaction mixture from hydrogenation of 1-penten-3-ol on 5%-Pd-on-alumina (left) and on 7-bilayer PEI-Pd(0)/PAA-on-alumina (right) catalysts. Substrate isomerization was greatly suppressed by the polyelectrolye films. The small unassigned peak in the left chromatogram is probably due to an isomerization intermediate.

6.4 Conclusions

Formation of a polyethyleneimine-Pd(II) complex followed by layer-by-layer polycation/polyanion deposition and post-deposition reduction is a convenient method to synthesize immobilized Pd catalysts. The polyelectrolyte matrix both stabilizes the particles and introduces selectivity. Moreover, the surrounding polyelectrolyte film significantly decreases the amount of unwanted isomerization. Specific modifications of the polyelectrolyte film such as cross-linking and capping with PAA/PAH enhance catalytic selectivity. Further exploitation of the versatility of polyelectrolyte films should increase selectivityity in hydrogenation as well as other reactions.

6.5 References

- 1 Fendler, J. H. Nanoparticles and Nanostructured Films: Preparation, Characterization and Applications; Wiley-VCH: Weinhein, 1998.
- 2 Schmid, G. In *Nanoscale Materials in Chemistry*; Klabunde, K. J., Ed.; Wiley-Interscience: New York, **2001**, pp 15-59.
- 3 Li, Y.; Boone, E.; El-Sayed, M. A. Langmuir 2002, 18, 4921 -4925.
- 4 Zhao, M.; Sun, L.; Crooks, R. M. J. Am. Chem. Soc. 1998, 120, 4877 -4878.
- 5 Bönnemann, H.; Richards, R. M. Eur. J. Inorg. Chem. 2001, 2455-2480.
- 6 Rao, C. N. R.; Kulkarni, G. U.; Thomas, P. J.; Edwards, P. P. Chem. Eur. J. 2002, 8, 28-35.
- 7 Li, Y.; El-Sayed, M. A. J. Phys. Chem. B 2001, 105, 8938-8943.
- 8 Crooks, R. M.; Zhao, M.; Sun, L.; Chechik, V.; Yeung, L. K. Accounts Chem. Res. **2001**, *34*, 181-190.
- 9 Underhill, R. S.; Liu, G. Chem. Mater. 2000, 12, 3633-3641.
- 10 Ding, J. H.; Liu, D. L. Chem. Mater. 2000, 12, 22-24.
- 11 Schmid, G.; Maihack, V.; Lantermann, F. J. Chem. Soc. Dalton Trans. Inorg. Chem. 1996, 589-595.
- 12 Niu, Y.; Yeung, L. K.; Crooks, R. M. J. Am. Chem. Soc. 2001, 123, 6840-6846.
- Mamedov, A. A.; Belov, A.; Giersig, M.; Mamedova, N. N.; Kotov, N. A. J. Am. Chem. Soc. 2001, 123, 7738-7739, and references therein.
- 14 Lvov, Y.; Munge, B.; Giraldo, O.; Ichinose, I.; Suib, S. L.; Rusling, J. F. *Langmuir* **2000**, *16*, 8850-8857.
- 15 Liu, Y.; Wang, A.; Claus, R. O. Appl. Phys. Lett. 1997, 71, 2265-2267.
- 16 Feldheim, D. L.; Grabar, K. C.; Natan, M. J.; Mallouk, T. E. J. Am. Chem. Soc. 1996, 118, 7640-7641.
- 17 Schrof, W.; Rozouvan, S.; Van Keuren, E.; Horn, D.; Schmitt, J.; Decher, G. Adv. Mater. 1998, 10, 338-341.
- 18 Iler, R. K. J. Coll. Int. Sci 1966, 21, 569-594.

- 19 Decher, G. Science 1997, 277, 1232-1237.
- Wang, T. C.; Rubner, M. F.; Cohen, R. E. *Langmuir* **2002**, *18*, 3370-3375.
- 21 Joly, S.; Kane, R.; Radzilowski, L.; Wang, T.; Wu, A.; Cohen, R. E.; Thomas, E. L.; Rubner, M. F. *Langmuir* **2000**, *16*, 1354-1359.
- 22 Fojas, A. M.; Murphy, E.; Stroeve, P. Ind. Eng. Chem. Res. 2002, 41, 2662-2667.
- 23 Dante, S.; Advincula, R.; Frank, C. W.; Stroeve, P. *Langmuir* **1999**, *15*, 193-201.
- 24 Dai, J.; Bruening, M. L. Nano Letters 2002, 2, 497-501.
- 25 Sullivan, D. M.; Bruening, M. L. J. Am. Chem. Soc. 2001, 123, 11805-11806.
- Sullivan, D. M.; Bruening, M. L. Chem. Mater. 2002, in press.
- 27 March, J. Advanced Organic Chemistry: reactions, mechanics, and structure; Wiley: New York, 1992.
- 28 Cerveny, L.; Ruzicka, V. Catal. Rev. Sci. Eng. 1982, 24, 503-566.
- Zharmagambetova, A. K.; Ergozhin, E. E.; Sheludyakov, Y. L.; Mukhamedzhanova, S. G.; Kurmanbayeva, I. A.; Selenova, B. A.; Utkelov, B. A. J. Mol. Catal. A 2001, 177, 165-170.

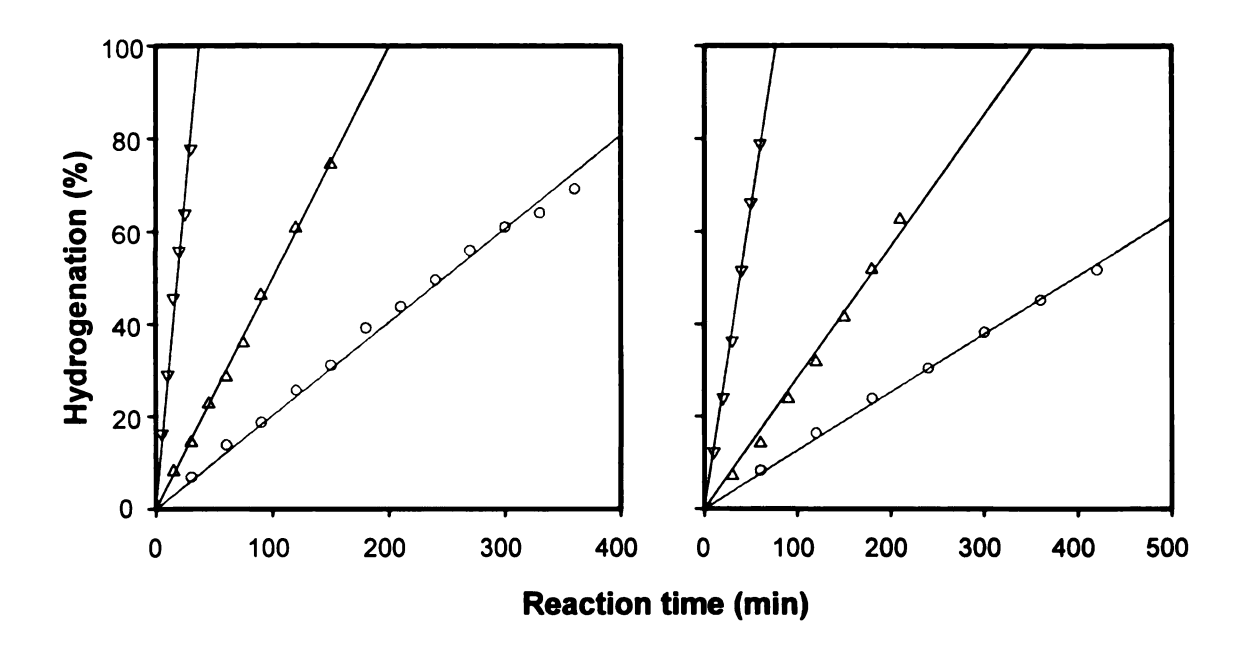


Figure 6.1, appendix. Hydrogenation vs reaction time of substrate 1 (inverted triangle), 2 (triangle), and 3 (circle) on 1 bilayer PAH/PAA-capped 7-PEI-Pd/PAA-on-alumina catalyst (left) and on cross-linked 7-PEI-Pd/PAA-on-alumina catalyst (right). Hydrogenation (%) was obtained from the integration of hydrogenated product peak of GC spectrum.

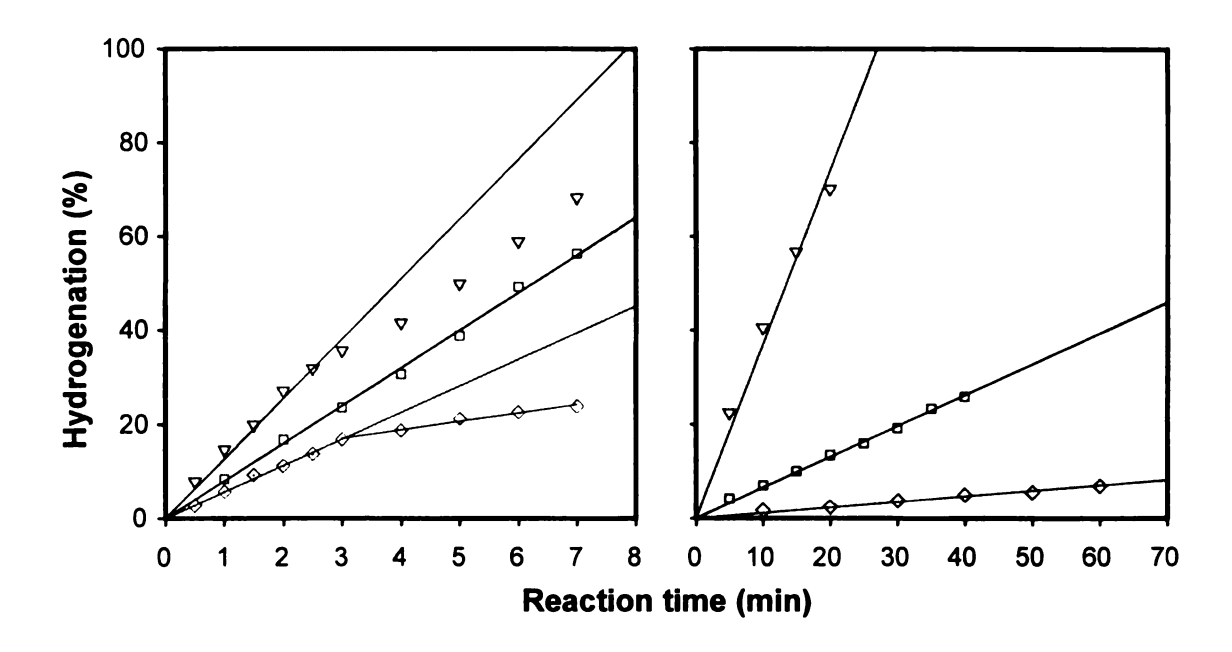


Figure 6.2, appendix. Hydrogenation vs reaction time of substrate 1 (inverted triangle), 4 (square), and 5 (diamond) on 5%-Pd-on-alumina catalyst (left) and on 7-PEI-Pd/PAA-on-alumina catalyst (right). Hydrogenation (%) was obtained from the integration of hydrogenated product peak of GC spectrum

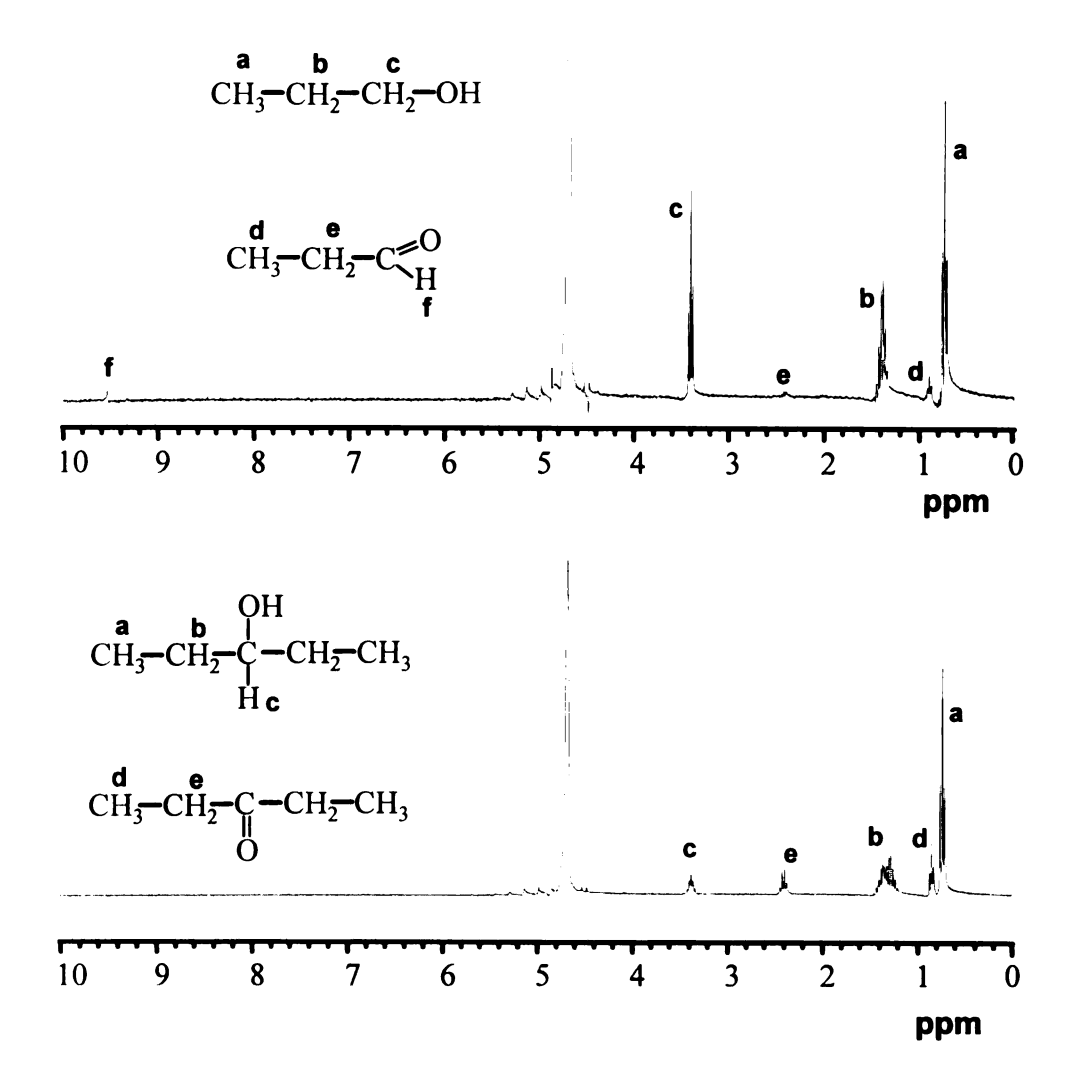


Figure 6.3, appendix. ¹H NMR spectra of the hydrogenation products of allyl alcohol (top, 7-PEI-Pd/PAA-on-alumina) and 1-penten-3-ol (bottom, 5%-Pd-on-alumina).

Chapter 7

Conclusions and future work

This thesis demonstrates the versatility of multilayer polyelectrolyte films in applications that require ultrathin coatings. Chapter 2 showed that control over the composition of PAA/PAH films through heat-induced amide formation yields highly passivating films. In chapters 3 and 4, we showed that manipulation of polyelectrolyte composition through derivatization affords control over coating hydrophobicity and charge density. This allowed enhancement of ion-transport selectivity and modeling of transport through PAA/PAH films and their derivatives. Chapters 5 and 6 explored the use of multilayer polyelectrolyte films for encapsulating catalytic nanoparticles. In addition to stabilizing nanoparticle size, the polyelectrolyte films function as a discriminating matrix that allows selective hydrogenation.

Although these studies clearly demonstrate the potential of multilayer polyelectrolyte films, real applications of these materials will require significant developments in deposition procedures as well as a better understanding of these systems. Coverage of porous supports on a large scale and studies of film durability must be performed to know if polyelectrolyte films can truly serve as practical separation membranes.

As work with nanoparticles encapsulated in polyelectrolyte films is just beginning, much research is needed to understand these systems. First of all, the mechanisms behind selective catalysis are not clear. Is selectivity reflective of hindered diffusion to the nanoparticles or different rates of reaction at the nanoparticle surface? Further studies of hydrogenation as a function of substrate concentration will help to clarify this issue.

Additionally, we have only begun to explore the reactions in which Pd nanoparticles may serve as catalysts. Selective hydrogenation within a molecule may be particularly interesting. For example, in the hydrogenation of dehydrolinalool, linalool is often the desired product, because it is an important building block in organic reactions (Scheme 7.1), However, dehydrolinalool is easily over-hydrogenated to dihydrolinalool. Bronstein and coworkers reported that Pd colloids surrounded by poly(4-vinylpyridine) (PVP) in polystyrene-block-PVP micelles provide high selectivity for hydrogenation to linalool. We expect that Pd nanoparticles in polyelectrolyte films will behave similarly and provide the additional convenience and versatility associated with polyelectrolyte films. This is just one example of the reactions that could be investigated using encapsulated nanoparticles.

Scheme 7.1

This dissertation clearly shows the potential of multilayer polyelectrolyte films in several areas. I am optimistic that with further work, the potential of these films will be truly exploited for practical applications.

Bronstein, L. M.; Chernyshov, D. M.; Volkov, I. O.; Ezernitskaya, M. G.; Valetsky, P. M.; Matveeva, V. G.; Sulman, E. M. J. Catalysis 2000, 196, 302-314.

131

